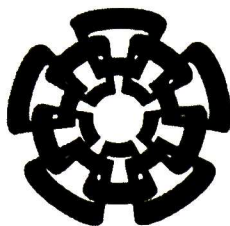xx(178585.1)

Centro de Investigación y de Estudios Avanzados del I.P.N. Unidad Guadalajara

Interpretación y Visualización de Atributos Instantáneos en Oscilaciones Inter-área

Tesis que presenta:
Francisco Román Lezama Zárraga

para obtener el grado de:
Maestro en Ciencias

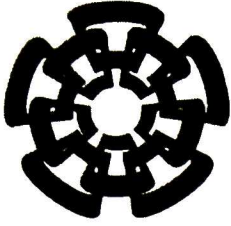en la especialidad de:
Ingeniería Eléctrica

Director de Tesis:
Dr. Arturo Román Messina

Guadalajara, Jalisco, Agosto de 2008.

Centro de Investigación y de Estudios Avanzados del I.P.N. Unidad Guadalajara

Interpretation and Visualization of Instantaneous Attributes in Inter-area Oscillations

A thesis presented by:
Francisco Román Lezama Zárraga

to obtain the degree of:
Master in Science

in the subject of:
Electrical Engineering

Thesis Advisors:
Dr. Arturo Román Messina

Guadalajara, Jalisco, August, 2008.

Interpretación y Visualización de Atributos Instantáneos en Oscilaciones Inter-área

**Tesis de Maestría en Ciencias
Ingeniería Eléctrica**

Por:

Francisco Román Lezama Zárraga

Ingeniero Mecánico Electricista
Universidad Autónoma de Campeche 1989-1994

Becario del CONACYT, expediente 203221

Director de Tesis:
Dr. Arturo Román Messina

Interpretation and Visualization of Instantaneous Attributes in Inter-area Oscillations

Master of Science Thesis
In Electrical Engineering

By:

Francisco Román Lezama Zárraga

Mechanical-Electrical Engineer
Universidad Autónoma de Campeche 1989-1994

Thesis Advisors:
Dr. Arturo Román Messina

Acknowledgments

To almighty God for giving me the strength in every moment of my life.

To my wife Sandra who has been my inspiration and always encouraged me to achieve my goals.

To my daughter Ximena and my son Damián who filled my life with infinite love.

In memory of my father Francisco who always supported my decisions and was the best example for me.

To my mother Ana María whose love and dedication towards me and my brother and sister were fundamental in forming a great family.

To my aunt Carmen who has been a mother for me.

To my mother-in-law María Antonia whose affection and advices has been very important in my professional and personal development.

Resumen

En esta tesis se propone un enfoque sistemático para analizar y caracterizar la evolución temporal de procesos no lineales variantes en el tiempo en sistemas de potencia. Primero, un modelo para la caracterización de la amplitud y el amortiguamiento de oscilaciones cuasi-estacionarias es propuesto. El método combina análisis tiempo-frecuencia y conceptos de la teoría de sistemas vibratorios para aproximar el comportamiento de oscilaciones no lineales variantes en el tiempo mediante osciladores de dos grados de libertad.

Se presenta, a continuación, un nuevo marco analítico en la caracterización y el modelado de la evolución temporal no lineal de las oscilaciones y técnicas para la identificación del contenido modal de los más dominantes componentes de movimiento son desarrolladas. Se obtienen expresiones analíticas que proporcionan soluciones aproximadas a los atributos instantáneos como frecuencia y amortiguamiento de las oscilaciones, y se ofrece una interpretación física del modelo. El método propuesto proporciona también un medio para la extracción de estructuras dinámicas en los procesos oscilatorios.

Como un ejemplo, se utilizan datos de estabilidad transitoria y eventos reales para examinar el potencial uso de técnicas en el análisis de series temporales no lineales en la caracterización de la evolución en el tiempo de oscilaciones no lineales y no estacionarias, y determinar la naturaleza y propagación del sistema perturbado. El enfoque propuesto también es comparado con técnicas convencionales y su eficiencia es completamente demostrada.

Abstract

In this thesis, a systematic approach to analyze and characterize the temporal evolution of nonlinear, time-varying processes in power systems is proposed. First, a model for characterizing the amplitude and damping of cuasi-stationary oscillations is proposed. The method combines time-frequency analysis and concepts from vibration systems theory for approximating the behavior of nonlinear, time-varying oscillations by second-order-degree-of-freedom oscillators.

A new analytic framework in characterizing and modelling the nonlinear temporal evolution of the oscillations is then presented and techniques for identifying the modal content of the most dominant motion components are developed. Analytic expressions are obtained that provide approximate solutions to the instantaneous attributes as frequency and damping of the oscillations, and a physical interpretation of the model is given. The proposed method provides also a means for extracting dynamic structures in oscillatory processes.

As an example, data from both transient stability and real events are used to examine the potential usefulness of nonlinear time series analysis techniques in characterizing the time evolution of nonlinear, non-stationary oscillations and to determine the nature and propagation of the system disturbance. The proposed approach is also compared with conventional techniques and its efficiency is fully demonstrated.

Index

Chapter 1
Introduction

Chapter 2
Generalized Hilbert-Huang Transforms

Chapter 3
Numerical Computation of the Hilbert Transform

Chapter 4
Free Vibration Analysis using the Hilbert Transform

Chapter 5
Modal Identification via Hilbert Analysis

Chapter 6
Application to complex inter-area oscillations

Chapter 7
Conclusions

Appendix A
Interpolation by spline functions

Index of figures and tables

Chapter1
Introduction

This introductory chapter presents a brief description of the research work in this thesis. The general introduction, the problem statement, the objectives and the study approach are presented.

After a motivation to the study of instantaneous attributes in the dynamic behavior of system oscillations, a review of recent work is presented.

The objectives of the work, the main results, and the limitations of the study are stated and the main contributions are then summarized.

The chapter concludes with an outline of the structure of the thesis.

1.1 Background and motivation

The analysis and characterization of nonlinear, non-stationary power system oscillations has attracted significant attention in recent years. Transient oscillations triggered by the loss of major transmission and generation resources may manifest highly complex spatial and temporal dynamics and involve a large number of machines and take place over a great range of space and time scales [1],[2].

Understanding the dynamic mechanisms that govern the leading modes of variability of the observed oscillations, and how these modes may be influenced by control or other changes, are questions of critical importance. Such features may be obscured or distorted in the normal spectral analysis approach.

Recent experience with the analysis of inter-area disturbances shows that many transient oscillations may manifest complex phenomena, including nonlinear, time-varying behavior and mode interaction [3]-[5]. In large, loosely interconnected power systems, the analysis and characterization of inter-area oscillations from measured data is a formidable challenge.

Non-stationary behavior may result from the effects of sequential faults, control actions, and changes in system topology and operating conditions. Successful analysis of complex dynamic events requires analysis approaches with high levels of sophistication including the ability to treat nonlinear and non-stationary data, increased time and frequency resolution, and ease of implementation among other features.

Accurate tracking of system behavior allows replicating the events leading to the observed oscillations, and analyzing the system conditions, control action or device on modal content.

Past studies have focused on identifying the causal mechanisms for instability and analyzing the temporal and spatial variability of measured data or simulations. Among such procedures, the evolutionary spectrum, the continuous wavelet transform, empirical orthogonal analysis, and the Hilbert-Huang

technique have proved to be useful tools for analyzing and studying the time-varying modal characteristics of complex systems subjected to large perturbations.

Of particle interest are applications where these techniques are used to extract modal information on an on-line basis or for real-time control of system behavior.

While some progress has been made, there are still some important issues that need to be addressed before such approaches can be realized for on-line monitoring and control of transient oscillations. Study experience with complex systems, suggests that various levels of refinement are required according to the application [3]-[5].

This work aims addressing some of these issues with emphasis on the analysis of nonlinear and non-stationary oscillations.

1.2 Problem statement

The detection of temporal changes in the dynamic behavior in nonlinear, non-stationary oscillatory processes is a problem of great theoretical and practical importance.

Characterization of non-stationary behavior is required for both, detailed understanding of the mechanisms leading to the instability, and addressing the key questions of how the temporal oscillation modes evolve over time. The issue of stationarity is particularly important in studying the system response to large and abrupt changes in system topology or operating conditions, and in tracking the system response to sequential faults.

Nonlinearity, on the other hand, causes the temporal modes to interact, leading to frequency and amplitude modulation and to a phase relationship known as quadratic phase coupling between the frequency components involved.

Detecting and identifying sources of nonlinearity and non-stationarity in observed time series are difficult problems. The non-stationarity of the data following the triggering event makes reliable estimates of the instantaneous frequency, damping and generator coherency of the observed oscillations difficult. Traditional methods of time series analysis do not address the problem of non-stationary in power system oscillations, and often assume linearity of the process which makes them unsuitable for the study of transient power system processes.

Because of the time-varying characteristics exhibited by the power system processes, the investigation of system behavior should employ methodologies that make proper use non-stationary approaches.

Besides the understanding of the temporal behavior of system oscillations, nonlinear models should be developed to understand complex behavior and enhance our ability of system prediction.

In what follows a critical review of methods for the analysis, modeling and characterization of transient processes in power systems is presented, with an emphasis on time-frequency methods of analysis of nonlinear, time-varying series.

1.3 A brief review of previous work

Time-frequency-energy analysis is a new field of research with a broad range of applications such as image processing and biomedical signal analysis.

In the past decade, many approaches have been proposed for spectral analysis of power system signals. Commonly used spectral analysis methods are based on linear analysis techniques. These include spectral estimation methods, eigenrealization algorithms and MIMO state-space identification methods, [6], [7], among other. These models are incapable of explaining important nonlinear phenomena and may not provide useful information needed in the assessment of transient signal dynamics.

4

In addition, most of the analysis techniques for system oscillations have one major shortcoming: the lack of realizable approach for damping estimation.

Approaches such as Prony analysis and block processing techniques have been successfully used to extract modal information from complex data set [8]-[10]. As the number of measured signals increases, however, accurate characterization of relevant modal behavior becomes difficult, especially in the presence of noise [9].

Other application areas include the analysis of generator coherency from simulated data and the extraction of spatial dynamic patterns. Algorithms such as those based on eigenvalue analysis [11] and principal component analysis [12] have been used to identify generator coherent groups as well as to analyze other aspects of system dynamic behavior.

In [13], a wide-area analysis method for generator coherency identification based on Fourier analysis was used for inter-area detection and generator grouping. A major limitation of this approach is the assumption of stationarity that makes it unsuitable for real-time applications, or applications involving control or topology changes.

Over the last few years, several time-energy-frequency analysis techniques have been developed with the ability to characterize non-stationary behavior. Among these emerging techniques, Hilbert and wavelet analysis, and higher order statistical techniques have been used to detect and quantify the effect of nonlinear mode interaction on the time evolution of non-stationary power system oscillations [3]-[5].

In [4], higher-order statistical (HOS) analysis techniques are used to study the interplay between modal interaction and nonlinear behavior in a complex system. HOS methods are mainly useful for the analysis of semi-stationary phenomena whose frequency components change slowly over time.

Also of interest is the approach of Levent *et al.* [14] who proposed a method to extract modal properties as damping and frequency from nonlinear transient signal

The proposed methods offer a powerful tool to analyzed sets of data obtained from simulations or measurements that supplements information on conventional analysis techniques. Also the modal information obtained of the analyzed signals is physically interpretable and provide meaningful insights into the observed dynamics.

1.4 Thesis objectives

Following the above problems, the objectives of this research are as follows:

- The development of an analytical framework based on time-energy-frequency representations to model, analyze and characterize the temporal dynamics of nonlinear and non-stationary oscillations in power systems that will be compatible with the models employed by the electric industry.

- The development and testing of improved numerical approaches for existing methods to analyze complex oscillations.

- The extension of existing approaches to analyze spatio-temporal dynamic patterns in transient processes.

- To investigate the applicability of HHT in the analysis of transient processes in power systems.

1.5 Research contributions

In this work, techniques to extract and characterize instantaneous attributes of nonlinear and non-stationary power system oscillations are proposed.

The main original contributions of this thesis include the followings:

The development of a mathematic and computational approach for extracting temporal information from nonlinear, time-varying processes. A new dynamic framework based on output-only information of a multiple-degree-of-freedom system is proposed to extract temporal modal information.

- The modification of standard EMD algorithms to allow demodulation of the extracted temporal components. Based on a modified sifting technique, temporal behavior is characterized in terms of mono-component analytic functions that admit well-behaved Hilbert transforms

- The extension of current algorithms for damping estimation and introduction of new measures based on the notion of averaged instantaneous damping. A simple model that combines splines with the log-decrement technique is used to define average instantaneous damping.

- The development and testing of alternative formulations for estimating instantaneous frequency and the computation of Hilbert transforms.

The development of analytical approaches to estimate dynamic coherency from transient stability simulations.

The combination of these methods is a new direction in power system research and has helped to gain new understanding in the variability of power system processes on midterm scales.

The results are also relevant to the identification of the critical period of activity of temporal modes and the development of corrective measures.

1.6 Organization of the thesis

This thesis is organized in seven chapters and one appendix.

After this introductory chapter, Chapter 2 introduces time-energy-frequency approaches for the analysis of temporal process.

Chapter 3 discusses different approach for the numerical implementation of the Hilbert transform in power signals for the estimation of instantaneous attributes. These methods are: the time-domain approach, the frequency-domain approach (Fourier method) and the convolution method. An application example is provided by determining the most viable approach.

Chapter 4 presents the analysis and identification of time-varying processes. A systematic method to analyze and characterize the temporal evolution of nonlinear, non-stationary process in power systems is developed. The method combines the Hilbert-Huang transform and concepts from vibrating systems theory and is used to approximate the dynamic behavior of quasi-stationary oscillations.

Chapter 5 demonstrates the efficiency of proposed method by comparing damping estimates with results obtained from conventional approaches. Alternative methods by computing instantaneous frequency are developed, and a method by estimating instantaneous generator coherency is proposed.

Chapter 6 presents the application of the time-varying algorithm model to the analysis of inter-are oscillations. Conclusions and suggestions for future work are presented in Chapter 7.

Appendix A describes the spline fitting technique used in this research.

1.7 References

[1] J. F. Hauer, and J. G. DeSteese, "A Tutorial on Detection and Characterization of Special Behavior in Large Electric Power Systems," *Pacific Northwest National Laboratory, Richland, WA,* Rep. PNNL-14655, July 2004.

[2] S. Liu, A. R. Messina, and V. Vittal, "Characterization of Nonlinear Modal Interaction using Normal Forms and Hilbert Analysis," in *Proc. IEEE Power Eng. Soc. Power System Conf. Expo.,* New York, October 2004.

[3] D. Ruiz-Vega, A. R. Messina, and G. Henriquez-Harper, "Analysis of Inter-area Oscillations via Non-linear Time Series Analysis Techniques," in *Proc. 15th Power System Computation Conf.,* Session 32, paper 2, pp. 1-7, Liege, Belgium, August 2005.

[4] A. R. Messina, and V. Vittal, "Nonlinear, Non-stationary Analysis of Inter-area Oscillations via Hilbert Spectral Analysis," in *IEEE Transactions on Power Systems,* vol. 21, No. 3, pp. 1234-1241, August 2006.

[5] A. R. Messina, V. Vittal, D. Ruiz-Vega, and G. Henriquez-Harper, "Interpretation and Visualization of Wide-Area PMU Measurements using Hilbert Analysis," in *IEEE Transactions on Power Systems,* vol. 21, No. 4, pp. 1763-1771, November 2006.

[6] D. J. Trudnowsky, M. K. Donnelly, and J. F. Hauer, "A procedure for oscillatory parameters identification," in *IEEE Transactions on Power Systems,* vol. 9, pp. 2049-2055, November 1994.

[7] I. Kamwa, and L. Gerin-Lajoie, "State-space system identification toward MIMO models for modal analysis and optimization of bulk power systems," in *IEEE Transactions on Power Systems,* vol. 15, pp. 326-335, February 2000.

[8] H. Okamoto, A. Kurita, J. J. Sanchez Gasca, K. Clark, N. W. Miller, and J. H. Chow, "Identification of equivalent linear power system models from

electromagnetic transient time domain simulations using Prony's method," in *Proc. 35ʰ IEEE Conf. on Decision and Control*, pp. 3857-3863, 1996.

[9] D. J. Trudnowsky, J. M. Johnson and J. F. Hauer, "Making Prony analysis more accurate using multiple signals," in *IEEE Transactions on Power Systems*, vol. 14, No. 1, pp. 226-231, February 1999.

[10] R. W. Wies, A. Balasubramanian, and J. W. Pierre, "Combining least mean adaptive filter and auto-regresive block processing techniques for estimating the low-frequency electromechanical modes in power systems," in *Proc. IEEE Power Engineering Society General Meeting,*" 2006.

[11] C. Liu, R. Yokoyama, K. Koyanagi, and K. Y. Lee, "PSS design for damping of inter-area power oscillations by coherency-based equivalent model," in *Electrical Power and Energy Systems*, vol.26, pp. 535-544, 2004.

[12] K. K. Anaparthi, B. Chaudhuri, N. F. Thornhill, and B. C. Pal, "Coherency Identification in Power Systems through Principal Component Analysis," in *IEEE Transactions on Power Systems*, vol. 20, No. 3, pp. 1658-1660, August 2005.

[13] M. Jonsson, M. Begovic, and J. Daalder, "A New Method Suitable for Real-Time Generator Coherency Determination," in *IEEE Transactions on Power Systems*, vol. 19, No. 3, pp. 1473-1482, August 2004.

[14] M. E. Levent, and K. Y. Sanliturk, "Characterisation of Vibration Isolators Using Vibration Test Data," in *10ᵗʰ International Congress on Sound and Vibration*, pp. 1-8, 2003.

Chapter2
Generalized Hilbert-Huang Transforms

The study of nonlinear, non-stationary power system processes has recently become the subject of intense interest and investigation in power system stability studies. In practice, the detection and characterization of temporal nonlinear oscillations in measured data is greatly complicated by non-stationary variations in system dynamic behavior.

Several representations have been explored over the last few years to analyze processes that are characterized by nonlinear and non-stationary characteristics.

This chapter presents a general review of modeling frameworks that explicitly acknowledge and incorporate nonlinear and non-stationary behavior. A two-stage time-frequency-energy (TFE) approach based on the Hilbert-Huang transform is first introduced that can be used to analyze temporal information. Variations to existing approaches are suggested along with a review of present limitations.

Numerical aspects associated with the use and interpretation of the proposed technique are discussed. In addition, we discuss various issues which influence the effectiveness of several time-frequency representations.

The notation utilized throughout the dissertation is also summarized.

2.1 The Hilbert-Huang technique

Recently, nonlinear and non-stationary analysis techniques based on the Hilbert-Huang Transform (HHT) [1],[2] have been used to analyze data from nonlinear and non-stationary processes. The HHT consists of two steps:

(a). The empirical mode decomposition of the signal into basis functions, and

(b). The application of the Hilbert transform to the intrinsic functions

The cornerstone to the whole HHT procedure is the Empirical Mode Decomposition (EMD) that separates a signal into amplitude and frequency modulated signal components that admit well-behaved Hilbert transforms [3],[4].

In the first step, the original system time histories $x(t)$ are decomposed into a finite number of intrinsic mode functions (IMFs) with time-variable amplitudes and frequencies, through EMD. Once the original signal has been decomposed into intrinsic mode functions, the Hilbert transform can be applied to each IMF to extract modal features.

In the following sections we offer a critical review of this approach. Enhancements, extensions and generalizations to the techniques are suggested along with an analysis of present limitations.

2.1.1 Empirical mode decomposition

The empirical mode decomposition (EMD) technique is a systematic method for numerically decomposing any time equally spaced time series, $x(t)$ into its own intrinsic mode functions, i.e. the IMFs.

Definition 2.1 (Intrinsic Mode Function). An IMF is defined as a time series which satisfies three critical requirements:

(a). In the whole data set, the number of extrema and the number of zero-crossing must either be equal or differ at most by one.

(b). At any point, the mean value of the envelope defined by the local maxima and the envelope defined by the local minima is zero.

(c). The linear superposition of all IMFs should reconstruct the time series.

The extraction of IMFs out of time series requires a repeated sifting procedure called empirical mode decomposition. EMD is briefly described as follows:

1. Starting with the original signal $x(t)$, set $r_0(t) = x(t)$, and $j = 1$.

2. Extract the jth IMF using the following sifting procedure

   a. Set $h_0(t) = r_j(t)$ and $i = 1$.

   b. Identify all extrema of $x(t)$ for $h_0(t)$ by passing a natural cubic spline through the local maxima and minima.

   c. Interpolate between maxima (minima) to obtain an envelope $e_{max}(t)$ $(e_{min}(t))$.

   d. Compute the running mean of the envelopes, $m_{i-1}(t) = \left[e_{max_{i-1}}(t) + e_{min_{i-1}}(t) \right]/2$ and subtract it from $h_{i-1}(t)$; determine a new estimate $h_i(t) = h_{i-1}(t) - m_{i-1}(t)$, such that $e_{min_{i-1}}(t) = \leq h_i(t) \leq e_{max_{i-1}}(t)$ for all t. Set $i = i + 1$.

The step 2(d) is then repeated until $h_i(t)$ satisfies a predetermined stopping criterion, and the first IMF component from the data is called $c_i(t) = h_i(t)$

3. Obtain an improved residue $r_j(t) = r_{j-1}(t) - c_j(t)$. Repeat steps 2(a) through 2(d) with $j = j + 1$ until the number of extremes in $r_j(t)$ is less than two.

In this model, the upper and lower envelopes are derived by fitting a cubic spline through the local maxima and minima, respectively, with the added requirement that the signal lies between these two envelopes. See Appendix A for details about cubic splines.

This decomposition is mathematically expressed in the form:

$$x(t) = \sum_{j=1}^{n} c_j(t) + r_n(t) \tag{2.1}$$

where the functions $c_j(t)$ are nearly orthogonal and have zero local means, n is the total number of IMFs and $r_n(t)$ is the non-oscillatory residual at the end of the sifting process, which represent the trend component of the signal $x(t)$. The algorithm does not impose a basis set on the data (does impose a predetermined basis function which makes it adaptive).

Each IMF is associated with a local time scale that can be amplitude or frequency modulated and even non-stationary, and involves only one mode of oscillation, where the first component (IMF1) contain the highest frequency oscillation; the frequency content then decrease with the increase in IMF and the last component is the residue $r_n(t)$.

The stopping criterion of the sifting process requires that the residue $r_n(t)$, becomes a monotonic function from which no more IMF can be extracted, or can still be different from zero mean.

To guarantee that the IMFs retain sufficient physical sense, a criterion to stop the sifting process is defined by calculating the standard deviation between two successive siftings as

$$SD = \frac{\sum_{t=0}^{T} \left(h_{1(k-1)}(t) - h_{1k}(t) \right)^2}{\sum_{t=0}^{T} h_{1(k-1)}^2(t)}$$

where SD is typically set between 0.2 and 0.3 [1]. The selection of an optimum threshold value is important, but difficult.

The sifting process serves two purposes: to separate out high-frequency, small-amplitude waves, which are 'riding' atop, or superimposed on, larger amplitude, lower frequency waves, and to smooth out uneven amplitudes in the IMF being extracted, i.e. to make the wave-profiles more symmetric about the local zero-mean line.

The first purpose must be achieved for the Hilbert transform to give a meaningful instantaneous frequency, while the second purpose must also be achieved in case the neighboring wave amplitudes have too large a disparity.

As pointed out in the literature, however, these goals are often conflicting for non-stationary signals, since riding waves may be transient in nature and/or highly variable in amplitude, and smoothing out the uneven amplitudes via sifting can prevent faithful extraction of these waves.

Moreover, repetitive sifting causes smearing of TFE information across different decomposition levels and an intra-level smoothing of TFE information, which is unlikely to reflect the intrinsic characteristics of the signal under analysis.

Physical insight into the nature of the EMD can be attained by seeing a nonlinear and non-stationary signal, $x(t)$, as composed of fast oscillations superimposed on slow oscillations. A simple example is shown in Fig. 2.1 to illustrate this notion. Here, the original signal (blue thick line) is seen as composed of a slow oscillation given by the mean of two envelopes $[e_{max}(t), e_{min}(t)]$ (dark broken line) and a fast oscillation given by

$$h(t) = x(t) - mean(t)$$

where

$$m_{i-1}(t) = [e_{max}(t) + e_{min}(t)]/2$$

Once the slow oscillation has been identified, it is considered as new signal onto which the same procedure is applied.
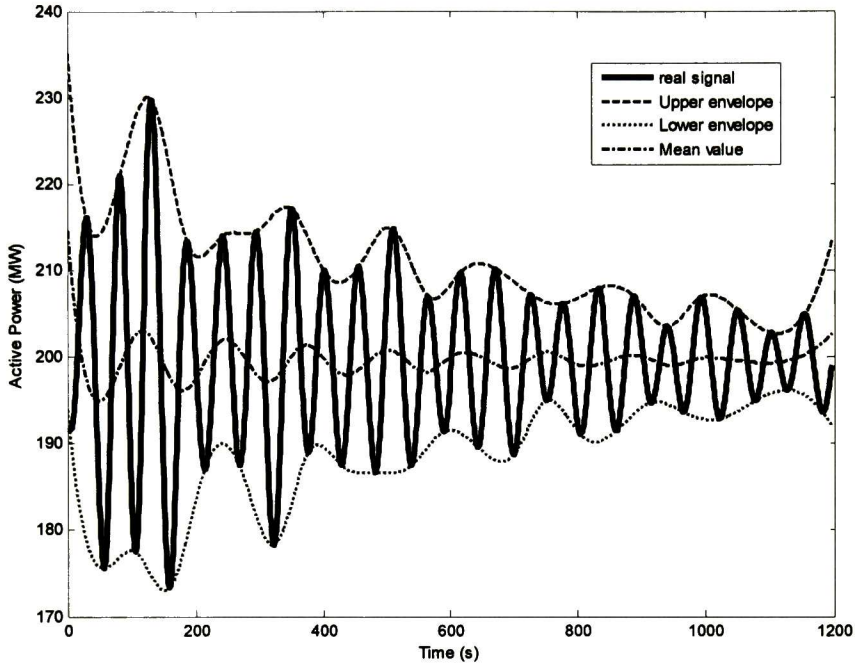
Figure 2.1. First step of the sifting process applied to a real signal showing the upper and lower envelopes and the instantaneous mean.

Other interpolation techniques such as trigonometric interpolation and higher order spline fitting hold promise in the development of improved EMD.

2.2 The Hilbert transform and the analytic signal

2.2.1 The Hilbert transform

Once the EMD technique has been applied to decompose the input signal into a set of IMFs and a residual signal, one may now analyze the components to extract instantaneous amplitude, phase and frequency information.

Suppose $u(t)$ is a general measured or simulated signal. The Hilbert transform (HT) of $u(t)$ is defined by [5]

$$v(t) = H[u(t)] = -\frac{1}{\pi} P \int_{-\infty}^{\infty} \frac{u(\eta)}{\eta - t} d\eta = \frac{1}{\pi} P \int_{-\infty}^{\infty} \frac{u(\eta)}{t - \eta} d\eta \qquad (2.2)$$

and the Hilbert inverse transform is given by

$$u(t) = H^{-1}[v(t)] = \frac{1}{\pi} P \int_{-\infty}^{\infty} \frac{v(\eta)}{\eta - t} d\eta = -\frac{1}{\pi} P \int_{-\infty}^{\infty} \frac{v(\eta)}{t - \eta} d\eta \qquad (2.3)$$

where the principal value of the integral is used and * indicates the convolution operator.

The integrals in (2.2) and (2.3) are improper integrals in the sense of the Cauchy principal value denoted by P, and they are represented in terms of convolution notation as

$$v(t) = \frac{1}{\pi t} * u(t) \qquad (2.4)$$

$$u(t) = -\frac{1}{\pi t} * v(t) \qquad (2.5)$$

where $1/(\pi t)$ is the kernel of the transformation. Equations (2.2) and (2.3) describe a unique pair $(u(t), H[u(t)])$ that contains temporal behavior.

2.2.2 The analytic signal

The real signal $u(t)$ and its HT define an analytic signal, $\Psi(t)$, given by

$$\Psi(t) = u(t) + jv(t) = A(t)e^{j\varphi(t)} \qquad (2.6)$$

where $A(t)$ and $\varphi(t)$ are the instantaneous amplitude and phase of the analytic signal $z(t)$, and the imaginary part $H[x(t)]$ is the Hilbert transform of $x(t)$:

$$H[x(t)] = \frac{1}{\pi} P \int_{-\infty}^{\infty} \frac{x(\eta)}{t - \eta} d\eta \qquad (2.7)$$

where the notation P indicates the Cauchy principal value of the integral.

Clearly,

$$u(t) = A(t)\cos[\varphi(t)] \qquad (2.8)$$

$$v(t) = A(t)\sin[\varphi(t)] \qquad (2.9)$$

It is important to emphasize that both, the amplitude $A(t)$, and phase function $\varphi(t)$, are single valued functions of time, and therefore can only be applied to a simple oscillatory function. The combined application of Hilbert analysis and the EMD allows the study of more complex signal behavior.

Meaningful results are obtained from mono-component Hilbert transform. This is discussed further in Chapter 6.

2.2.3 Instantaneous time-frequency information

The analytic signal represents a local time-varying wave in the complex plane (u,v) and is a phasor that rotates about the Cartesian plane (u,v), as shown in Fig. 2.2.
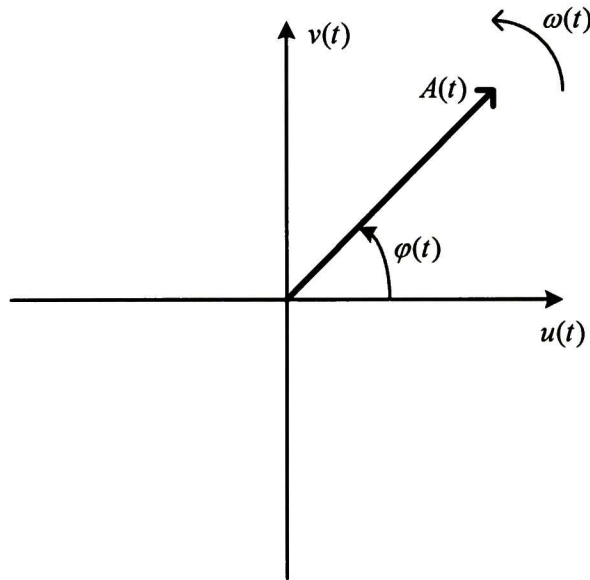
Figure 2.2. A rotating phasor representing the analytic signal $\Psi(t) = u(t) + jv(t)$.

The length of the rotating phasor $A(t)$, is named the instantaneous amplitude, defined as

$$A(t) = \sqrt{u^2(t) + v^2(t)} \qquad (2.10)$$

and the instantaneous phase is defined as the instantaneous angle

$$\varphi(t) = \arctan\left[\frac{v(t)}{u(t)}\right] \qquad (2.11)$$

in which, the instantaneous phases are obtained by unwrapping the phase angles $\varphi_j(t)$.

The rotating phasor and its instantaneous angular speed define the instantaneous angular frequency of the analytic signal. Following Gabor [2], the instantaneous frequency is defined as the phase velocity of any given phase:

$$\omega(t) = \dot{\varphi}(t) = \frac{d}{dt}\left[\arctan\left(\frac{v(t)}{u(t)}\right)\right] = \frac{u(t)\dot{v}(t) - v(t)\dot{u}(t)}{u^2(t) + v^2(t)} \qquad (2.12)$$

Therefore, the instantaneous frequency in cycles/s or Hertz can be calculated by

$$F(t) = \frac{\omega(t)}{2\pi} = \frac{1}{2\pi}\dot{\varphi}(t) \qquad (2.13)$$

Techniques to compute the instantaneous frequency that avoid computing the local time derivative are introduced in Chapter 5. Several practical procedures for computing the Hilbert transform are given in Chapter 3.

2.2.4 Mathematical challenges in Hilbert-Huang analysis

While the introduction of the EMD constitutes a conceptual advance in TEF analysis for non-stationary and nonlinear signals, it has several practical limitations that reduce its practical utility and may cause inaccuracies in depicting signal dynamics.

Numerical problems include:

- End swings caused by spline interpolation that result in large variations in the envelope estimation. These large swings can eventually propagate into the data series and corrupt the whole signal, especially the low frequency components, thus making the EMD ineffective.

    Convergence problems in the sifting procedure,

- Difficulty with intermittency and modulation, and

    Distortion in the Hilbert transform, and

A number of analytical issues remain open for research and include:

    Finding physical and mathematical meaning for the IMFs,

- Determining the most appropriate interpolating schemes, and

- Identifying criteria for stopping the sifting process.

Despite the aforementioned weaknesses, the HHT is finding increased application.

There have been several approaches to handling these issues. These include the use of signal masking techniques, higher-order spline fits, the use of trigonometric interpolation, bitting-off of the beginning and the end of a signal, and decreasing sampling intervals, among other methods.

2.3 Use of signal masking techniques to improve EMD

The conventional EMD method introduced by Huang is based on a progressive sifting process by extracting the IMFs, which requires that a local average of the signal be defined [6].

As we remarked above, however, the IMFs may contain riding waves which create intermittency and modulation making physical interpretation of

mixed modes difficult. Further IMFs may be multi-harmonic functions and therefore, the instantaneous frequencies extracted from them show irregularities which raise difficulties in interpreting the signal.

2.3.1 Intermittency and intermodulation

The problem of intermittency prevents the use of EMD on many types of signals. Intermittency occurs in any signal that is constantly changing and is usually defined as erratic changes wave heights.

Following Huang [7], we refer to intermittency as a component at a particular time scale either into existence or disappearing from a signal. This can introduce mode mixing, that is, having different time or spatial scales mixed in one IMF. In turn, this has the effect of producing additional spurious variations in the IMFs and their associated instantaneous frequencies.

In the standard analysis procedure, the nonlinear and multi-component signal is decomposed into a finite number of high-frequency and low-frequency components (IMFs) by cubic spline interpolation to create envelopes around the signal and find the local average. If we knew the components a priori through EMD method we would naturally define the local average to be the lowest frequency component.

In most practical modeling situations, however, the nonlinear, non-stationary temporal functions may include one or more modes whose associated amplitudes and frequencies are modulated and coupled in time; these modes are difficult to interpret in term of conventional modal analysis.

The need for improved descriptions of the EMD has led to the development of signal masking techniques.

2.3.2 Solution to mode mixing

A solution to the problem of mode mixing is to insert a sinusoidal masking signal that prevents lower frequency components from being included in the IMF obtained through traditional EMD method.

This is accomplished as follows [8]:

(i). Perform a Fast Fourier Transform (FFT) on the original signal $x(t)$, to estimate frequency components $f_1, f_2, ..., f_n$ in an IMF, where $f_1 < f_2 < ... < f_n$. The frequencies $f_1, f_2, ..., f_n$, are the stationary equivalents of the possibly time-varying frequency components of $x(t)$.

(ii). Construct the masking signals $mask_2$, $mask_3, ...,$ $mask_n$, where $mask_k(t) = M_k \sin[2\pi(f_k + f_{k-1})t]$, in which $|f_k|$ is the magnitude of f_k obtained from the FFT spectrum. The value of M_k is empirical.

(iii). Obtain two signals $c_n(t)_+ = x(t) + mask_n(t)$ and $c_n(t)_- = x(t) - mask_n(t)$. Perform EMD (steps 1-2 from section 2.1.1) on both signals to obtain their first IMFs only, $c_1(t)_+$ and $c_1(t)_-$; then $c_1(t) = (c_1(t)_+ + c_1(t)_-)/2$.

(iv). Obtain the residue, $r_1(t) = x(t) - c_1(t)$.

(v). Perform steps A3-A4 iteratively using the other masking signals and replacing $x(t)$ with the residue obtained, until $n-1$ IMFs containing frequency components $f_2, f_3, ..., f_n$ are extracted. The final residue $r_n(t)$ will contain the remaining component f_1.

(vi). Compute the residue, $r_1(t) = x(t) - c_1(t)$.

(vii). If the residue, $r_1(t)$, is above a threshold value of error tolerance, then repeat step (i) through (iii) on $r_1(t)$, to obtain the next IMF and a new residue.

By using a masking signal higher that the highest frequency component, it is possible to separate two components whose frequencies are within a factor

of 2 of each other. Further, this preprocessing technique decomposes the signal into IMFs that have better-behaved Hilbert transforms.

In recent work by Senroy [8], the improved HHT, developed in [4], was used to characterizing the time-frequency-magnitude response of a high-temperature superconducting motor, in which its algorithm uses the FFT of a time-varying waveform to generate appropriate masking signals. Other variations to enhance empirical mode decomposition employing this approach are described in [9] and [10].

Special techniques to deal with mode mixing are discussed in Chapter 6.

The masking signal method allows EMD to be used to separate components that are similar in frequency that would be inseparable with traditional EMD techniques.

2.4 The Hilbert spectrum and instantaneous frequency

2.4.1 The Hilbert spectrum

After performing the Hilbert transform on each IMF component, the original data can be recovered as

$$x(t) = \sum_{j=1}^{n} IMF_j(t) = \Re\left\{ \sum_{j=1}^{n} a_j(t) e^{i\int \omega_j(t)dt} \right\} \tag{2.14}$$

where $\Re$ is the real part of the complex number. The time-frequency distribution of the amplitude is designated as the Hilbert spectrum $H(\omega,t)$, the term $a_j(t)$ is a time-dependent expansion coefficient similar to the constant in the Fourier expansion and $\omega_j(t)$ is the instantaneous frequency at time τ which differs from the constant frequency ω_j in the Fourier transform.

Equation (2.14) shows that a time series $x(t)$ can be represented by a triplet $\{t, \omega(t), a(t)\}$, i.e. an effective time-frequency distribution of the amplitude is generated for the associated time series.

2.4.2 *Instantaneous complex phase and complex frequency*

The instantaneous phase of a signal may be derived from the instantaneous frequency using the integral [5]

$$\varphi(t) = \int_0^t \omega(t)dt + \varphi_0 \tag{2.15}$$

This formula may be regarded as a solution of the first-order differential equation given by

$$\dot{\varphi}(t) = \omega(t) = 2\pi f(t) \tag{2.16}$$

The integral of the angular speed $\omega(t)$ equals the angular distance $\varphi(t)$ and the integration constant φ_0 is given by the angular position of the phasor at $t = 0$. In order to get a uniform exponential notation of the analytic signal, let us define the instantaneous radial velocity of the phasor or instantaneous radial frequency of Figure 2.2 as

$$\alpha(t) = \frac{\dot{A}(t)}{A(t)} \tag{2.17}$$

where $\alpha(t)$ is a measure of the relative speed of elongation of the radius vector A(t); in others word, $\alpha(t)$ gives a measure of the radial velocity representing the speed of change of the radius or amplitude of the phasor.

The solution of this differential equation enables us to write the instantaneous amplitude in the form

$$A(t) = A_0 e^{\int_0^t \alpha(t)dt} \tag{2.18}$$

and the analytic signal in a uniform exponential notation

$$\Psi(t) = A_0 e^{j\varphi_0} e^{\int_0^t [\alpha(t) + j\omega(t)]dt} \tag{2.19}$$

where $A_0 e^{j\varphi_0}$ is a constant defining the notion of a complex amplitude at $t = 0$.

The integrand in this formula defines the notion of the instantaneous complex frequency

$$s(t) = \alpha(t) + j\omega(t) \qquad (2.20)$$

Alternatively, we can define the instantaneous complex phase of the analytic signal of the form [11]

$$\Phi_C(t) = Ln[\Psi(t)] = Ln[A(t) + j\varphi(t)] \qquad (2.21)$$

Here, the capital L denotes the multibranch character of the logarithm of a complex function. The time derivate of the complex phase yields the complex frequency (2.20), since

$$s(t) = \dot{\Phi}_C(t) = \frac{\dot{A}(t)}{A(t)} + j\dot{\varphi}(t) = \alpha(t) + j\omega(t) \qquad (2.22)$$

Subsequent sections of this paper discuss briefly the use of alternate modeling approaches to characterize temporal behavior.

2.5 Generalized time-varying transformations

In spite of the wide applicability of the time-frequency-energy representations described in the preceding sections, numerous other techniques have been developed as well. The following is a summary of recent approaches existing in the literature.

2.5.1 Projections in time-frequency: continuous time case

The orthogonal bases can also be computed with other techniques, in a relatively straightforward manner. Figure 2.3 gives a schematic representation in which the EMD is replaced by other techniques. These can include wavelet decomposition, proper rotation, and empirical orthogonal analysis, among other approaches.

Care must be taken, however, in ensuring that the issues of non-stationarity and non-linearity are addressed in the study of nonlinear phenomena.
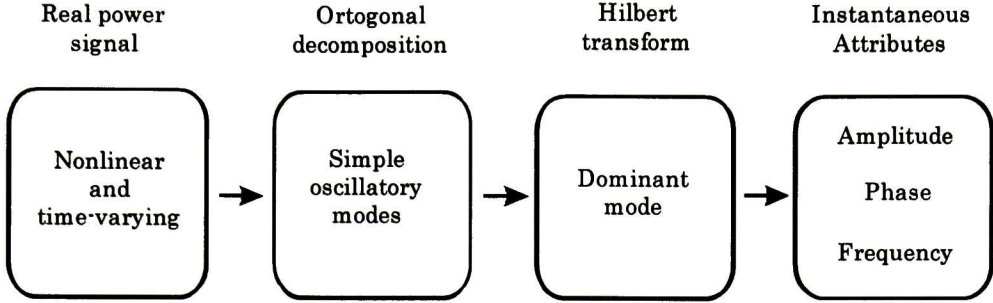
Figure 2.3. Processing of a signal to obtain its instantaneous attributes.

2.5.2 Wavelet projections

An alternative to the EMD is to use a wavelet projection to compute the basis. Once the basis has been computed, Hilbert analysis can be used to determine instantaneous parameters.

In practice, other projections could be used including both projections on continuous and discrete time [12].

Projections in time-frequency: continuous time

Given a real-valued continuous-time signal $x(t)$, consider a series of projection operators P_{R_j} which project $x(t)$ into a time-frequency region R_j. These operators need not be orthogonal but we assume that $\sum_{j=1}^{J_0+1}(P_{R_j}x)(t) = x(t)$ for some J_0. For $j = 1,...,J_0$ define $d_j(t) = (P_{R_j}x)(t)$ and $s_{J_0}(t) = (P_{R_{J_0+1}}x)(t)$. Then

$$x(t) = \sum_{j=1}^{J_0} d_j(t) + s_{J_0}(t) \tag{2.23}$$

Such an additive decomposition of $x(t)$ is achieved by the empirical mode decomposition technique or alternatively, wavelet decomposition.

Discrete time wavelet decomposition

Analogous to decomposition anterior we consider projections of a real-valued signal which attempt to produce monocomponent separation, only here we use discrete-time methods. Assume we have sampled a continuous-time signal at intervals $\Delta t = 1$ to get a vector of observations $\mathbf{X} = [X_0, ..., X_{N-1}]^T$ Assume also we have a series of projection matrices $\mathbf{P}_{R_j}$, which project a vector $\mathbf{X}$ into a particular time-frequency region R_j. These operators need not be orthogonal but we shall assume $\sum_{j=1}^{J_0+1} \mathbf{P}_{R_j} \mathbf{X} = \mathbf{X}$ for same particular J_0. For $j = 1, ..., J_0$ define $\widetilde{D}_j = \mathbf{P}_{R_j} \mathbf{X}$ and $\widetilde{S}_{J_0} = \mathbf{P}_{R_{J_0+1}} \mathbf{X}$. Then

$$\mathbf{X} = \sum_{j=1}^{J_0} \widetilde{D}_j + \widetilde{S}_{J_0} \qquad (2.24)$$

Decomposition (2.24) is the discrete equivalent of (2.23). So we can decompose the sampled signal into a linear combination of the contributions of $\mathbf{X}$ in projected spaces. In the time-frequency plane has been tiled ideally, each projection will contain at most one monocomponent signal for which the concept of instantaneous frequency is well defined.

2.5.3 Time-Varying VARMA models

In this approach, a time-varying vector autoregressive moving average (VARMA) model based method is proposed to calculate the instantaneous frequency of the IMFs obtained from the EMD. By representing the IMFs as a time varying VARMA model and using a Kalman filter to estimate the time varying model parameters [13], the instantaneous frequencies can be calculated according to the time varying parameters; the instantaneous frequencies and the envelopes derived from the cubic spline interpolation of the maxima of IMFs are then used to yield the Hilbert spectrum.

The method can be summarized as follows:

(a). The state-space representation is through a time-varying vector auto-regressive (VARMA) model that consists of two equations: the measurement equation and the transition equation.

(b). The Kalman filter is used to estimate the time-varying parameters of VARMA model; the goal is to minimize the difference between the observation (the measurement equation) and the prediction based on the previous observations (the prediction equations). The instantaneous frequencies are obtained.

(c). The cubic spline interpolation and the instantaneous frequencies derived from VARMA model are then used by to yield an improved Hilbert-Huang transform.

2.6 Other approaches

Several other approaches are being developed that expand on previous results. These approaches are beyond the scope of this research and only summarized as follows: (1) the wavelet transform, (2) the Hilbert transform considering high harmonics, (3) the global Hilbert vibration decomposition (HVD) method, (4) the High-order statistic (HOS), and (5) Wavelet-Hibert Huang transform among other approaches.

2.7 References

[1] N. E. Huang, Z. Sheng, S. R. Long, M. C. Wu, H. H. Shih, Q. Zheng, N. C. Yen, C. C. Tung, and H. H. Liu, "The empirical mode decomposition and the Hilbert spectrum for nonlinear and non-stationary time series analysis," in *Proceedings of the Royal Society of London. A*, vol. 454, pp. 903–995, 1998.

[2] D. Gabor, "Theory of communication," in *Journal of Institute for Electrical Engineering.*, vol. 93, No. 23, pp. 429-457, 1946.

[3] A. R. Messina, M. A. Andrade, J. H. Hernández, and R. Betancourt, "Analysis and characterization of power system nonlinear oscillations using Hilbert Spectral Analysis," in *The Open Electrical and Electronic Engineering Journal*, vol. 1, pp. 1-8, June 2007.

[4] A. R. Messina, V. Vittal, D. Ruiz-Vega, and G. Enríquez-Harper, "Intrepretation and visualitation of wide-area PMU measurements using Hilbert analysis," in *IEEE Transactions on Power Systems*, vol. 21, No. 4, pp. 1763-1771, Nov. 2006.

[5] S. L. Hahn, "Hilbert Transforms in Signal Processing", Ed. The Artech House Signal Processing Library, ISBN 0-89006-886-0, 1st ed., vol.1, Boston, London, 1996.

[6] J. N. E. Huang, and S. S. P. Shen, "Hilbert-Huang Transform and its applications," in *Interdisciplinary Mathematical Science, 1st ed.*, vol. 5, Ed. World Scientific, ISBN 981-256-376-8, pp. 1-26, 2005.

[7] N. E. Huang, Z. Shen, and S. R. Long, "A new view of nonlinear water waves: the Hilbert spectrum," in *Ann. Rev. Fluid Mech.*, vol. 31, pp. 417-457, 1999.

[8] N. Senroy, S. Suryanarayanan, and P. F. Ribeiro, "An Improved Hilbert-Huang Method for Analysis of Time-Varying Waveforms in Power Quality," in *IEEE Transactions on Power Systems*, vol.22, No. 4, pp. 1843-1850, November 2006.

[9] N. Senroy, S. Suryanarayanan, M. Steurer and S. L. Woodruff, "Application of a Time-Frequency Algorithm for Adaptive Estimation of Transfer Function of a Notional High-Temperature Superconducting Motor," in *Electric Ship Technologies Symposium 2007 IEEE*, pp. 238-244, May 2007.

[10] N. Senroy, and S. Suryanarayanan, "Two Techniques to Enhance Empirical Mode Decomposition for Power Quality Applications," in *Power Engineering Society General Meeting 2007 IEEE*, pp. 1-6, June 2007.

[11] S. L. Hahn, "On the uniqueness of the definition of the amplitude and phase of the analytic signal", in *Signal Processing*, vol. 83, pp. 1815-1820, 2003.

[12] S. Olhede, and A. T. Walden, "The Hilbert spectrum via wavelet projections," in *Proceedings of the Royal Society of London. A*, vol. 460, pp. 955–975, 2004.

[13] C. F. Ansley, and R. Kohn, "A note on square root filtering for Vector AutoRegressive Moving-Average models," in *Journal of Time Series Analysis*, vol. 11, No. 3, pp. 181-183, 1990.

Chapter 3
Numerical Computation of the Hilbert Transform

Existing approaches to the numerical calculation of the Hilbert transform are based on the computation of the analytic signal using the Fourier transform and are not well adapted for estimation of instantaneous characteristics of a real signal producing numerical errors in the computing of instantaneous parameters in the initial and end data points.

In this chapter, methods for the calculation of the Hilbert transform are developed.

The present study presents and contrasts three methods for computing the Hilbert transform of arbitrary signals. These are: a time-domain approach, a frequency-domain approach based on Fourier analysis and a convolution-based method.

3.1 Frequency-domain approach (FFT-based method)

The Hilbert transform is usually computed in the frequency-domain through the Fourier transform according to the convolution theorem. From our previous development in Chapter 2, the Hilbert transform can be considered to be the convolution of $h(t) = 1/\pi t$ with $u(t)$ such that

$$v(t) = u(t) * \frac{1}{\pi t}$$

This representation of the Hilbert transform as a convolution leads to an alternative way to compute the Hilbert transform in the frequency domain via Fourier transform.

Assume that $U(f)$ and $V(f)$ are the Fourier transform of $u(t)$ and $v(t)$. Then $U(f)$ and $V(f)$ are defined by [1]

$$U(f) = \int_{-\infty}^{\infty} u(t)e^{-j\omega t}dt \; ; \; \omega = 2\pi f$$

$$V(f) = -j\,\text{sgn}(f)U(f)$$

in which

$$\text{sgn}(\omega) = \{-1,0,-1\} \text{ for } \omega \in \{-\infty,0,\infty\}$$

where f is called Fourier frequency with units 1/units of the independent variable and the signum function is defined by

$$\text{sgn}(f) = \begin{cases} 1 & for \quad f > 0 \\ 0 & for \quad f = 0 \\ -1 & for \quad f < 0 \end{cases}$$

Applying the Fourier transform to the convolution in the equation above, we obtain the Hilbert transform in the frequency domain as

$$V(j\omega) = FT[v(t)] = FT[1/\pi t]U(j\omega) = -j\,\text{sgn}(\omega)U(j\omega) \tag{3.1}$$

where FT denotes the Fourier transform.

Let x_k be a real signal; its HT $\hat{x}_k$ can be computed using the fast Fourier transform (FFT) techniques as

$$\hat{x}_k = FFT^{-1}\left[-j\,\text{sgn}(\omega)FFT[x_k]\right] \tag{3.2}$$

where FFT is the fast Fourier transform, FFT^{-1} is the inverse fast Fourier transform, ω is the nth frequency of the discrete Fourier transform, and sgn is the sign function.

Therefore the Hilbert transform is a $-\pi/2$ phase shifter when observed as a linear system whose input is x_k and output is $\hat{x}_k$.

In the present implementation, the Hilbert transform is computed using the function *hilbert* in Matlab. This function is a 90-degree phase shift operator and it does not change the amplitude of the original signal x_k. Its operation can be described in either as a convolution in the time-domain or frequency-domain.

This transform has a global character and hence is not well suited for characterization of local signal parameters. Further, this approach is subject to the problems that normally attend Fourier analysis, e.g. aliasing, end effects, etc. Thus, for instance, the Gibbs' phenomenon makes the Hilbert-Huang transform analysis inaccurate around the two data ends caused by discontinuity of each IMF during the cubic spline process of local extreme [2].

3.2 Time-domain approach

Consider a real signal $x(t)$. Assume further that the signal $x(t)$ has been sampled every Δt seconds to give the sequence $x_k = x(k\Delta t)$, $k = 1,2,3,...,n$ and that the Hilbert transform signal $\hat{x}(k)$ can be computed.

If the signal $x(t)$ is assumed to vary linearly within the sampling interval [Δt to $n\Delta t$], its Hilbert transform at time Δt can be written as [3]

$$\hat{x}_k = \hat{x}(k\Delta t) = \frac{1}{\pi}\int_{\Delta t}^{n\Delta t}\frac{x(\tau)}{k\Delta t - \tau}d\tau$$

$$= \frac{1}{\pi}(\int_{\Delta t}^{2\Delta t} \frac{x(\tau)}{k\Delta t - \tau} d\tau + \ldots + \int_{(k-2)\Delta t}^{(k-1)\Delta t} \frac{x(\tau)}{k\Delta t - \tau} d\tau + \int_{(k-1)\Delta t}^{k\Delta t} \frac{x(\tau)}{k\Delta t - \tau} d\tau$$

$$+ \int_{k\Delta t}^{(k+1)\Delta t} \frac{x(\tau)}{k\Delta t - \tau} d\tau + \int_{(k+1)\Delta t}^{(k+2)\Delta t} \frac{x(\tau)}{k\Delta t - \tau} d\tau + \ldots + \int_{(n-1)\Delta t}^{n\Delta t} \frac{x(\tau)}{k\Delta t - \tau} d\tau)$$

$$= \frac{1}{\pi}(\sum_{i=1}^{k-2} I_i^{(f)} + I_k^{(c)} + \sum_{i=k+2}^{n} I_i^{(r)}) \tag{3.3}$$

where

$$I_i^{(f)} \equiv \int_{\Delta t}^{(i+1)\Delta t} \frac{x(\tau)}{k\Delta t - \tau} d\tau \tag{3.4}$$

$$I_k^{(c)} \equiv \int_{(k-1)\Delta t}^{k\Delta t} \frac{x(\tau)}{k\Delta t - \tau} d\tau + \int_{k\Delta t}^{(k+1)\Delta t} \frac{x(\tau)}{k\Delta t - \tau} d\tau \tag{3.5}$$

$$I_i^{(r)} \equiv \int_{(i-1)\Delta t}^{i\Delta t} \frac{x(\tau)}{k\Delta t - \tau} d\tau \tag{3.6}$$

When $x(t)$ is linear during the sampling period, that is

$$x(t) = \begin{cases} x_i + (x_{i+1} - x_i)(t - i\Delta t)/\Delta t & for \quad i\Delta t \le t \le (i+1)\Delta t \\ x_i + (x_{i-1} - x_i)(t - i\Delta t)/(-\Delta t) & for \quad (i-1)\Delta t \le t \le i\Delta t \end{cases} \tag{3.7}$$

we obtain

$$I_i^{(f)} = \int_0^{\Delta t} \frac{x_i + (x_{i+1} - x_i)\tau/\Delta t}{(k-i)\Delta t - \tau} d\tau$$

$$= x_i \ln \frac{k-i}{k-i-1} + (x_{i+1} - x_i)(-1 + (k-i)\ln \frac{k-i}{k-i-1}) \tag{3.8}$$

$$I_k^{(c)} = \int_{-\Delta t}^{0} \frac{x_k + (x_k - x_{k-1})\tau/\Delta t}{-\tau} d\tau + \int_0^{\Delta t} \frac{x_k + (x_{k+1} - x_k)\tau/\Delta t}{-\tau} d\tau$$

$$= x_{k-1} - x_{k+1} \tag{3.9}$$

$$I_i^{(r)} = -\int_0^{\Delta t} \frac{x_i + (x_{i-1} - x_i)\tau / \Delta t}{(i-k)\Delta t - \tau} \, d\tau$$

$$= x_i \ln \frac{i-k-1}{i-k} + (x_{i-1} - x_i)(1 + (i-k)\ln \frac{i-k-1}{i-k}) \qquad (3.10)$$

Therefore, the Hilbert transform of x_k is

$$\hat{x}_k = \frac{1}{\pi}(\sum_{i=1}^{k-2} I_i^{(f)} + I_k^{(c)} + \sum_{i=k+2}^{N} I_i^{(r)})$$

$$= \frac{1}{\pi}(\sum_{i=1}^{k-2}(x_i \ln \frac{k-i}{k-i-1} + (x_{i+1} - x_i)(-1 + (k-i)\ln \frac{k-i}{k-i-1}))$$

$$+ (x_{k-1} - x_{k+1})$$

$$+ \sum_{i=k+2}^{N}(x_i \ln \frac{i-k-1}{i-k} + (x_{i-1} - x_i)(1 + (i-k)\ln \frac{i-k-1}{i-k}))) \qquad (3.11)$$

The results given in [4] are

$$I_i^{(f)} = x_i \ln \frac{k-i}{k-i-1} + (x_{i+1} - x_i)(-1 + (k-i)\ln \frac{k-i}{k-i-1}) \qquad (3.12)$$

$$I_k^{(c)} = x_{k-1} - x_{k+1} \qquad (3.13)$$

$$I_i^{(r)} = x_i \ln \frac{i-k}{i-k-1} + (x_{i-1} - x_i)(-1 + (i-k)\ln \frac{i-k}{i-k-1}) \qquad (3.14)$$

We observe that $I_i^{(f)}$ and (3.8), $I_k^{(c)}$ and (3.9) are exactly the same, but $I_i^{(r)}$ is different from (3.10). This equation does influence the result of the Hilbert transform of a signal.

3.3 Convolution-based method

In this method we consider complex sequences for which the real and imaginary components of analytic signal can be related through a convolution. These Hilbert transform relations are particularly useful in representing bandpass signals as complex signals.

This method has not been used in power signals applications.

Causal sequences

Any sequences can be expressed as the sum of an even sequence and an odd sequence. Specifically, with $x_e(n)$ and $x_o(n)$ denoting the even and odd parts of $x(n)$, then

$$x(n) = x_e(n) + x_o(n) \tag{3.15}$$

where

$$x_e(n) = \frac{1}{2}[x(n) + x(-n)] \tag{3.16}$$

and

$$x_o(n) = \frac{1}{2}[x(n) - x(-n)] \tag{3.17}$$

Equations (3.15)-(3.17) apply to an arbitrary sequence whether or not it is causal or whether or not it is real. However, if $x(n)$ is causal, then it is possible to recover $x(n)$ from $x_e(n)$ and to recover $x(n)$ for $n \neq 0$ from $x_o(n)$.

Hilbert transform relations for complex sequences

As the Fourier transform of a complex sequence cannot be zero for $\omega < 0$ since it is periodic, the requirement must be changed for being zero in the second half of each period. Thus, being $x(n)$ a sequence whose Fourier transform is $X(e^{j\omega})$, it is required that

$$X(e^{j\omega}) = 0, \qquad -\pi \leq \omega < 0 \tag{3.18}$$

If the time series $x(n)$ is complex, we can express it as

$$x(n) = x_r(n) + jx_i(n) \tag{3.19}$$

where $x_r(n)$ and $x_i(n)$ are real sequences.

With $X_r(e^{j\omega})$ and $X_i(e^{j\omega})$ denoting the Fourier transforms of the real sequences $x_r(n)$ and $x_i(n)$, respectively, we obtain

$$X(e^{j\omega}) = X_r(e^{j\omega}) + jX_i(e^{j\omega}) \tag{3.20}$$

in which is easily shown that

$$X_r(e^{j\omega}) = \frac{1}{2}\left[X(e^{j\omega}) + X^*(e^{-j\omega})\right] \tag{3.21}$$

and

$$jX_i(e^{j\omega}) = \frac{1}{2}\left[X(e^{j\omega}) - X^*(e^{-j\omega})\right] \tag{3.22}$$

If $X(e^{j\omega})$ is zero for $-\pi \le \omega < 0$, there is no overlap between the nonzero portions of $X(e^{j\omega})$ and $X^*(e^{j\omega})$. Thus $X(e^{j\omega})$ can be recovered from either $X_r(e^{j\omega})$ or $X_i(e^{j\omega})$ as

$$X(e^{j\omega}) = \begin{cases} 2X_r(e^{j\omega}), & 0 \le \omega < \pi, \\ 0, & -\pi \le \omega < 0. \end{cases} \tag{3.23}$$

and

$$X(e^{j\omega}) = \begin{cases} 2jX_i(e^{j\omega}), & 0 \le \omega < \pi, \\ 0, & -\pi \le \omega < 0. \end{cases} \tag{3.24}$$

From (3.23) and (3.24) it is possible to relate $X_r(e^{j\omega})$ and $X_i(e^{j\omega})$, directly by

$$X_i(e^{j\omega}) = \begin{cases} -jX_r(e^{j\omega}), & 0 \le \omega < \pi, \\ jX_r(e^{j\omega}), & -\pi \le \omega < 0, \end{cases} \tag{3.25}$$

or

$$X_i(e^{j\omega}) = H(e^{j\omega})X_r(e^{j\omega}) \qquad (3.26)$$

where

$$H(e^{j\omega}) = \begin{cases} -j, & 0 \le \omega < \pi, \\ j, & -\pi \le \omega < 0. \end{cases} \qquad (3.27)$$

According to (3.25) and (3.26), $x_i(n)$ can be obtained by processing $x_r(n)$ with a linear time-invariant discrete-time system with frequency response $H(e^{j\omega})$ as is given by (3.27). Such system is called an ideal 90-degree phase shifter or a Hilbert transformer, whose frequency response has unity magnitude and a phase angle of $-\pi/2$ for $0 < \omega < \pi$, and a phase angle of $+\pi/2$ for $-\pi < \omega < 0$.

From (3.26) it follows that

$$X_r(e^{j\omega}) = \frac{1}{H(e^{j\omega})}X_i(e^{j\omega}) \qquad (3.28)$$

Thus $-x_r(n)$ can also be obtained from $x_i(n)$ with a 90-degree phase shifter.

In other words, the Hilbert transformer is an all-pass filter called quadrate filter, than produce a displacement ± 90-degree phase shifter in the input signal. For negative frequency is +90-degree and for positive frequency is -90-degree. The input and output signals of the Hilbert filter are named a pair of quadrate signals. The Hilbert filter can be analog or digital.

The transfer function of an ideal nonrealizable analog Hilbert transformer is

$$H(jf) = F[1/\pi t] = |H(jf)|e^{j\varphi(f)} = -j\,\mathrm{sgn}(f) \qquad (3.29)$$

Therefore, the transfer function is given by

$$H(jf) = \begin{cases} -j & for \quad f > 0 \\ 0 & for \quad f = 0 \\ j & for \quad f < 0 \end{cases} \qquad (3.30)$$

The magnitude $|H(jf)| = 1$, $\forall f$ and the phase function is

$$\varphi(f) = \arg[H(jf)] = -(\pi/2)\,\mathrm{sgn}(f) \qquad (3.31)$$

The Hilbert transformer

The estimate Hilbert transformer of an analytic signal will be obtained by performing a filtering operation on the analytic signal itself. The integral of Cauchy given by equation (2.6) can be rewritten in the form of a convolution as

$$x_i(n) = \sum_{l=-L}^{L} x_r(n-l)h(l) \qquad (3.32)$$

where (3.32) is the desired Hilbert transform of the imaginary part of a discrete-time analytic signal. L indicate the order of the filter and its maximum order is given by

$$L = Nimf - 1 \qquad (3.33)$$

where *Nimf* indicates the total number of IMFs, including the residue $r(t)$. The filtering process eliminates the residue to avoid the mistake in the initial and end data points of recording.

The filter with the desired features which has the impulse response $h(n)$ of a 90-degree phase shifter, corresponding to a frequency response given by (3.25) is given by Oppenheimer and Schafer [5] as

$$h(n) = \frac{1}{2\pi}\int_{-\pi}^{0} je^{j\omega n}d\omega - \frac{1}{2\pi}\int_{0}^{\pi} je^{j\omega n}d\omega \qquad (3.34)$$

or

$$h(n) = \begin{cases} \dfrac{2}{\pi}\dfrac{\sin^2(\pi n/2)}{n} & n \neq 0 \\ 0 & n = 0 \end{cases} \qquad (3.35)$$

In this study $L=1$ in (3.32) provided an adequate amplitude response and perfect 90-degree phase response. Future research for decomposition of signals should compare the above filter to other filters.

Other promising approaches are the use of Chebyshev filters.

Figure 3.1 show how a discrete-time Hilbert transformer system can be used to form a complex analytic signal, which is simply a pair of real signals.
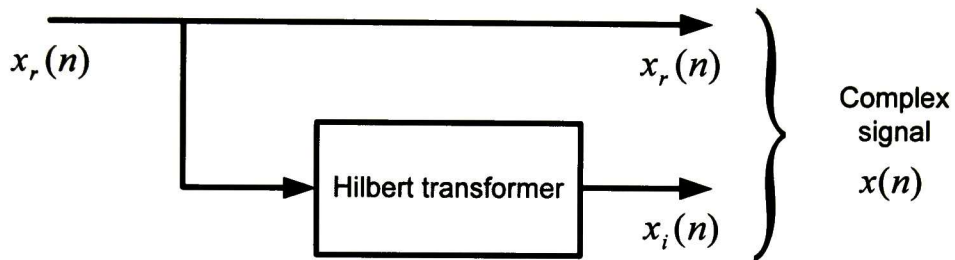
Figure 3.1. Block diagram representation of the creation of a complex sequence whose Fourier transform is one-sided.

In practice, one can implement the Hilbert transform by using a finite impulse response approximation to $h(n)$. Such FIR filter designs can be obtained either via the window method or the equiripple method.

3.4 Summary

Three different methods for computation of the Hilbert transform have been presented and discussed. The approaches to the numerical calculation of the Hilbert transform are based on the computation of the analytic signal in nonlinear and non-stationary power system signals and the comparison is made on the instantaneous frequency of an oscillatory signal.

The convolution method and the time-domain approach algorithm identify the instantaneous attributes from a similar manner and the frequency-domain approach algorithm differs from the others two methods.

As demonstrated in this study, convolution method is the most feasible way to obtain reliable dynamic behaviour of the system, whose nonlinear and non-stationary oscillations over all the study period, require precise and accurate analysis to determine the instantaneous characteristics, mainly in the estimation of the instantaneous frequency. In this approach, filtering operation on the analytic signal eliminates noise and fluctuations in the initial and end data points and allows us to obtain a more accurate estimate of the instantaneous frequency during the analysis of the dynamics of the system under study.

3.5 References.

[1] J. A. Inaudi, and J. M. Kelly, "Linear hysteretic damping and the Hilbert transform," in *Journal of Engineering Mechanics*, vol. 121, pp. 626–632, May 1995.

[2] P. F. Pai, "Nonlinear vibration characterization by signal decomposition," in *Journal of Sound and Vibration*, vol. 307, pp. 527-544, June 2007.

[3] X. Wang, M. Sc. Thesis, "Numerical implementation of the Hilbert transform," University of Saskatchewan, 2006.

[4] M. Johansson, M. Sc. Thesis, "The Hilbert transform," VaxJo University, 1999.

[5] A. V. Oppenheim, and R. W. Schafer, "Digital Signal Processing," Ed. Prentice Hall, ISBN 0-13-214635-5, 1975.

Chapter 4
Free Vibration Analysis using the Hilbert Transform

An accurate model of transient processes must capture dominant temporal features of the observed system dynamics such as abrupt changes in modal content and to relate these features to specific aspects of interest. This chapter discusses the development of time-frequency representations of system behavior based on Hilbert analysis.

Methods for investigating the free response of time-varying linear systems are developed. Classical vibration theory is combined with Hilbert analysis to construct a multi-degree-of-freedom time-varying system identification framework that is utilized to extract modal properties. Use of these two approaches makes it possible to study spatio-temporal behavior in an efficient manner. The method is constructive for dynamic analysis of measure data and can be used to study quasi-stationary oscillations.

A systematic method for studying free oscillations of a class of system models, based on Hilbert analysis, is first introduced. Then, the FREEVIB approach for estimating nonlinear modal characteristics is discussed. The model serves as a foundation for more efficient algorithms for modal estimation en Chapter 5.

Explicit approximate expressions for instantaneous parameters are obtained. Techniques for extracting instantaneous parameters, estimating the modeling errors, and minimizing numerical issues are all examined. Finally, issues concerning the implementation of the algorithms and numerical calculations are briefly discussed. A numerical example is used to illustrate the practical application of the proposed algorithm.

4.1 Extraction of modal information from time-varying linear models

4.1.1 Description of dynamic Model

Linear, time-varying systems are frequently used to model systems that have non-stationary properties and undergo low magnitude vibrations. These models capture the instantaneous dynamical behavior of the system, and could be used to assess the temporal condition of the system or to diagnose modal properties.

To interpret the physical meaning of the proposed technique let us consider the analysis of modal properties of a MDOF system by using output-only response information. The equations of motion describing the natural vibration of a viscously damped linear, time-varying multiple degree-of-freedom (*MDOF*) system can be written as [1]

$$\left[\mathbf{M}(t_0)...\mathbf{M}(t_n)\right]\frac{d^2}{dt^2}\begin{bmatrix}\mathbf{x}_1(t)\\ \vdots\\ \mathbf{x}_n(t)\end{bmatrix}+\left[\mathbf{C}(t_0)...\mathbf{C}(t_n)\right]\frac{d}{dt}\begin{bmatrix}\mathbf{x}_1(t)\\ \vdots\\ \mathbf{x}_n(t)\end{bmatrix}+\left[\mathbf{K}(t_0)...\mathbf{K}(t_n)\right]\begin{bmatrix}\mathbf{x}_1(t)\\ \vdots\\ \mathbf{x}_n(t)\end{bmatrix}=0 \quad (4.1)$$

In equation (4.1), $\mathbf{x}(t) = \left[\mathbf{x}_1(t)...\mathbf{x}_n(t)\right]^T$ is an $(n \times 1)$ displacement vector, and $\mathbf{M}(t)$, $\mathbf{C}(t)$ and $\mathbf{K}(t)$ are the time-varying diagonal mass, damping and stiffness matrices of dimension $(n \times n)$, respectively.

The system is called a slowly-variant-system if $\mathbf{M}(t)$, $\mathbf{C}(t)$ and $\mathbf{K}(t)$ are all slow variables of t compared with $\mathbf{x}(t)$ $\dot{\mathbf{x}}(t)$, and $\ddot{\mathbf{x}}(t)$ [2]. The validity of this assumption is studied further in Chapters 5 and 6.

If the system response $\mathbf{x}(t)$ is known, then the modal properties of the MDOF system can be determined. It follows from arguments given in Chapter 2 that the system output $\mathbf{x}(t)$ can be decomposed into a series of time-varying modes. More precisely, let the motion of the system be described by an n-dimensional column vector $x(t) = \left[x_1(t) \quad x_2(t) \quad \cdots \quad x_n(t)\right]^T$ with components

$$x_i(t) = \sum_{j=1}^{n} x_{ij}(t) = \sum_{j=1}^{n} A_{ij}(t)\cos(\varphi_{ij}(t)), \quad (j=1,2,...n) \quad (4.2)$$

in which $A_{ij}(t)\cos(\varphi_{ij}(t))$ is the time-dependent coefficient extracted for the ith element of the displacement vector. The corresponding complex form of the signal is

$$z(t) = x_i(t) + H[x_i(t)] = A_{ij}(t)\exp(i\varphi_{ij}(t)) \tag{4.3}$$

where $z(t)$ is the analytic signal, and $H[x_i(t)]$ is the Hilbert transform of $x_i(t)$. We remark that this representation includes both, amplitude and frequency modulation.

In practice, equation (4.2) could be obtained from empirical mode decomposition of measured or simulated data. A general approach to determining the modal coefficients is to use Hilbert analysis to estimate modal quantities from knowledge of the solution $x(t)$. The proposed approach involves viewing instantaneous parameters as a measure of the best fit harmonic at each point of the complex signal.

According to Bedrosian's theorem [3] the Hilbert transform of the product of two signals $f(t)$ and $g(t)$ can be defined as

$$H[f(t)g(t)] = f(t)H[g(t)] \tag{4.4}$$

if the Fourier spectra of $f(t)$ and $g(t)$ are non-overlapping in frequency space and $g(t)$ has a higher frequency content than $f(t)$[1], or both $f(t)$ and $g(t)$ are analytic.

Making use of this property in (4.2), one obtains

$$H[\mathbf{M}(t)\mathbf{x}(t)] = \mathbf{M}(t)H[\mathbf{x}(t)]$$

$$H[\mathbf{C}(t)\mathbf{x}(t)] = \mathbf{C}(t)H[\mathbf{x}(t)]$$

$$H[\mathbf{K}(t)\mathbf{x}(t)] = \mathbf{K}(t)H[\mathbf{x}(t)]$$

---

[1] We can consider, equivalently, that $f(t)$ is a high-pass signal and $g(t)$ is a low-pass signal

or, equivalently

$$H[\mathbf{M}(t)\mathbf{x}(t)] = \mathbf{M}(t)\tilde{\mathbf{x}}(t) \qquad (4.5a)$$

$$H[\mathbf{C}(t)\mathbf{x}(t)] = \mathbf{C}(t)\tilde{\mathbf{x}}(t) \qquad (4.5b)$$

$$H[\mathbf{K}(t)\mathbf{x}(t)] = \mathbf{K}(t)\tilde{\mathbf{x}}(t) \qquad (4.5c)$$

Equation (4.5) implies that the coefficients, $\mathbf{M}(t)$, $\mathbf{C}(t)$ and $\mathbf{K}(t)$, do not vary quickly over time. i.e, equation (4.3) is not suitable for the analysis of abrupt changes in system behavior. This is confirmed in our numerical application of the method in Chapter 5.

Applying the Hilbert transform to (4.1), one obtains

$$\mathbf{M}(t)\ddot{\tilde{\mathbf{x}}}(t) + \mathbf{C}(t)\dot{\tilde{\mathbf{x}}}(t) + \mathbf{K}(t)\tilde{\mathbf{x}}(t) = 0 \qquad (4.6)$$

Multiplying each term of equation (4.6) by j and adding it to the corresponding term of equation (4.1), a differential equation on the analytic signal is obtained as

$$\mathbf{M}(t)\ddot{\mathbf{X}}(t) + \mathbf{C}(t)\dot{\mathbf{X}}(t) + \mathbf{K}(t)\mathbf{X}(t) = 0 \qquad (4.7)$$

in which $\mathbf{X}(t) = [X_1(t), X_2(t), \ldots, X_n(t)]^T$ is the analytic signal of the displacement vector, and the ith element (which corresponds to the ith DOF) of the analytic signal.. A mono-mode analytical function corresponding to each component can be constructed using the Hilbert transform as

$$X_i(t) = \sum_{j=1}^{n} X_{ij}(t) = \sum_{j=1}^{n} A_{ij}(t) e^{j\varphi_{ij}(t)} \qquad (4.8a)$$

in which

$$x_{ij}(t) = A_{ij}(t)\cos\varphi_{ij}(t) \qquad (4.8b)$$

$$A_{ij}(t) = \sqrt{x_{ij}^2(t) + \tilde{x}_{ij}^2(t)} \qquad (4.8c)$$

$$\varphi_{ij}(t) = \arctan\left[\frac{\tilde{x}_{ij}(t)}{x_{ij}(t)}\right] \tag{4.8d}$$

$$\omega_{ij}(t) = \dot{\varphi}_{ij}(t) = \frac{x_{ij}(t)\dot{\tilde{x}}_{ij}(t) - \dot{x}_{ij}(t)\tilde{x}_{ij}(t)}{A_{ij}^2(t)} \tag{4.8e}$$

and

$$\dot{A}_{ij}(t) = \frac{x_{ij}(t)\dot{x}_{ij}(t) + \tilde{x}_{ij}(t)\dot{\tilde{x}}_{ij}(t)}{A_{ij}(t)} \tag{4.8f}$$

Using the analytic signal from equations (4.8a)-(4.8f), we have

$$\dot{X}_{ij}(t) = X_{ij}(t)\left[\frac{\dot{A}_{ij}(t)}{A_{ij}(t)} + j\omega_{ij}(t)\right] \tag{4.9}$$

$$\ddot{X}_{ij}(t) = X_{ij}(t)\left[\frac{\ddot{A}_{ij}(t)}{A_{ij}(t)} - \omega_{ij}^2(t) + j\left(2\frac{\dot{A}_{ij}(t)\omega_{ij}(t)}{A_{ij}(t)} + \dot{\omega}_{ij}(t)\right)\right] \tag{4.10}$$

where

$$\omega_{ij}(t) = \dot{\varphi}_{ij}(t) = \frac{x_{ij}(t)\dot{\tilde{x}}_{ij}(t) - \dot{x}_{ij}(t)\tilde{x}_{ij}(t)}{A_{ij}^2(t)} = \mathrm{Im}\left[\frac{\dot{X}_{ij}(t)}{X_{ij}(t)}\right] \tag{4.11a}$$

$$\dot{A}_{ij}(t) = \frac{x_{ij}(t)\dot{x}_{ij}(t) + \tilde{x}_{ij}(t)\dot{\tilde{x}}_{ij}(t)}{A_{ij}(t)} = A_{ij}(t)\mathrm{Re}\left[\frac{\dot{X}_{ij}(t)}{X_{ij}(t)}\right] \tag{4.11b}$$

$$\dot{\omega}_{ij}(t) = \mathrm{Im}\left[\frac{\ddot{X}_{ij}(t)}{X_{ij}(t)}\right] - 2\frac{\dot{A}_{ij}(t)\omega_{ij}(t)}{A_{ij}(t)} \tag{4.11c}$$

$$\ddot{A}_{ij}(t) = A_{ij}(t)\left(\mathrm{Re}\left[\frac{\ddot{X}_{ij}(t)}{X_{ij}(t)}\right] + \omega_{ij}^2(t)\right) \tag{4.11d}$$

The free vibration of the linear time-varying MDOF system in equation (4.7) can be solved by substituting $\ddot{X}(t)$ and $\dot{X}(t)$ of equations (4.9) and (4.10), and using equations (4.8) and (4.11). Assuming the mass matrix to be known,

equation (4.7) can be simplified and written in compact matrix notation for the j th IMF of the analytic signal.

$$\mathbf{P}_j^c \boldsymbol{\beta}_j^c + \mathbf{P}_j^k \boldsymbol{\beta}_j^k = \mathbf{P}_j^m \tag{4.12}$$

in which $\boldsymbol{\beta}_j^c = \{c_1 c_2 \cdots c_i \cdots c_n\}^T$ $\boldsymbol{\beta}_j^k = \{k_1 k_2 \cdots k_i \cdots k_n\}^T$ and the diagonal matrix are given by

$$\mathbf{P}_j^c = \begin{bmatrix} h_{1j}^c X_{1j} & h_{1j}^c X_{1j} - h_{2j}^c X_{2j} & & & \\ & h_{2j}^c X_{2j} - h_{1j}^c X_{1j} & h_{2j}^c X_{2j} - h_{3j}^c X_{3j} & & \\ & & \cdots & \cdots & \\ & & & h_{ij}^c X_{ij} - h_{i-1j}^c X_{i-1j} & h_{ij}^c X_{ij} - h_{i+1j}^c X_{i+1j} & \\ & & & & \cdots & \cdots \\ & & & & & h_{nj}^c X_{nj} - h_{n-1j}^c X_{n-1j} \end{bmatrix} \tag{4.13}$$

$$\mathbf{P}_j^k = \begin{bmatrix} X_{1j} & X_{1j} - X_{2j} & & & \\ & X_{2j} - X_{1j} & X_{2j} - X_{3j} & & \\ & & \cdots & \cdots & \\ & & & X_{ij} - X_{i-1j} & X_{ij} - X_{i+1j} & \\ & & & & \cdots & \cdots \\ & & & & & X_{nj} - X_{n-1j} \end{bmatrix} \tag{4.14}$$

$$\mathbf{P}_j^m = \left\{ -m_1 h_{1j}^m X_{1j} \quad -m_2 h_{2j}^m X_{2j} \quad \cdots \quad -m_i h_{ij}^m X_{ij} \quad \cdots \quad -m_n h_{nj}^m X_{nj} \right\}^T \tag{4.15}$$

The coefficients h_{ij}^c and h_{ij}^m in equations (4.13) and (4.15) are given as follows:

$$h_{ij}^c = \frac{\dot{A}_{ij}(t)}{A_{ij}(t)} + j\omega_{ij}(t) \tag{4.16}$$

$$h_{ij}^m = \left[\frac{\ddot{A}_{ij}(t)}{A_{ij}(t)} - \omega_{ij}^2(t) \right] + j \left[2\frac{\dot{A}_{ij}(t)\omega_{ij}(t)}{A_{ij}(t)} + \dot{\omega}_{ij}(t) \right] \tag{4.17}$$

The complex equation (4.12) can be separated into two equations according to the real and imaginary parts, and then the two parts can be assembled in the following matrix representation

$$\begin{bmatrix} \mathrm{Re}(\mathbf{P}_i^c) & \mathrm{Re}(\mathbf{P}_i^k) \\ \mathrm{Im}(\mathbf{P}_i^c) & \mathrm{Im}(\mathbf{P}_i^k) \end{bmatrix} \begin{Bmatrix} \beta_i^c \\ \beta_i^k \end{Bmatrix} = \begin{Bmatrix} \mathrm{Re}(\mathbf{P}_i^m) \\ \mathrm{Im}(\mathbf{P}_i^m) \end{Bmatrix} \tag{4.18}$$

Determination of modal parameters involves finding n independent solutions for the above equation.

For an n-DOF linear time-varying system, equation (4.18) contains $2n$ time-varying unknown parameters and $2n$ time-varying equations for each IMF of the original signal. Therefore, each mode extracted from the original signal can be used in equation (4.18) to solve for one set of identification results. This is an important advantage of the proposed method in practical system identification as only one set of IMFs is required for solving all the time-varying unknown system parameters.

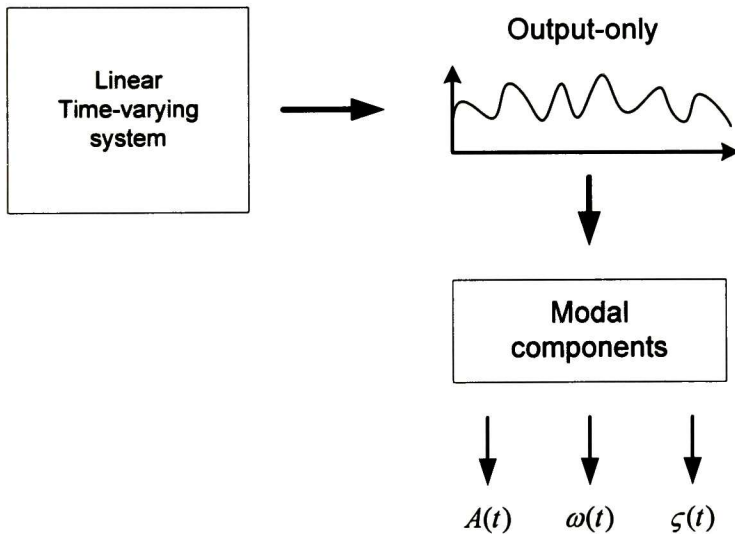Figure 4.1 gives a pictorial representation of the output-only modal identification algorithm.

Figure 4.1. Modal identification algorithm.

For a SDOF system, the identified results from equation (4.18) can be simplified as [4]

$$c(t) = -m\left(2\frac{\dot{A}(t)}{A(t)} + \frac{\dot{\omega}(t)}{\omega(t)}\right) \qquad (4.19)$$

where $c(t)$ is the instantaneous damping function, and the instantaneous stiffness is given by

$$k(t) = m\omega_0^2(t) \qquad (4.20)$$

where $\omega_0(t)$ is the instantaneous undamped natural frequency of the system. If follows immediately that,

$$\omega_0^2(t) = \frac{k(t)}{m} = \omega^2(t) - \frac{\ddot{A}(t)}{A(t)} + 2\frac{\dot{A}^2(t)}{A^2(t)} + \frac{\dot{A}(t)\dot{\omega}(t)}{A(t)\omega(t)} \qquad (4.21a)$$

$$\omega(t) = \dot{\varphi}(t) = \frac{x(t)\dot{\tilde{x}}(t) - \dot{x}(t)\tilde{x}(t)}{A^2(t)} = \text{Im}\left[\frac{\dot{X}(t)}{X(t)}\right] \qquad (4.21b)$$

$$\dot{A}(t) = \frac{x(t)\dot{x}(t) + \tilde{x}(t)\dot{\tilde{x}}(t)}{A(t)} = A(t)\,\text{Re}\left[\frac{\dot{X}(t)}{X(t)}\right] \qquad (4.21c)$$

$$\dot{\omega}(t) = \text{Im}\left[\frac{\ddot{X}(t)}{X(t)}\right] - 2\frac{\dot{A}(t)\omega(t)}{A(t)} \qquad (4.21d)$$

$$\ddot{A}(t) = A(t)\left(\text{Re}\left[\frac{\ddot{X}(t)}{X(t)}\right] + \omega^2(t)\right) \qquad (4.21e)$$

where $A(t)$ and $\omega(t)$ are the instantaneous amplitude (or envelope) and frequency respectively of the vibration with their first and second derivatives $\dot{A}(t)$, $\ddot{A}(t)$ and $\dot{\omega}(t)$. Both, $A(t)$ and $\omega(t)$ are calculated as functions of time and can therefore be related to all temporal events during the measurement.

The processing steps are detailed in the sections that follow.

4.1.2 Damped system response

In the more general and interesting case, the ith modal response can be expressed as

$$x(t) = \sum_{i=1}^{n} IMF_i(t) = \left[\sum_{i=1}^{n} A_i(t) e^{-(2\pi\varsigma_i f_i t)} \cos(2\pi f_{di} + \phi_i) \right] \qquad (4.22)$$

where $A_i(t)$ is the amplitude of the ith mode, $\phi_i(t)$ is the phase lag, $f_i(t)$ is the undamped natural frequency, $f_{di}(t) = f_i \sqrt{1 - \varsigma_i^2}$ is the damped natural frequency, and ς_i is the damping ratio.

$$X(t) = \begin{bmatrix} x_1 + jy_1 \\ x_2 + jy_2 \\ \vdots \\ x_n + jy_n \end{bmatrix} = \begin{bmatrix} A_1 e^{-2\pi\varsigma_1 f_1 t} e^{j(2\pi f_{d1} t + \phi_1)} \\ A_2 e^{-2\pi\varsigma_2 f_2 t} e^{j(2\pi f_{d2} t + \phi_2)} \\ \vdots \\ A_n e^{-2\pi\varsigma_n f_n t} e^{j(2\pi f_{dn} t + \phi_n)} \end{bmatrix} \qquad (4.23)$$

The original data can then be expressed as the real part of the sum of all of the IMF components, that is,

$$x(t) = \Re \left[\sum_{i=1}^{n} H_i(t) e^{(2\pi\varsigma \int f_i(t) dt \; f_i t)} \right] \qquad (4.24)$$

Several variations to the above model are available in the literature. For its importance and relation to this work, the FREEVIB method introduced by Feldman will be discussed in detail.

4.2 The FREEVIB method

In this section, the FREEVIB method is applied to a SDOF oscillator and compared with the standard approach based on log-decrement. First, the model form of a linear damped multiple-degree-of-freedom system is presented. Then, the results are shown and compared with experimental data. The reader is referred to [4] for a detailed account of the FREEVIB methodology.

4.2.1 Description of dynamic model

In the previous section we saw that the knowledge of the output of a linear MDOF system allowed us to deduce the time-varying modal properties of the process. Here we extend this approach to deal with nonlinear systems.

Following the work of Worden and Tomlinson, consider a second degree-of-freedom (SDOF) nonlinear system under free vibration

$$\ddot{x} + h(x)\dot{x} + \omega_0^2(x)x = 0 \qquad (4.25)$$

where $\ddot{x}, \dot{x}$, and $x(t)$ are the acceleration, velocity and displacement, respectively, of the oscilator, $\omega_0(t)$ is the undamped natural frequency and $h_0(t)$ is the effective viscous damping characteristic. It is assumed that they are all slow variables of t compared with the response signal $x(t)$.

Using the definition of analytical signal yields

$$X(t) = x(t) - \tilde{x}(t) = A(t)e^{i\varphi(t)} \qquad (4.26)$$

in which

$$x(t) = A(t)\cos(\varphi(t)) \quad \text{and} \quad \tilde{x}(t) = -iA(t)\sin(\varphi(t)) \qquad (4.27)$$

where $A(t)$ is the instantaneous magnitude or envelope and $\varphi(t)$ is the instantaneous phase [4]. Thus,

$$A(t) = \sqrt{x^2(t) - \tilde{x}^2(t)} \qquad (4.28)$$

$$\varphi(t) = \arctan\left(\frac{-\tilde{x}(t)}{ix(t)}\right) \qquad (4.29)$$

and

$$\dot{A}(t) = \frac{x(t)\dot{x}(t) - \tilde{x}(t)\dot{\tilde{x}}(t)}{\sqrt{x^2(t) - \tilde{x}^2(t)}} = A(t)\,\text{Re}\left[\frac{\dot{X}(t)}{X(t)}\right] \qquad (4.30)$$

$$\omega(t) = \dot{\varphi}(t) = \frac{i\left(x(t)\dot{\tilde{x}}(t) - \dot{x}(t)\tilde{x}(t)\right)}{x^2(t) - \tilde{x}^2(t)} = \text{Im}\left[\frac{\dot{X}(t)}{X(t)}\right] \qquad (4.31)$$

where $\omega(t)$ is the instantaneous frequency.

Equations (4.25) and (4.26) are employed to generate the first and two derivatives of the analytic signal

$$\dot{X}(t) = X(t)\left[\frac{\dot{A}(t)}{A(t)} + i\omega(t)\right] \tag{4.31}$$

$$\ddot{X}(t) = X(t)\left[\frac{\ddot{A}(t)}{A(t)} - \omega(t)^2 + 2i\frac{\dot{A}(t)\omega(t)}{A(t)} + i\dot{\omega}(t)\right] \tag{4.32}$$

where the derivatives $\dot{X}(t)$ and $\ddot{X}(t)$ are functions of A and ω.

Coming back to the equation (4.25) and recalling the properties of the Hilbert transform, we have

$$H[\dot{x}] = \dot{\tilde{x}} \quad \text{and} \quad H[\ddot{x}] = \ddot{\tilde{x}}$$

Using equation (4.4) yields

$$H[\varsigma(t)\omega_0(t)\dot{x}(t)] = \varsigma(t)\omega_0(t)H[\dot{x}(t)] = \varsigma(t)\omega_0(t)\dot{\tilde{x}}(t) \tag{4.33}$$

$$H[\omega_0^2(t)x(t)] = \omega_0^2(t)H[x(t)] = \omega_0^2(t)\tilde{x}(t) \tag{4.34}$$

where in (4.23) the low-pass portion consist of two variables: $\varsigma(t)$ and $\omega_0(t)$.

Now, taking the Hilbert transform of (4.25), then multiplying each side of the obtained new equation by i and adding to the corresponding sides of (4.25) we can get a differential equation for the analytic signal of $x(t)$

$$\ddot{X} + h(t)\dot{X} + \omega_0^2(t)X = 0$$

or in quasi-linear form

$$\ddot{X} + h(A)\dot{X} + \omega_0^2(A)X = 0 \tag{4.35}$$

Substitution of (4.21) and (4.24) into (4.25), results in

$$X\left[\frac{\ddot{A}}{A} - \omega^2 + \omega_0^2 + h\frac{\dot{A}}{A} + i\left(2\omega\frac{\dot{A}}{A} + \dot{\omega} + \omega\right)\right] = 0. \tag{4.36}$$

Separating out real and imaginary parts of equation (4.36), one may obtain the expressions for the instantaneous undamped natural frequency and the instantaneous damping characteristic

$$h(t) = -2\frac{\dot{A}}{A} - \frac{\dot{\omega}}{\omega} \qquad (4.37)$$

$$\omega_0^2(t) = \omega^2 - \frac{\ddot{A}}{A} + 2\frac{\dot{A}^2}{A^2} + \frac{\dot{A}\dot{\omega}}{A\omega} \qquad (4.38)$$

The corresponding effective damping ratio can then be easily found as

$$\varsigma(t) = h_o(t) / \omega_o(t) \qquad (4.39)$$

In most practical applications, one starts with a measurement of the system response $x(t)$. Application is then straightforward; the Hilbert transform can then be computed using the various approaches in Chapter 3; the instantaneous modal parameters are determined using (4.27) and (4.30).

Also, nonlinear effects can be accounted for as discussed in Chapter 5.

4.3 References.

[1] Z. Y. Shi, and S. S. Law, "Identification of Linear Time-Varying Dynamical Systems Using Hilbert Transform and Empirical Mode decomposition method," in *Journal of Applied Mechanics*," vol. 74, pp. 223-230, 2007.

[2] W. Lili, Z. Jinghui, and H. Shiyue, "The Accompanied Slowly-Variant-System of Nonlinear Dynamic Systems," in *The Chinese Society of Theoretical and Applied Mechanics, Acta Mechanica Sinica (English Series)*, vol. 15, pp. 73-81, 1999.

[3] S. L. Hahn, "Hilbert Transforms in Signal Processing", Ed. The Artech House Signal Processing Library, ISBN 0-89006-886-0, 1st ed., vol.1, Boston, London, 1996.

[4] M. Feldman, "Non-linear System Vibration Analysis Using Hilbert Transform I: Free Vibration Analysis Method -FREEVIB-," in *Mechanical Systems and Signal Processing*, vol. 8, pp. 119-127, 1994.

Chapter 5
Modal Identification via Hilbert Analysis

Power systems contain nonlinear temporal evolution and time-varying processes that it is very difficult to identify with the conventional techniques. In most practical modeling situations, many transient oscillations may manifest highly complex phenomena and its analysis presents modal interaction that is particularly difficult to characterize because of the large number of potential modes involved in the interaction and the time scales in which they interact.

Inspired by models developed with the framework of vibration analysis, we describe the behavior of the system assuming that the observed power signal can be approximated by family of simple oscillatory functions with time-varying parameters. With this characterization, an approach based on the FREEVIB method and a modified Hilbert analysis is proposed for estimating modal parameters from measured data. This approach improves the ability of the HHT to capture abrupt changes in the observed data. It is shown that in addition to providing estimates of time dependent mode shapes, the analysis also provides a method to identify the modes with the most energy embedded in the analyzed oscillations.

Analytical criteria to describe the energy relationships in the observed oscillations are derived and a physical interpretation of the system modes is suggested. A simple example illustrates the main idea of the proposed method.

5.1 Identification of linear time-varying dynamical systems

5.1.1 Modal parameter identification

Our previous developments suggest that each IMF is nearly orthogonal to each other and that each IMF can be considered to be a harmonic oscillator of variable amplitude and frequency [1]. Based on this notion, an efficient technique to extract temporal modal behavior from the EMD of a signal is proposed.

The approach assumes that a nonlinear model is sought for a set of nearly orthogonal time series. Since each IMF admits an unambiguous definition of instantaneous frequency and amplitude through the Hilbert transform, the above theory can be readily applied.

Our HHT-based method is summarized in Figure 5.1. It consists of the following steps:

- Improved empirical mode decomposition

- Temporal analysis of system behavior

- Feature reconstruction

Assume in order to introduce the nature of this model, that a signal $x(t)$ has been decomposed into a set of nearly orthogonal IMFs, IMF_1, IMF_2, $\cdots$, IMF_n through continuous time projections, i.e. empirical mode decomposition of the signal. These components are then interpreted in terms of N independent undamped oscillators

$$\ddot{x}_i(t) + 2\varsigma\omega_o(t)\dot{x}_i + \omega_o^2(t)x_i = 0 \qquad i = 1,..,N$$

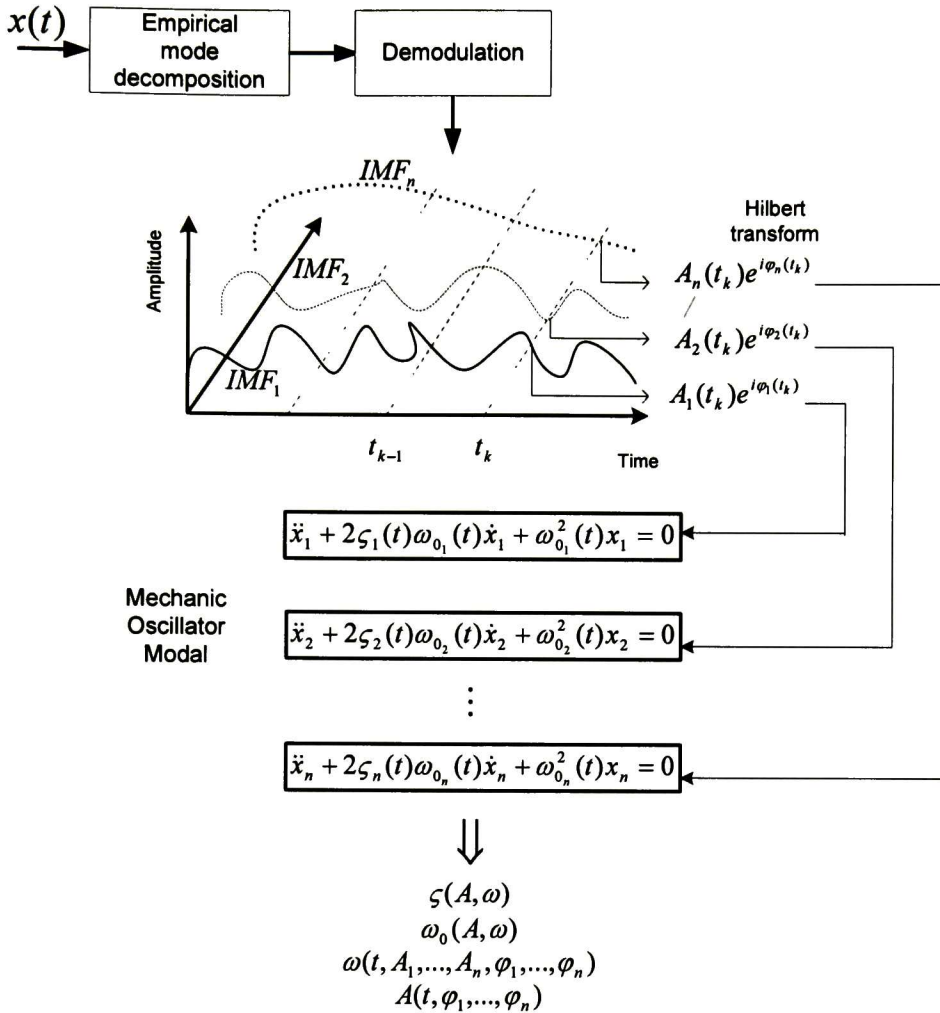whose modal characteristics are to be determined.

Figure 5.1. Conceptual representation of the proposed analysis method.

The sections that follow provide information on the various steps in the procedure.

5.1.2 Improved EMD

The basic idea to insert a masking signal, in this case a single sine tone, that prevents lower frequency components from being included in the IMF. Since the

masking signal is know, it can be removed from the IMF obtained through EMD in the following manner.

1. Construct a masking signal, $f(t)$ from the frequency information of the original data, $x(t)$.

2. Perfom EMD on $x_+(t) = x(t) + f(t)$ to obtain the IMF $y_+(t)$. Similarly obtain $y_-(t)$ from $x_-(t) = x(t) - f(t)$.

3. Define the IMF as $y(t) = (y_+(t) + y_-(t))/2$.

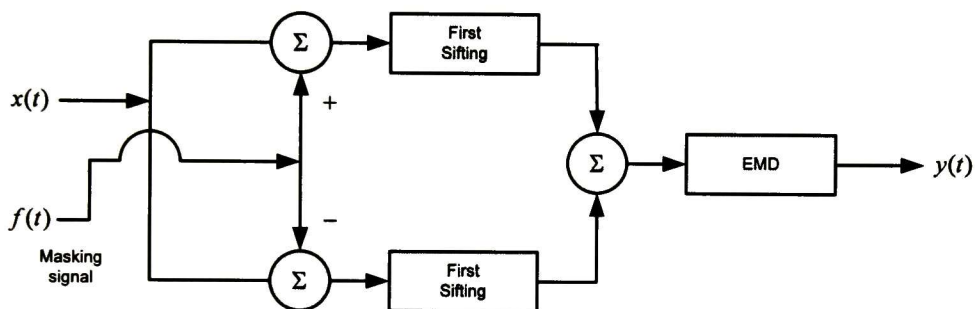Figure 5.2 describes this algorithm.

Figure 5.2. Ilustrated proposed approach.

5.1.3 Natural damping estimation

Damping is a critical consideration in the analysis and design of power systems. In this section, a technique to compute nonlinear damping in power signals is presented.

To build intuition about how the algorithm works consider a general signal $x(t)$. Once the individual IMFs are identified through EMD, the Hilbert transform is applied to each IMF independently to determine the local damping and frequency. More precisely, assume that each IMF can be described by a second-DOF system with nonlinear damping as

$$x(t) + 2\varsigma\omega_o(t)\dot{x} + \omega_o^2(t)x = 0 \tag{5.1}$$

where $x(t)$ is the displacement of the fictitious mass, ω_o is the undamped natural frequency, and ς is the dimensionless damping coefficient. The solution entails fitting a second-order model of the form (5.1) to the observed oscillation $y(t)$.

Applying the HT to (5.1) and combining the real and imaginary parts yields a differential equation of the ith analytical signal [2]

$$\ddot{z}(t) + 2\varsigma\omega_o(t)\dot{z} + \omega_o^2(t)z = 0 \tag{5.2}$$

Letting

$$z_k(t) = A_k(t)e^{i\varphi_k(t)} = \Lambda_k(t)e^{-\eta_k(t)}e^{i\varphi_k(t)} \tag{5.3}$$

where the envelope $A_k(t)$ and the phase $\varphi_k(t)$ are both slowly varying functions of time, $\Lambda_j(t)$ is time-dependent amplitude that can be interpreted as the source-related intensity, and $\eta(t)$ is an exponential factor characterizing the time-dependent decay of the solution [3], it can be readily proved that

$$\dot{z}_k(t) = z_k(t)\left[i\omega_k(t) - \dot{\eta}_k(t)\right]$$
$$\ddot{z}_k(t) = z_k(t)\left[i\dot{\omega}_k(t) - \omega_k^2(t) - 2i\omega_k(t)\dot{\eta}_k(t) - \ddot{\eta}_k(t) + \dot{\eta}_k^2(t)\right] \tag{5.4}$$

and

$$\frac{\dot{A}_k(t)}{A_k(t)} = -\dot{\eta}_k(t)$$
$$\frac{\ddot{A}_k(t)}{A_k(t)} = -\ddot{\eta}_k(t) \tag{5.5}$$

Substituting (5.5) into (5.4) and separating out the real and imaginary parts gives

$$2\varsigma\omega_o(t) = 2\dot{\eta}_k(t) - \frac{\dot{\omega}_k(t)}{\omega_k(t)}$$
$$\omega_{ko}^2(t) = \omega_k^2(t) + \ddot{\eta}_k(t) - \dot{\eta}_k^2(t) - 2\varsigma\omega_o(t)\dot{\eta}_k(t) \tag{5.6}$$

where the instantaneous frequency is given by

$$\omega_k(t) = \dot{\phi}_k(t) = \frac{z_k(t)\dot{\tilde{x}}(t) - \dot{z}_k(t)\tilde{z}_k(t)}{z_k^2(t) - \tilde{z}_k^2(t)} \tag{5.7}$$

Having determined the instantaneous amplitudes and phases, equation (5.6) provides the natural damping and natural frequency of the k th IMF. In its present form, however, these equations are sensitive to numerical errors caused by the computation of instantaneous frequency. This issue is discussed in detail in section 5.3.

5.1.4 Instantaneous energy

Hilbert analysis does not directly provide a measure of energy. In this section a technique to compute the instantaneous energy based on the developed mechanical model is proposed.

Consider the mass normalized equation of motion [4]

$$\ddot{z} + \omega_n^2 z + \hat{f}_D(z, \dot{z}) = 0 \tag{5.8}$$

where $\omega_n = \sqrt{k/m}$ is the natural frequency, and $\hat{f}_D$ is the mass normalized damping force, including both linear and nonlinear damping.

Assuming that nonlinear forces are relatively small, the free response can be assumed to be a simple sinusoid with a time-varying amplitude

$$z(t) = A(t)e^{i\varphi(t)} = A(t)\sin\left(\omega_d t + \phi\right) \tag{5.9}$$

Differentiation of this relation with respect to time produces the following dependence of the instantaneous parameters:

$$
\begin{aligned}
x(t) &= A(t)\omega_d \cos\left(\omega_d t + \phi\right) + \dot{A}(t)\sin\left(\omega_d t + \phi\right) \\
x(t) &= -A(t)\omega_d^2 \sin\left(\omega_d t + \phi\right) + \cos\left(\omega_d t + \phi\right)\dot{A}(t)\omega_d + \\
&\quad \dot{A}(t)\omega_d \cos\left(\omega_d t + \phi\right) + \sin\left(\omega_d t + \phi\right)\ddot{A}(t)
\end{aligned}
\tag{5.10}
$$

If the damping is assumed to be small in comparison to the stiffness and inertial forces, the response of the system can be written as

$$x(t) \approx A(t)\sin\left(\omega t + \phi\right)$$
$$\dot{x}(t) \approx A(t)\omega\cos\left(\omega t + \phi\right) \qquad (5.11)$$
$$\ddot{x}(t) \approx -A(t)\omega^2(t)\sin\left(\omega t + \phi\right)$$

The mass normalized instantaneous mechanical energy in the system is

$$e(t) = \frac{1}{2}kx^2(t) + \frac{1}{2}m\dot{x}^2(t) = \frac{1}{2}\omega^2 x^2(t) + \frac{1}{2}\dot{x}^2(t) \qquad (5.12)$$

Substituting (5.12) into (5.9) and assuming that damping is small in comparison to the stiffness and inertial forces[2] it can be proved that

$$e(t) = \frac{1}{2}\omega_n^2 A^2(t) \qquad (5.13)$$

Equations (5.6) and (5.13) completely characterize the modal behavior of each IMF.

The algorithm described in this section will now be illustrated for the computation of damping of a nonlinear oscillator.

Based upon this discussion, we express the time evolution of each IMF in the form of a simple time-varying oscillatory mode with different amplitude and frequency content and can have both amplitude and frequency modulation.

Using the same procedure as before, the linear time-varying systems using HHT are frequently used to model systems that have non-stationary properties and undergo low magnitude vibrations.

5.2 Motivating example: a nonlinear Duffing oscillator

To further illustrate the use of the method to identify nonlinear, non-stationary characteristics, we consider the study of a nonlinear Duffing oscillator with cubic damping. The equation governing the motion for the oscillator is given by

---

[2] In this case, the rate of change of the amplitude of oscillation is small, i.e. $\dot{A}(t) = 0$ and $\omega_d \approx \omega$.

$$\frac{d^2x(t)}{dt^2} + 2\xi\omega_n \frac{dx(t)}{dt} + \omega_n^2 x(t) + \omega_n^2 \varepsilon x^3(t) = u(t) \qquad (5.14)$$

where ξ is the damping ratio, ω_n is the natural frequency of the Duffing oscillator and ε is the spring stiffness. The presence of the cubic nonlinear restoring force term $x^3(t)$ in (5.14) represents a nonlinear hard spring.

Numerical data for the model was obtained by integrating the system model (5.14) using a fourth-order Runge-Kutta method. Table 5.1 provides the data used in our computations corresponding to the nonlinear model

$$\frac{d^2x(t)}{dt^2} + 10 \frac{dx(t)}{dt} + 10^4 x(t) + 5 \times 10^4 x^3(t) = 0$$

with initial conditions $x_0 = 0$ and $\dot{x}_0 = 200$. For numerical solutions to the nonlinear equations, fourth and fifth order Runge-Kutta formulas were employed. All numerical results were obtained by using Matlab.

Figure 5.3 shows the time evolution of the displacement and speed.

Table 5.1. Parameters of the Duffing oscillator.

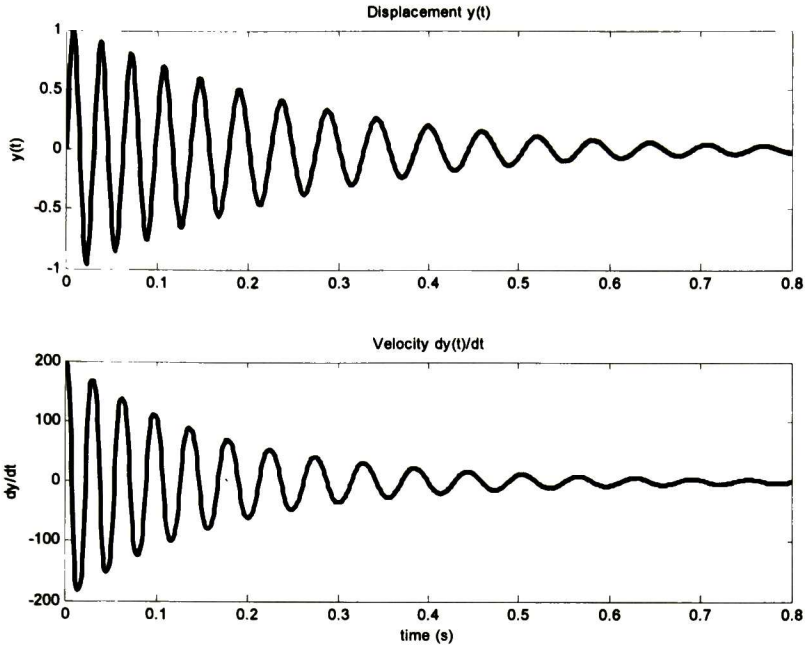| Parameters	Value
Damping ratio	$\xi = 0.05s^{-1}$
Natural frequency	$\omega_n = 100 rad/s = 15.91 Hz$
Spring sttifness	$\varepsilon = 5$

Figure 5.3. Duffing oscillator. *Top*: displacement. *Bottom*: velocity.

The model developed in the previous section was used to determine the temporal behavior of the oscillator. Figure 5.4 shows the instantaneous amplitude, phase and frequency obtained using equations (4.28), (4.29) and (4.31).

As a further illustration, Figure 5.4 shows the instantaneous attributes. The results show that the method is capable of accurately representing the nonlinear system dynamics. Examination of simulation results in Figure 5.4a shows that the method accurately captures the envelope of the oscillation. Also of interest, Figure 5.4b reveals that the instantaneous phase increases almost linearly with time indicating an essentially constant frequency. In turn the analysis of instantaneous frequency in Figure 5.4c shows that the instantaneous frequency reaches a steady state after a few seconds in close agreement with the expected physical behavior.
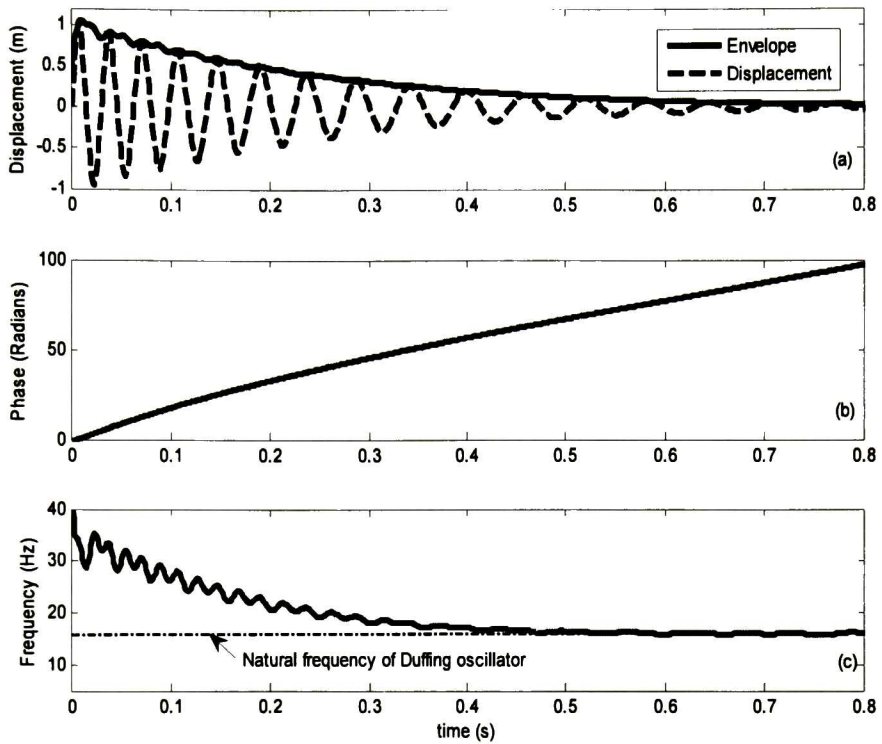
Figure 5.4. Instantaneous attributes. (a) amplitude or envelope, (b) phase, and (c) frequency.

Finally, examination of Figure 5.5 shows that the instantaneous damping fluctuates around the natural damping $\xi = 0.05s^{-1}$ As may be observed from this figure, in steady state the instantaneous damping coincides with the natural damping showing the accuracy of the model.
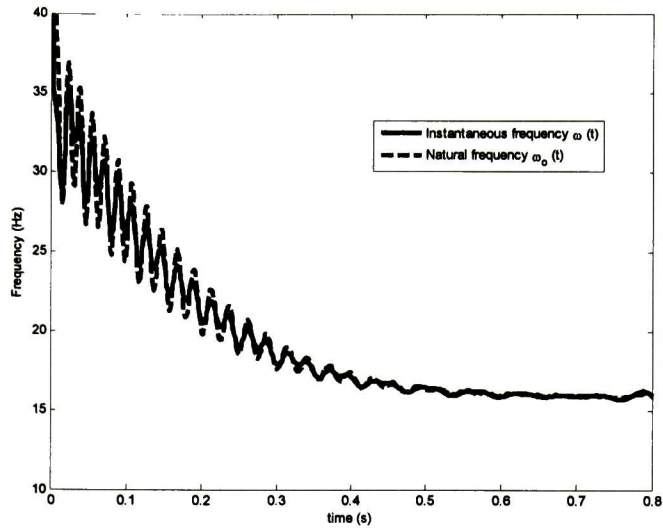
Figure 5.6. Comparison between natural frequency and instantaneous frequency.

We return now to the problem of frequency estimation.

5.3 Frequency estimation

In Chapter 2, instantaneous frequency was defined as the derivative of the instantaneous phase. If $x(t)$ is a time-varying trace and $H[x(t)]$ its Hilbert transform, the following equation can be used to calculate the instantaneous frequency of a time-varying trace

$$f(t) = \left(\frac{1}{2\pi}\right)\frac{x(t)\dfrac{dy(t)}{dt} - y(t)\dfrac{dx(t)}{dt}}{x^2(t) + y^2(t)} = \left(\frac{1}{2\pi}\right)\frac{x(t)\dfrac{dy(t)}{dt} - y(t)\dfrac{dx(t)}{dt}}{A^2(t)} \tag{5.15}$$

The computation of instantaneous frequency requires the evaluation of two time derivatives and it is numerically sensitive to the effects of low-amplitudes areas, $A(t)$, i.e. relative minima in the envelope. This results in spurious spikes which are physically meaningful. Another problem that affects the LSR method is the ringing effect caused by Gibbs' phenomenon.

Alternative methods for the calculation of instantaneous frequency are discussed below.

5.3.1 Central finite difference (CDF) of second order

Let $f(t)$ the instantaneous frequency of an analytic signal $\Psi(t) = u(t) + jv(t)$ given by

$$f(t) = \frac{\omega(t)}{2\pi} = \frac{1}{2\pi} \frac{d}{dt} [\varphi(t)] = \frac{1}{2\pi} \frac{d}{dt} \left[\arctan\left(\frac{v(t)}{u(t)}\right) \right] \qquad (5.16)$$

where $u(t)$ is a real signal and $v(t)$ is its Hilbert transform.

By definition, the derivative of a function $f(t)$ is given by

$$f'(t) = \lim_{h \to 0} \frac{f(x+h) - f(x)}{h} \qquad (5.17)$$

Therefore, the derivative of the phase is

$$\varphi'(t) = \frac{1}{2\pi} \lim_{T \to 0} \frac{\varphi(t+T) - \varphi(t)}{T} \qquad (5.18)$$

Assume that $\varphi \in C^3[a,b]$, $t - T$, $t + T \in [a,b]$ as is given in [5], then

$$\varphi'(t) \approx \frac{\varphi(t+T) - \varphi(t-T)}{2T} \qquad (5.19)$$

Furthermore, these exists a number $\alpha = \alpha(t) \in [a,b]$ such that

$$\varphi'(t) \approx \frac{\varphi(t+T) - \varphi(t-T)}{2T} + E_T(\varphi, T) \qquad (5.20)$$

where $E_T(\varphi, T) = -\frac{T^2 \varphi'''(\alpha)}{6} = O(T^2)$ is called the truncation error.

Proof. Taylor's series of second-order for $\varphi(t+T)$ and $\varphi(t-T)$ about t are

$$\varphi(t+T) = \varphi(t) + \varphi'(t)(t+T-t) + \frac{\varphi''(t)}{2!}(t+T-t)^2 + \frac{\varphi'''(t)}{3!}(t+T-t)^3$$

$$\varphi(t+T) = \varphi(t) + \varphi'(t)T + \frac{\varphi''(t)}{2!}T^2 + \frac{\varphi'''(\alpha_1)}{3!}T^3 \qquad (5.21)$$

and

$$\varphi(t-T) = \varphi(t) + \varphi'(t)(t-T-t) + \frac{\varphi''(t)}{2!}(t-T-t)^2 + \frac{\varphi'''(t)}{3!}(t-T-t)^3$$

$$\varphi(t-T) = \varphi(t) - \varphi'(t)T + \frac{\varphi''(t)}{2!}T^2 - \frac{\varphi'''(\alpha_2)}{3!}T^3 \qquad (5.22)$$

After (5.22) is subtracted from (5.21), the result is

$$\varphi(t+T) - \varphi(t-T) = 2\varphi'(t)T + \frac{\varphi'''(\alpha_1) + \varphi'''(\alpha_2)}{3!}T^3 \qquad (5.23)$$

If $\varphi \in C^3[a,b]$, then by intermediate value theorem exist $\alpha \in [a,b]$ that

$$\varphi'''(\alpha) = \frac{\varphi'''(\alpha_1) + \varphi'''(\alpha_2)}{2}$$

$$2\varphi'''(\alpha) = \varphi'''(\alpha_1) + \varphi'''(\alpha_2)$$

This can be substituted into (5.23) and we obtain

$$\varphi(t+T) - \varphi(t-T) = 2T\varphi'(t) + \frac{2\varphi'''(\alpha)}{3!}T^3$$

and the terms rearranged to yield

$$\varphi'(t) = \frac{\varphi(t+T) - \varphi(t-T)}{2T} - \frac{\varphi'''(\alpha)}{6}T^2 \qquad (5.24)$$

The first term on the right side of (5.24) is the central finite difference of second-order and the second term is the truncation error.

Finally we have equation (2.13)

$$F(t) = \frac{1}{2\pi}\varphi'(t) = \frac{1}{4\pi T}[\varphi(t+T) - \varphi(t-T)] \qquad (5.25)$$

To minimize the bias error and also to make the estimator more robust in the presence of noise, additional neighboring points may be included in the formula.

5.3.2 Central finite difference of fourth order

Suppose that the value of the third derivative $\varphi'''(\alpha)$ does not change too rapidly; then the truncation error in (5.20) goes zero in the same manner as T^2 which is expressed by using the notation $O(T^2)$. When computer calculations are used, it is not desirable to choose T too small. For this reason it is useful to have a formula for approximating $\varphi'(t)$ that has a truncation error of the order $O(T^4)$ as can be observed in [5]

Assume that $\varphi \in C^5[a,b]$, $t-2T$ $t-T$, t, $t+T$ $t+2T \in [a,b]$, then

$$\varphi'(t) \approx \frac{-\varphi(t+2T) + 8\varphi(t+T) - 8\varphi(t-T) + \varphi(t-2T)}{12T} \tag{5.26}$$

Furthermore, there exists a number $\alpha = \alpha(t) \in [a,b]$ such that

$$\varphi'(t) \approx \frac{-\varphi(t+2T) + 8\varphi(t+T) - 8\varphi(t-T) + \varphi(t-2T)}{12T} + E_T(\varphi,T) \tag{5.27}$$

where $E_T(\varphi,T) = -\dfrac{T^4 \varphi^V(\alpha)}{30} = O(T^4)$ is the truncation error of four-order.

Proof. Taylor's series of four-order of $\varphi(t+2T)$ and $\varphi(t-2T)$ about t are

$$\varphi(t+2T) = \varphi(t) + \varphi'(t)(t+2T-t) + \frac{\varphi''(t)}{2!}(t+2T-t)^2 + \frac{\varphi'''(t)}{3!}(t+2T-t)^3$$

$$+ \frac{\varphi^{IV}(t)}{4!}(t+2T-t)^4 + \frac{\varphi^V(t)}{5!}(t+2T-t)^5$$

$$\varphi(t+2T) = \varphi(t) + 2\varphi'(t)T + \frac{4\varphi''(t)}{2!}T^2 + \frac{8\varphi'''(t)}{3!}T^3 + \frac{16\varphi^{IV}(t)}{4!}T^4 + \frac{32\varphi^V(t)}{5!}T^5 \tag{5.28}$$

and

$$\varphi(t-2T) = \varphi(t) + \varphi'(t)(t-2T-t) + \frac{\varphi''(t)}{2!}(t-2T-t)^2 + \frac{\varphi'''(t)}{3!}(t-2T-t)^3$$

$$+ \frac{\varphi^{IV}(t)}{4!}(t-2T-t)^4 + \frac{\varphi^{V}(t)}{5!}(t-2T-t)^5$$

$$\varphi(t-2T) = \varphi(t) - 2\varphi'(t)T + \frac{4\varphi''(t)}{2!}T^2 - \frac{8\varphi'''(t)}{3!}T^3 + \frac{16\varphi^{IV}(t)}{4!}T^4 - \frac{32\varphi^{V}(t)}{5!}T^5 \qquad (5.29)$$

After (5.29) is subtracted from (5.28), the result is

$$\varphi(t+2T) - \varphi(t-2T) = 4\varphi'(t)T + \frac{16\varphi'''(t)}{3!}T^3 + \frac{64\varphi^{V}(\alpha_2)}{5!}T^5 \qquad (5.30)$$

In addition, differences between the Taylor's series of four-order of $\varphi(t+T)$ and $\varphi(t-T)$ about t is given by

$$\varphi(t+T) - \varphi(t-T) = 2\varphi'(t)T + \frac{2\varphi'''(t)}{3!}T^3 + \frac{2\varphi^{V}(t)}{5!}T^5 \qquad (5.31)$$

Multiply the terms in (5.31) by 8 we get

$$8\varphi(t+T) - 8\varphi(t-T) = 16\varphi'(t)T + \frac{16\varphi'''(t)}{3!}T^3 + \frac{16\varphi^{V}(\alpha_1)}{5!}T^5 \qquad (5.32)$$

Subtract (5.30) to (5.32)

$$-\varphi(t+2T) + 8\varphi(t+T) - 8\varphi(t-T) + \varphi(t-2T) = 12\varphi'(t)T + \frac{16\varphi^{V}(\alpha_1) - 64\varphi^{V}(\alpha_2)}{120}T^5 \qquad (5.33)$$

If $\varphi^{V}(t)$ has one sign and if its magnitude does not changes rapidly, we can find a value α that lies in $[t-2T, t+2T]$ so that

$$16\varphi^{V}(\alpha_1) - 64\varphi^{V}(\alpha_2) = -48\varphi^{V}(\alpha)$$

This can be substituted into (5.33) and we obtain

$$-\varphi(t+2T) + 8\varphi(t+T) - 8\varphi(t-T) + \varphi(t-2T) = 12\varphi'(t)T - \frac{48\varphi^{V}(\alpha)}{120}T^5$$

and the terms rearranged to yield

$$\varphi'(t) = \frac{-\varphi(t+2T) + 8\varphi(t+T) - 8\varphi(t-T) + \varphi(t-2T)}{12T} + \frac{\varphi^{V}(\alpha)}{30}T^4 \quad (5.34)$$

The first term on the right side of (5.34) is the central finite difference of four-order and the second term is the truncation error.

Finally we obtain equation (2.13)

$$F(t) = \frac{1}{2\pi}\varphi'(t) = \frac{1}{24\pi T}\left[\varphi(t-2T) - 8\varphi(t-T) + 8\varphi(t+T) - \varphi(t+2T)\right] \quad (5.35)$$

The above equation is named centered five-point equation and requires using another equation at the endpoints. By obtaining this equation is necessary to use the Lagrange interpolation polynomial [6], which is given by

$$f(x) = \sum_{i=0}^{n} f(x_i)L_{n,i}(x) + \frac{(x-x_0)(x-x_1)(x-x_2)...(x-x_n)}{(n+1)!}f^{(n+1)}(c),$$

for some $c = c(x) \in [a,b]$ and $L_{n,i}(x)$ is the ith Lagrange polynomial for f at $x_0, x_1, ..., x_n$, thus

$$f'(x) = \sum_{i=0}^{n} f(x_i)L'_{n,i}(x) + \frac{d[(x-x_0)(x-x_1)(x-x_2)...(x-x_n)]}{dx}\frac{f^{(n+1)}(c)}{(n+1)!}$$

$$+ \frac{(x-x_0)(x-x_1)(x-x_2)...(x-x_n)}{(n+1)!}f^{(n+2)}(c),$$

so that

$$f'(x) = \sum_{i=0}^{n} f(x_i)L'_{n,i}(x) + \frac{f^{(n+1)}(c)}{(n+1)!}\left[(x-x_0)(x-x_1)(x-x_2)...(x-x_n)\right.$$

$$+ (x-x_0)(x-x_2)(x-x_3)...(x-x_n) + (x-x_0)(x-x_1)(x-x_3)...(x-x_n) + ...$$

$$\left. + (x-x_0)(x-x_1)(x-x_2)...(x-x_{n-1})\right] + \frac{\Pi_{j=0, j\neq k}^{n}(x_j - x_k)}{(n+1)!}f^{(n+2)}(c)$$

If $x = x_j$, $j = 0,1,2,...,n$, then we have

$$f'(x) = \sum_{l=0}^{n} f(x_i) L'_{n,i}(x_j) + \frac{f^{(n+2)}(c)}{(n+1)!} \prod_{j=0, j \neq k}^{n} (x_j - x_k) \qquad (5.36)$$

Equation (5.36) is called equation of the $n+1$ points, of course there is a better approximation to the derivative if it takes a greater amount of points, but this in turn implies a high cost computational due to the large number of assessments to be carried out. It is enough to take 3 or 5 points.

To deduce the five-point equation at the endpoints consider

$$L_{4,0}(x) = \frac{(x-x_1)(x-x_2)(x-x_3)(x-x_4)}{(x_0-x_1)(x_0-x_2)(x_0-x_3)(x_0-x_4)},$$

$$L_{4,1}(x) = \frac{(x-x_0)(x-x_2)(x-x_3)(x-x_4)}{(x_1-x_0)(x_1-x_2)(x_1-x_3)(x_1-x_4)},$$

$$L_{4,2}(x) = \frac{(x-x_0)(x-x_1)(x-x_3)(x-x_4)}{(x_2-x_0)(x_2-x_1)(x_2-x_3)(x_2-x_4)},$$

$$L_{4,3}(x) = \frac{(x-x_0)(x-x_1)(x-x_2)(x-x_4)}{(x_3-x_0)(x_3-x_1)(x_3-x_2)(x_3-x_4)}.$$

$$L_{4,4}(x) = \frac{(x-x_0)(x-x_1)(x-x_2)(x-x_3)}{(x_4-x_0)(x_4-x_1)(x_4-x_2)(x_4-x_3)},$$

with $x_1 = x_0 + h$, $x_2 = x_0 + 2h$, $x_3 = x_0 + 3h$, $x_4 = x_0 + 4h$, in other words x_0, x_1, x_2, x_3 and x_4 equally spaced, then

$$L'_{4,0}(x) = \frac{1}{(x_0-x_1)(x_0-x_2)(x_0-x_3)(x_0-x_4)} [(x-x_2)(x-x_3)(x-x_4)$$

$$+ (x-x_1)(x-x_3)(x-x_4) + (x-x_1)(x-x_2)(x-x_4) + (x-x_1)(x-x_2)(x-x_3)],$$

$$L'_{4,1}(x) = \frac{1}{(x_1-x_0)(x_1-x_2)(x_1-x_3)(x_1-x_4)} [(x-x_2)(x-x_3)(x-x_4)$$

$$+ (x-x_0)(x-x_3)(x-x_4) + (x-x_0)(x-x_2)(x-x_4) + (x-x_0)(x-x_2)(x-x_3)],$$

$$L'_{4,2}(x) = \frac{1}{(x_3 - x_0)(x_3 - x_1)(x_3 - x_2)(x_3 - x_4)}[(x - x_1)(x - x_2)(x - x_4)$$

$$+ (x - x_0)(x - x_2)(x - x_4) + (x - x_0)(x - x_1)(x - x_4) + (x - x_0)(x - x_1)(x - x_2)],$$

and

$$L'_{4,4}(x) = \frac{1}{(x_4 - x_0)(x_4 - x_1)(x_4 - x_2)(x_4 - x_3)}[(x - x_1)(x - x_2)(x - x_3)$$

$$+ (x - x_0)(x - x_2)(x - x_3) + (x - x_0)(x - x_1)(x - x_3) + (x - x_0)(x - x_1)(x - x_2)],$$

so that

$$L'_{4,0}(x_0) = -\frac{25}{12h}, \ L'_{4,1}(x_0) = \frac{4}{h}, \ L'_{4,2}(x_0) = -\frac{3}{h}, \ L'_{4,3}(x_0) = \frac{4}{3h}, \text{ and } L'_{4,4}(x_0) = -\frac{1}{4h}$$

Therefore

$$f'(x_0) = -\frac{25}{12h}f(x_0) + \frac{4}{h}f(x_1) - \frac{3}{h}f(x_2) + \frac{4}{3h}f(x_3) - \frac{1}{4h}f(x_4) + \frac{f^V(c_0)h^4}{5},$$

so that

$$f'(x_0) = \frac{1}{12h}[-25f(x_0) + 48f(x_0 + h) - 36f(x_0 + 2h) + 16f(x_0 + 3h)$$

$$-3f(x_0 + 4h)] + \frac{f^V(c_0)h^4}{5} \tag{5.37}$$

but also

$$L'_{4,0}(x_1) = -\frac{1}{4h}, \ L'_{4,1}(x_1) = -\frac{5}{6h}, \ L'_{4,2}(x_1) = \frac{3}{2h}, \ L'_{4,3}(x_1) = -\frac{1}{2h}, \text{ and } L'_{4,4}(x_1) = \frac{1}{12h}$$

then

$$f'(x_0 + h) = -\frac{1}{4h}f(x_0) - \frac{5}{6h}f(x_0 + h) + \frac{3}{2h}f(x_0 + 2h) - \frac{1}{2h}f(x_0 + 3h)$$

$$+ \frac{1}{12h}f(x_0 + 4h) - \frac{f^V(c_1)h^4}{20},$$

Hence

$$f'(x_0 + h) = \frac{1}{12h}\left[-3f(x_0) - 10f(x_0 + h) + 18f(x_0 + 2h) - 6f(x_0 + 3h)\right.$$

$$\left. + f(x_0 + 4h)\right] - \frac{f^V(c_1)h^4}{20} \tag{5.38}$$

Now

$$L'_{4,0}(x_2) = \frac{1}{12h}, \; L'_{4,1}(x_2) = -\frac{2}{3h}, \; L'_{4,2}(x_2) = 0, \; L'_{4,3}(x_2) = \frac{2}{3h}, \text{ and } L'_{4,4}(x_2) = -\frac{1}{12h}$$

so

$$f'(x_0 + 2h) = \frac{1}{12h}f(x_0) - \frac{2}{3h}f(x_0 + h) + \frac{2}{3h}f(x_0 + 3h) - \frac{1}{12h}f(x_0 + 4h) + \frac{f^V(c_2)h^4}{30},$$

and hence

$$f'(x_0 + 2h) = \frac{1}{12h}\left[f(x_0) - 8f(x_0 + h) + 8f(x_0 + 3h) - f(x_0 + 4h)\right.$$

$$\left. + f(x_0 + 4h)\right] - \frac{f^V(c_2)h^4}{30} \tag{5.39}$$

but

$$L'_{4,0}(x_3) = \frac{1}{3h}, \; L'_{4,1}(x_3) = \frac{1}{2h}, \; L'_{4,2}(x_3) = -\frac{2}{3h}, \; L'_{4,3}(x_3) = \frac{17}{6h}, \text{ and } L'_{4,4}(x_3) = \frac{1}{4h}$$

Therefore

$$f'(x_0 + 3h) = \frac{1}{3h}f(x_0) + \frac{1}{12h}f(x_0 + h) - \frac{2}{3h}f(x_0 + 2h) + \frac{17}{6h}f(x_0 + 3h)$$

$$+ \frac{1}{4h}f(x_0 + 4h) - \frac{f^V(c_3)h^4}{20}.$$

and

$$f'(x_0 + 3h) = \frac{1}{12h}\left[4f(x_0) + 6f(x_0 + h) - 8f(x_0 + 2h) + 34f(x_0 + 3h)\right.$$

$$\left. + 3f(x_0 + 4h)\right] - \frac{f^V(c_3)h^4}{20} \tag{5.40}$$

in addition

$$L_0'(x_4) = \frac{1}{4h}, \ L_1'(x_4) = -\frac{4}{3h}, \ L_2'(x_4) = \frac{3}{h}, \ L_3'(x_4) = -\frac{4}{h}, \ \text{and} \ L_4'(x_4) = \frac{25}{12h}$$

Therefore

$$f'(x_0 + 4h) = \frac{1}{4h} f(x_0) - \frac{4}{3h} f(x_0 + h) + \frac{3}{h} f(x_0 + 2h) - \frac{4}{h} f(x_0 + 3h)$$

$$-\frac{25}{12h} f(x_0 + 4h) - \frac{f^V(c_4)h^4}{5},$$

and

$$f'(x_0 + 4h) = \frac{1}{12h} \left[f(x_0) - 3f(x_0 + h) + 4f(x_0 + 2h) - 36f(x_0 + 3h) \right.$$

$$\left. + 25f(x_0 + 4h) \right] - \frac{f^V(c_4)h^4}{5} \tag{5.41}$$

But if in equation (5.38) is replecad $x_0 + h$ by x_0, in (5.39) $x_0 + 2h$ by x_0 in (5.40) $x_0 + 3h$ by x_0, and in (5.41) $x_0 + 4h$ by x_0, we have

$$f'(x_0) = \frac{1}{12h} \left[-25f(x_0) + 48f(x_0 + h) - 36f(x_0 + 2h) + 16f(x_0 + 3h) \right.$$

$$\left. - 3f(x_0 + 4h) \right] + \frac{f^V(c_1)h^4}{5} \tag{5.42}$$

Performing the change of variable $t = x_0$, and $h = T$ in equation (5.42), and employing this equation at the initial and endpoint, we obtain the centered five-point equation for the instantaneous frequency

$$f'(t) = \pm \frac{1}{12T} \left[-25f(t) + 48f(t \pm T) - 36f(t \pm 2T) + 16f(t \pm 3T) - 3f(t \pm 4T) \right] \tag{5.43}$$

5.3.3 Approximation using analytic signal

Inspired by a model developed by Barnes [7], an algorithm to compute the instantaneous frequency directly from the notion of instantaneous phase is now developed.

74

Mathematically, instantaneous frequency is expressed as the derivative of the phase which is given in equation (5.15). If a time interval the instantaneous frequency is represented by only one value, the average of the instantaneous frequency is arguably the best value use; the instantaneous frequency at any point can vary greatly from this average.

Following Barnes [7], we define the average instantaneous frequency $\bar{f}_{(t+T/2)}$ as the temporal average of instantaneous frequency in a time interval from t to $t+T$ as

$$\bar{f}_T(t+T/2) = \frac{1}{T}\int_t^{t+T} f(\tau)d\tau \qquad (5.44)$$

where τ is a dummy variable of integration. Substitution of the definition given above for $f(t)$ into (5.15) yields

$$\bar{f}_T(t+T/2) = \frac{1}{2\pi}\frac{\Delta\varphi(t)}{\Delta(t)} = \frac{1}{2\pi}\left[\frac{\varphi(t+T)-\varphi(t)}{t+T-t}\right] = \frac{1}{2\pi}\left[\frac{\varphi(t+T)-\varphi(t)}{T}\right]$$

$$\bar{f}_T(t+T/2) = \frac{1}{2\pi T}\left[\varphi(t+T)-\varphi(t)\right] \qquad (5.45)$$

Replacing the definition of instantaneous phase $\varphi(t) = \arctan\dfrac{v(t)}{u(t)}$ in equation (5.45) we get

$$\bar{f}_T(t+T/2) = \frac{1}{2\pi T}\left[\arctan\frac{v(t+T)}{u(t+T)} - \arctan\frac{v(t)}{u(t)}\right] \qquad (5.46)$$

Applying the identity trigonometry $\arctan(A) - \arctan(B) = \arctan\left[\dfrac{A-B}{1+AB}\right]$ in (5.46) yields

$$\bar{f}_T(t+T/2) = \frac{1}{2\pi T}\arctan\left[\frac{v(t+T)/u(t+T)-v(t)/u(t)}{1+\big(v(t+T)/u(t+T)\big)\big(v(t)/u(t)\big)}\right]$$

or

$$\bar{f}_T(t+T/2) = \frac{1}{2\pi T}\arctan\left[\frac{u(t)v(t+T)-u(t+T)v(t)}{u(t)u(t+T)+v(t)v(t+T)}\right] \tag{5.47}$$

and thus

$$\bar{f}_T(t+T/2) = \frac{1}{2\pi T}\arctan\left[\frac{u(t-T)v(t+T)-u(t+T)v(t-T)}{u(t-T)u(t+T)+v(t+T)v(t-T)}\right] \tag{5.48}$$

This approximation is faster to compute that the instantaneous frequency (5.35) because it avoids the two differentiations that the computation of instantaneous frequency requires.

Table 5.2 summarizes the formula used in this work to compute instantaneous frequency.

Table 5.2. Formulae for computation of instantaneous frequency.

Approach	Formula
Standard	$f(t) = \left(\dfrac{1}{2\pi}\right)\dfrac{x(t)\dfrac{dy(t)}{dt}-y(t)\dfrac{dx(t)}{dt}}{x^2(t)+y^2(t)} = \left(\dfrac{1}{2\pi}\right)\dfrac{x(t)\dfrac{dy(t)}{dt}-y(t)\dfrac{dx(t)}{dt}}{A^2(t)}$
Second order CFD	$F(t) = \dfrac{1}{2\pi}\varphi'(t) = \dfrac{1}{4\pi T}\left[\varphi(t+T)-\varphi(t-T)\right]$
Fourth order CFD	$F(t) = \dfrac{1}{2\pi}\varphi'(t) = \dfrac{1}{24\pi T}\left[\varphi(t-2T)-8\varphi(t-T)+8\varphi(t+T)-\varphi(t+2T)\right]$, and $f'(t) = \pm\dfrac{1}{12T}\left[-25f(t)+48f(t\pm T)-36f(t\pm 2T)+16f(t\pm 3T)-3f(t\pm 4T)\right]$
Barnes	$\bar{f}_T(t+T/2) = \dfrac{1}{2\pi T}\arctan\left[\dfrac{u(t-T)v(t+T)-u(t+T)v(t-T)}{u(t-T)u(t+T)+v(t+T)v(t-T)}\right]$

5.4 Estimation of damping using Log-decrement techniques

Nonlinear damping plays a critical role in the long-term behavior of weakly nonlinear systems.

5.4.1 Averaged instantaneous damping

Simulation results in previous sections suggest the need for an averaged instantaneous damping that could be compared with well established linear and stationary techniques such as Prony analysis. More formally, based on the notion of instantaneous frequency we defined an averaged instantaneous damping can be defined as [8]

$$\overline{2\varsigma\omega_0} = T^{-1}\int_0^T 2\varsigma(t)\omega_0(t)t = T^{-1}\int_0^T \frac{\dot{A}(t)}{A(t)}t = T^{-1}\ln\left[\frac{A(t)}{A_0}\right] \tag{5.49}$$

An alternative approach to the computation of average instantaneous damping from the combined application of the log-decrement technique and splines as discussed next.

5.4.2 Log-decrement techniques

The use of the log decrement method is a well established technique for the estimation of the modal properties of a linear sdof system [9]. In this section, we extend this approach to characterize instantaneous damping.

Consider a decaying transient signal. In the case of typical transient signal where the amplitude $A(t)$ decays exponentially and the period T between the consecutive cycles remains constant. The logarithmic decrement (δ), damping ratio (η), and the natural frequency (f) of the system are defined as [9]

$$\delta = \frac{1}{n}\ln\frac{A(t_1)}{A(t_1 + nT)}, \tag{5.50}$$

$$\eta = \frac{2\delta}{\sqrt{4\pi^2 + \delta^2}}, \tag{5.51}$$

$$f = \frac{1}{T} \tag{5.52}$$

where $A(t_1)$ is the modulus of the peak response at time t_i and n is number of cycles after t_i. If the system is linear, the same modal properties are obtained irrespective of which cycle or how many cycles are used in the evaluation of the above equations. For nonlinear systems, however, the arguments stated above are no longer valid; the modal properties estimated using equations (5.50)-(5.52) will vary depending on the amplitude at which these properties are estimated. This is precisely the property that will be utilized to extract the instantaneous damping from the transient signal.

Based on the use of splines, and the notion of nonlinear log-decrement, a technique to estimate the average modal damping is proposed. Figure 5.7 we offer a conceptual idea of the proposed technique. Let A_{i-2}, A_{i-1}, A_i and A_{i+1} be the peak amplitudes of the instantaneous damping determined using cubic spline.

Using the logarithmic decrement, the averaged instantaneous damping, ς_{av}, can be calculated as follows

$$\delta_i = \ln\left(\frac{A_{i-2} + A_{i-1}}{A_i + A_{i+1}}\right), \tag{5.53}$$

where $A_{i-2}, A_{i-1}, A_i, A_{i+1}$, are the modulus of the peak response signal at time $t_{i-2}, t_{i-1}, t_i, t_{i+1}$, respectively. It then follows that the damping ratio, η_i, can be approximated as

$$\eta_i = \frac{2\delta_i}{\sqrt{\delta_i^2 + 4\pi^2}} \tag{5.54}$$

Further, the natural frequency f_i, is given by

$$f_i = \frac{1}{0.5(t_{i+1} + t_i) - 0.5(t_{i-1} + t_{i-2})},$$ (5.55)
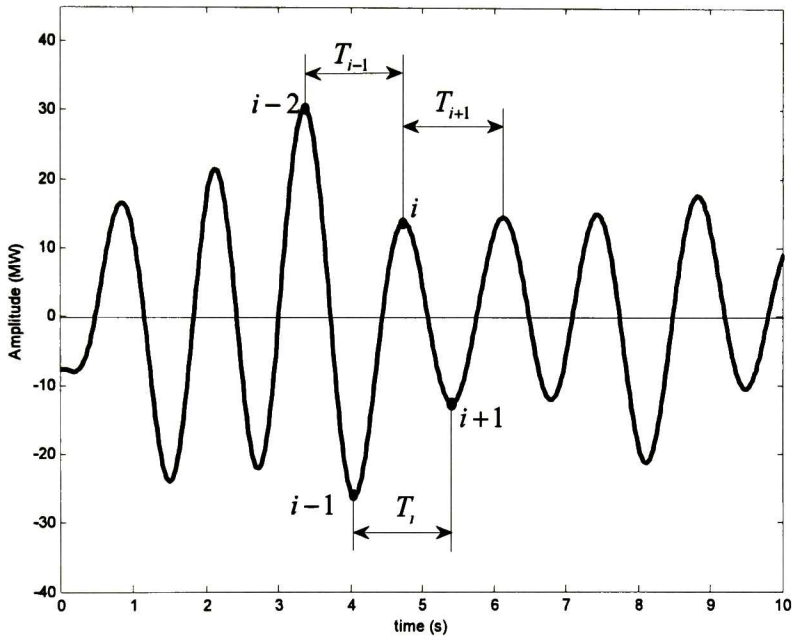
Figure 5.7. Nonlinear oscillatory signal.

The algorithm is simple to implement, and computational requirements are small. Figure 5.8 provides a comparison between the log-decrement approximation and the damping coefficient computed from equation (5.6).
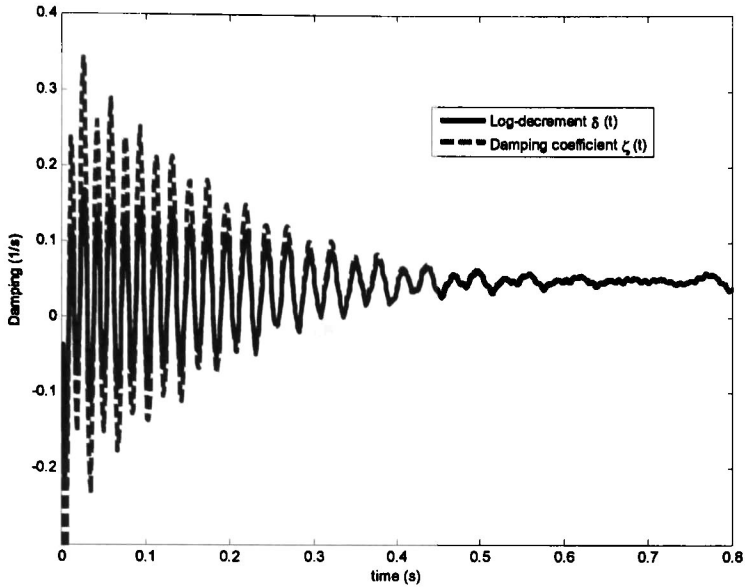
Figure 5.8. Comparison between logarithmic decrement and damping coefficient.

Several other variations are possible using techniques such as autoregressive moving average. The above approach, however, is simple to implement, and computational requirements are small.

5.5 Instantaneous coherency identification

5.5.1 Proposed method

Traditionally, generator coherency has been determined from the difference between the corresponding inter-area oscillations, using a linearized power system model or nonlinear time-domain simulations [10], [11]. An alternative approach is to use the phase of the generator oscillations, instead of the actual swing curves, to determine coherency.

The proposed approach consists of three steps:

1. Determine the dominant modes from oscillation signals of each generator.

2. Compute the instantaneous phase of the dominant mode in each case.

3. Define the angular difference between instantaneous phase angles using an appropriate metric.

In the first step, empirical mode decomposition is applied to extract meaningful modal components of complicated signals arising out of nonlinear and non-stationary power system oscillations. The dominant modes in each signal can then be clearly identified on the basis of the energy distribution of the intrinsic mode function (IMF) components.

The IMFs are orthogonal in nature, and are extracted in decreasing order of their local frequency content. In other words, the first IMF extracted contains the modes with highest local frequency content. If n IMFs are thus obtained iteratively, the original signal is recoverable according to equation (2.1). The relative importance of each IMF in capturing the modal information of the original signal is computed as a ratio of its norm to the norm of the original signal

$$\rho_j = \frac{\|c_j(t)\|_2}{\|x(t)\|_2} \tag{5.56}$$

where $\|\|$ refers to the l^2 norm of the signal, $c_j(t)$ is the jth IMF and $x(t)$ is the original signal. The IMF with the highest relative importance is referred to as the dominant IMF.

Hilbert transform is applied on the dominant IMF of each generator in second step to obtain analytic signals from which the instantaneous amplitude, phase and frequency can be computed. The EMD along with Hilbert transform constitute the Hilbert-Huang transform, proposed to study nonlinear and non-stationary signals. In power system, this technique has been applied to study of nonlinear oscillations [2].

In the third step, the instantaneous phase information is further utilized to identify coherency between generators that have negligible phase difference.

Hence, variation of generator coherency is interpreted as the instantaneous phase-difference between the dominant modes of generator oscillations.

Using equation (2.11), the instantaneous phase of any real signal $x(t)$ can be computed. Let the instantaneous phase of signal $x_1(t)$ be $\varphi_1(t)$, and that of signal $x_2(t)$ be $\varphi_2(t)$. The two signals $x_1(t)$ and $x_2(t)$ are coherent at any instant t, if

$$\left|\varphi_1(t) - \varphi_2(t)\right| = 2n\pi, \qquad n = 0,1,2,... \qquad (5.57)$$

An instantaneous coherency index for two signals may be defined as the difference between their instantaneous phase angle.

In the next chapter, results of the analysis of inter-area oscillations demonstrate that is possible to extract coherency between different areas using the Hilbert-Huang transform.

5.6 References.

[1] J. F. Hauer, and J. G. DeSteese, "A tutorial on detection and characterization of special behavior in large electric power systems," *Pacific Northwest National Laboratory, Richland, WA.*, Rep. PNNL-14655, July 2004.

[2] A. R. Messina, M. A. Andrade, J. H. Hernández, and R. Betancourt, "Analysis and characterization of power system nonlinear oscillations using Hilbert Spectral Analysis," in *The Open Electrical and Electronic Engineering Journal*, vol. 1, pp. 1-8, June 2007.

[3] R. R. Zhang, L. VanDemark, J. Liang, and Y. Hu, "On estimating site damping with soil non-linearity from earthquake recordings," in *International Journal of Non-Linear Mechanics*, vol. 39, pp. 1501-1517, Nov. 2004.

[4] C. Meskell, "A decrement method for quantifying nonlinear and linear damping parameters," in *journal of Sound and Vibration*, vol. 296, pp. 643-649, 2006.

[5] J. H. Mathews, and K. D. Fink, "Numerical Methods Using Matlab", Ed. Prentice-Hall, ISBN 0-1327-0042-5, 3rd ed., vol. 1, 1999.

[6] R. L. Burden, and J. D. Faires, "Numerical Analysis," Ed. Brooks Cole Publishing, ISBN 0-534-95532-0, 6th ed., vol.1, Pacific Grove, CA., 1997.

[7] A. E. Barnes, "A tutorial on complex seismic trace analysis," in *Society of Exploration Geophysicists*, vol. 72, Issue 6, October 2007.

[8] M. Feldman, "Non-linear System Vibration Analysis Using Hilbert Transform I: Free Vibration Analysis Method -FREEVIB-," in *Mechanical Systems and Signal Processing*, vol. 8, No. 2, pp. 119-127, 1994.

[9] M. E. Levent, and K. Y. Sanliturk, "Characterisation of Vibration Isolators Using Vibration Test Data," in *Tenth International Congress on Sound and Vibration*, pp. 1-8, 2003.

[10] C. Liu, R. Yokoyama, K. Koyanagi, and K. Y. Lee, "PSS design for damping of inter-area power oscillations by coherency-based equivalent model," in *Electrical Power and Energy Systems*, vol. 26, pp. 535-544, 2004.

[11] K. K. Anaparthi, B. Chaudhuri, N. F. Thornhill, and B. C. Pal, "Coherency Identification in Power Systems Through Principal Component Analysis," in *IEEE Transactions on Power Systems*, vol. 20, pp. 1658-1660, August 2005.

Chapter 6
Application to complex inter-area oscillations

This chapter describes the application of the developed theory to the modeling, simulation and analysis of nonlinear oscillations in power systems. Hilbert spectral analysis is used to characterize and visualize the time evolution of power system oscillatory phenomena following large perturbations. Data from transient stability simulations are used to examine the potential usefulness of nonlinear time series analysis techniques to characterize the temporal evolution of nonlinear, non-stationary oscillations and to determine the nature and propagation of the system disturbance.

The viability of the technique is demonstrated on both, simulation- based transient stability data. Attention is also focused on assessing the effect of coherency on system dynamic performance. Finally some concluding remarks are made.

A 68-bus, 16-machine power system is analyzed to examine the onset of nonlinear, non-stationary behavior. Examples of the developed procedures to characterize and visualize spatio-temporal behavior and to estimate the instantaneous damping are provided.

The results obtained from proposed approach are compared with conventional time-domain analysis techniques and its efficiency is demonstrated. Challenges involved in realistic modal analysis of large linear systems are emphasized and relationships with other modern modal analysis techniques are discussed.

The study demonstrates the feasibility of time-frequency analysis to characterize signals that are nonlinear and/or non-stationary in nature.

6.1 Outline of the study

6.1.1 System description

The test system under study is a 16-machine model of an NPCC system which is a reduced order model of the New England/New York interconnection [1]. Figure 6.1 shows a schematic representation of this system showing the main areas of concern for this study areas and major transmission elements selected for analysis. System parameters used for the simulations are based on data given in [2].

For illustration purposes in the analysis of inter-area oscillations, the system is divided into five coherent machine groups.

These are:

Area 1: Machines 1-9

Area 2: Machines 10-13

Area 3: Machine 14

Area 4: Machine 15

Area 5: Machine 16
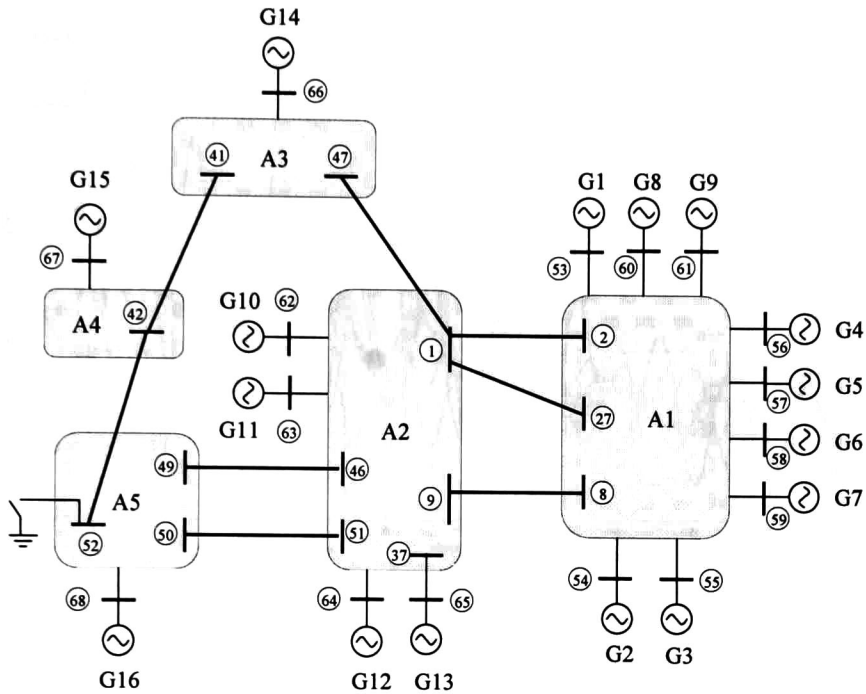
Figure 6.1. Sixteen-machine NPCC system.

6.1.2 Test cases and modeling considerations

Output data from transient stability simulations were considered to verify the ability of the method to extract the dominant features of complex oscillations.

Detailed numerical simulations for the above contingency were performed to generate the snapshots used in the POD method. The fault considered to analyze system behavior is a three-phase fault at bus 52, cleared in 6 cycles by removing the fault.

Figures 6.2 shows selected simulation results. Each recording is 20 s long. The sampling time is 0.01 s.
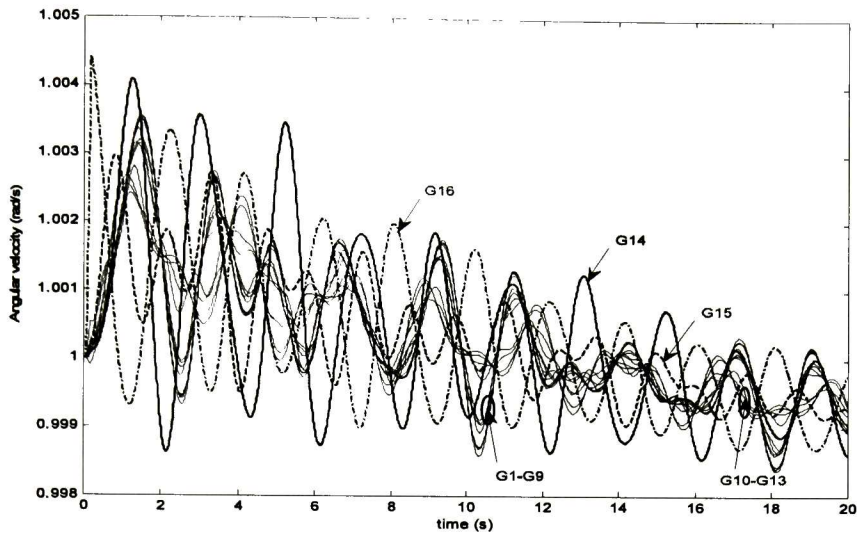
(a)
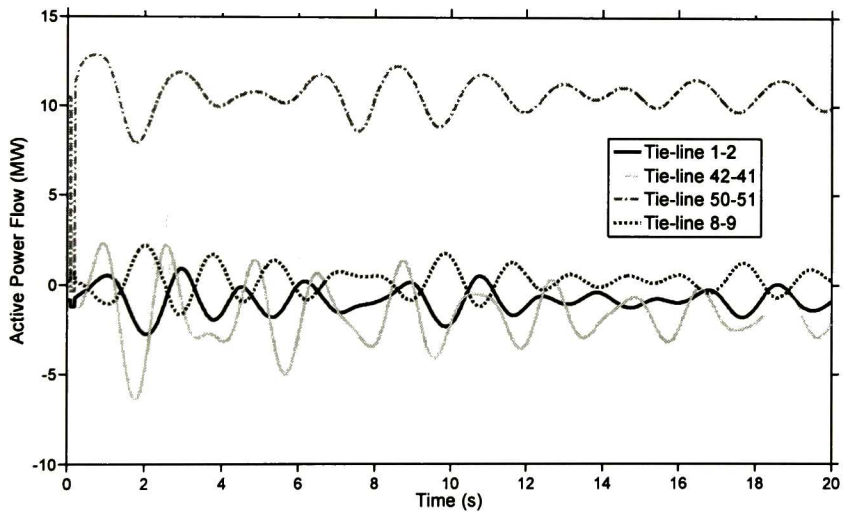
(b)

Figure 6.2. System response to a three phase fault at bus 52: (a) Speed deviations; (b) Tie-line power flows.

The dynamic data obtained from these simulations are used for Hilbert analysis in the following sections.

Before applying Hilbert analysis, some background information on the small-signal characteristics is introduced. For direct comparison to proposed method, we employ the algorithm used to.

6.1.3 Linear stability analysis

The overall system small signal stability analysis was performed using eigen-value calculation methodologies. To this end, a linear model of the system of the form $\mathbf{x} = A\mathbf{x}$ was developed and the linear response was computed.

The first five electromechanical modes of oscillation of the system are summarized in Table 6.1. Modal analysis results in Table 6.1 show four domi-nant inter-area modes with frequencies of 0.39 Hz, 0.50 Hz, 0.64 Hz and 0.78 Hz with damping ratios below 5% involving the exchange of swing energy between areas.

a)   A critical inter-area mode at 0.3929 Hz involving the interaction of generators in area-1 and area-4.

b)   An 0.5028 Hz inter-area mode shown the interaction of genera-tors in area-3 and area-5,

c)   The inter-area mode at 0.6427 Hz is present due to interaction of generators in area-1 and area-2, and

d)   The inter-area mode that exhibits a high frequency at 0.7873 Hz is observed by the interaction of generators in area-3 and area-4.

Table 6.1. The slowest oscillatory modes of the system.

Mode description	Eigenvalue (*)	Oscillation pattern	Frequency (Hz)	Damping ratio (%)
Inter-area mode 1	$-0.0616 \pm j2.4687$	$G_5 \leftrightarrow G_{15}$	0.392	2.49
Inter-area mode 2	$-0.0693 \pm j3.1594$	$G_{14} \leftrightarrow G_{16}$	0.502	2.19
Inter-area mode 3	$-0.0531 \pm j4.0388$	$G_5 \leftrightarrow G_{13}$	0.642	1.31
Inter-area mode 4	$-0.0809 \pm j4.9471$	$G_{14} \leftrightarrow G_{15}$	0.787	1.63

(*)Real part (1/s) and Imaginary part (rad/s)

Examination of the power spectra of the tie-line flows in Figure 6.3, reveals that the selected tie-lines have a strong participation in the critical inter-area modes. Studies below are aimed at disclosing the temporal evolution of these modes.
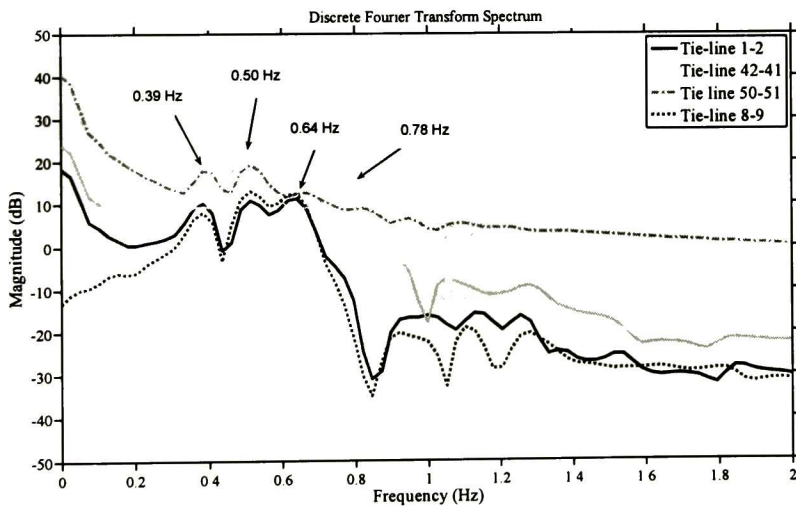
Figure 6.3. Power spectra of tie-line power flows.

Figure 6.4 gives the rotor modes shapes of the inter-area mode illustrating the nature of energy exchange.
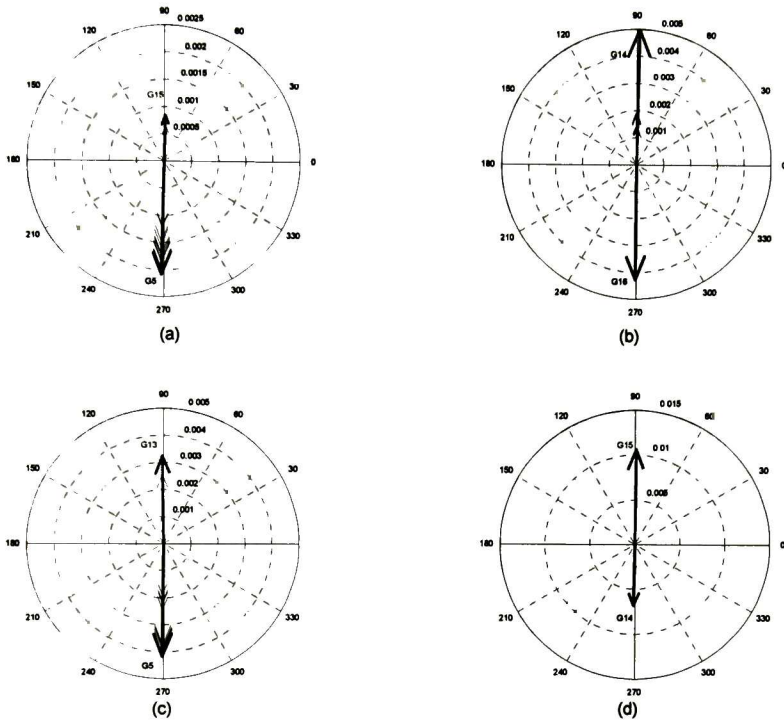
Figure 6.4. Mode shapes of inter-area modes. (a) inter-area mode 1, (b) inter-area mode 2, (c) inter-area mode 3, and (d) inter-area mode 4.

6.2 Conventional HHT analysis of tie-line power flows

In the subsections that follow conventional Hilbert analysis is used to characterize the time evolution of the test signals. In this approach, the conventional empirical mode decomposition algorithm in section 2.1.1 was utilized; the Hilbert transform is computed using the FFT-based approach [3].

For comparison, each case is analyzed separately.

---

[3] The Hilbert transform is computed using the matlab script *hilbert*

6.2.1 Tie-line flow between buses 1 and 2

This transmission line interconnecting areas 1 and 2 has a strong participation in the three slowest inter-area modes (0.39 Hz, 0.50 Hz and 0.64 Hz) as shown in Figure 6.3.

Using the proposed analysis, the tie-line signal is decomposed into five non-stationary temporal modes and a trend.

Figure 6.5 shows the IMF components for the tie line signal extracted following the standard procedure in Chapter 2. For this signal, application of the HHT in Figure 6.6 identifies two IMFs centered at 0.63 Hz and 0.37 Hz Visual inspection of the 0.64 Hz component suggests some degree of mode mixing in which a second mode modulates the 0.64 Hz IMF to produce an FM signal. The analysis of the 0.37 Hz component suggests, on the other hand, mono-component behavior.
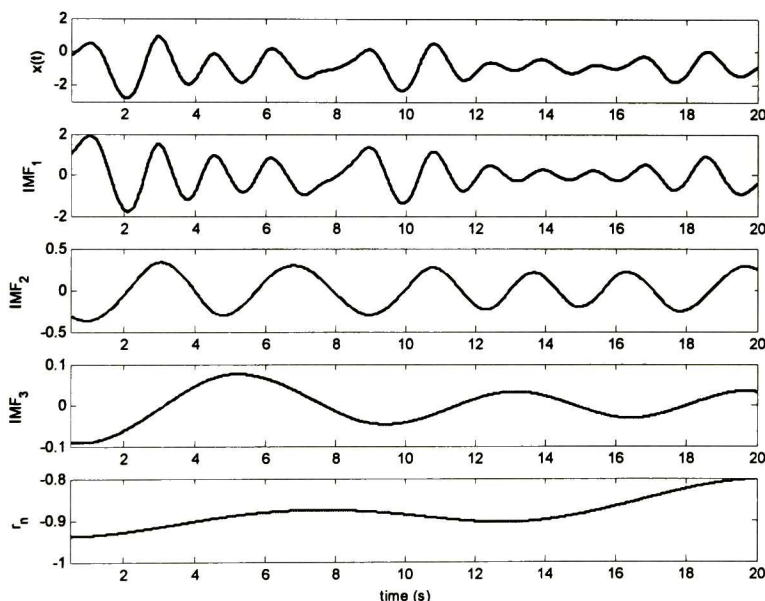
Figure 6.5. Test power signal with its four IMFs and residue component obtained through the EMD method.

Comparison with the power spectra in Figure 6.7 shows some discrepancy in the frequencies extracted. In both cases, the techniques can not identify the underlying modal components in the Fourier spectra.
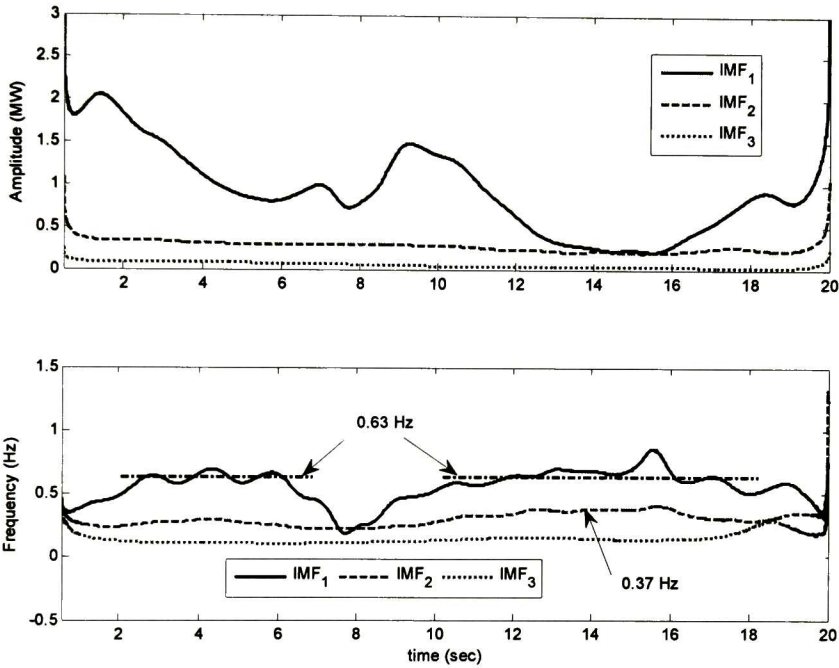
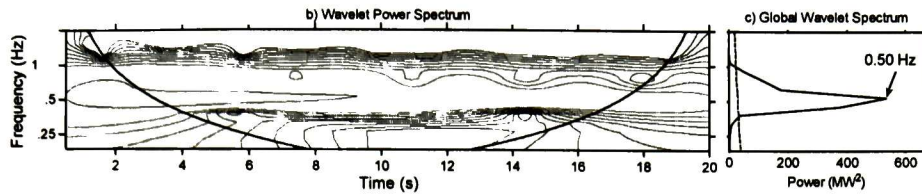Figure 6.6. Hilbert spectral analysis of tie line flow 1-2. Instantaneous characteristics.
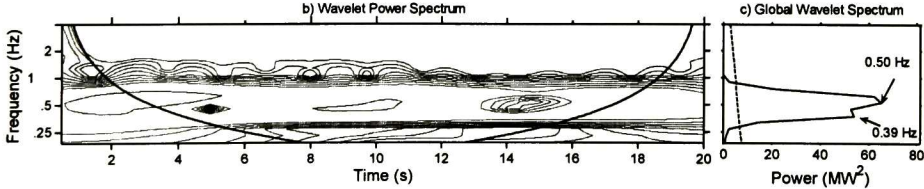
Figure 6.7. Wavelet spectra.

6.2.2 Tie-line flow between buses 42 and 41

This transmission line has a strong participation in the 0.50 Hz and 0.78 Hz inter-area modes 1 and 4.

Examination of the modal components in Figure 6.8 shows two distinct stages in which IMFs 1 and 2 make a significant contribution to the observed oscillation. During the initial stage, the system exhibits two dominant IMFs at 0.78 Hz and 0.39 Hz (lower panel). As may be observed from the plot, the degree of modulation of very small. As time progresses, the frequency of IMF 1 decreases to about 0.50 Hz; the degree of modulation is seen to increase. Analysis of the temporal amplitudes in the top panel indicates that the 0.39 Hz component decays rapidly indicating the transient nature of this oscillation. Also of interest, wavelet analysis in Figure 6.9 indicates a dominant component at 0.50 Hz. Here, the presence of two frequency components is shown as variations in the contour plot.
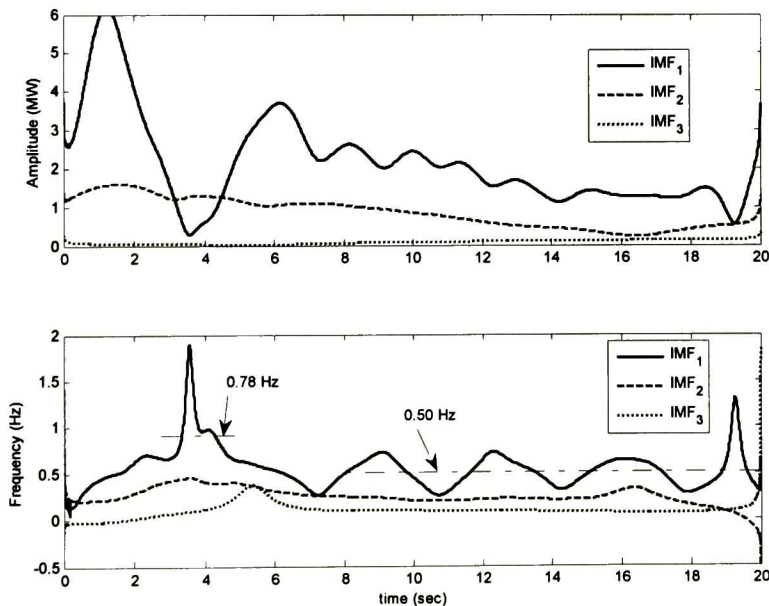
Figure 6.8. Hilbert spectral analysis of tie line flow 42-41. Instantaneous amplitude and frequency.

Figure 6.9. Wavelet spectra.

6.2.3 Tie-line flow between buses 50 and 51

This transmission line has a strong participation in the 0.39 Hz and 0.50 Hz inter-area modes 1 and 2.

The analysis of the instantaneous amplitude in Figure 6.10 shows two nearly stationary modes centered at 0.50 Hz (dominant mode) and 0.34 Hz in close agreement with the Fourier results in Figure 6.3. Visual inspection of the time evolution of the 0.50 Hz component indicates some degree of modulation.

Wavelet analysis in Figure 6.11 confirms these findings.

As shown, the estimation of instantaneous parameters is noisy in areas of low signal energy.
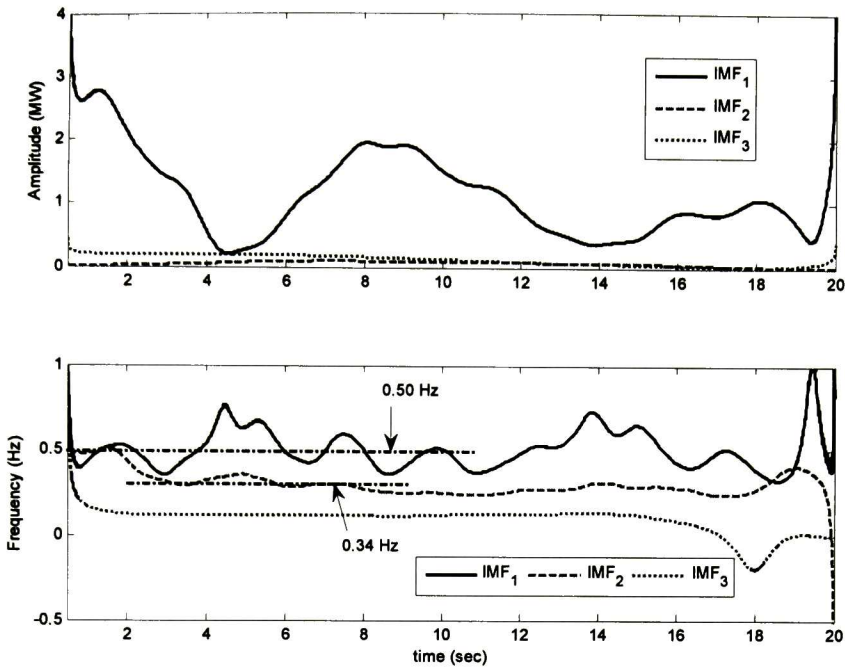
Figure 6.10. Hilbert spectral analysis of tie-line 50-51. *Top*: Instantaneous amplitude, *Bottom*: Instantaneous frequency.
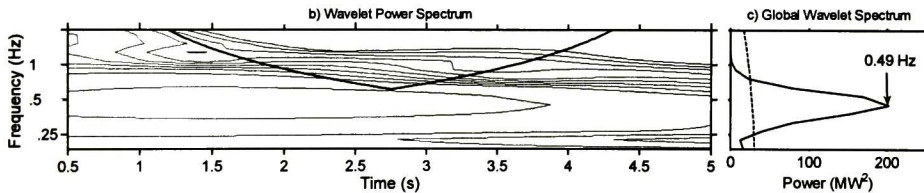
Figure 6.11. Wavelet spectra of tie-line 50-51.

6.2.4 Tie-line flow between buses 8 and 9

This transmission line has a strong participation in the three slowest inter-area modes at 0.39 Hz, 0.50 Hz and 0.64 Hz. Simulation results shown in Figure 6.12 are very similar to those of transmission line 50-51 as expected.
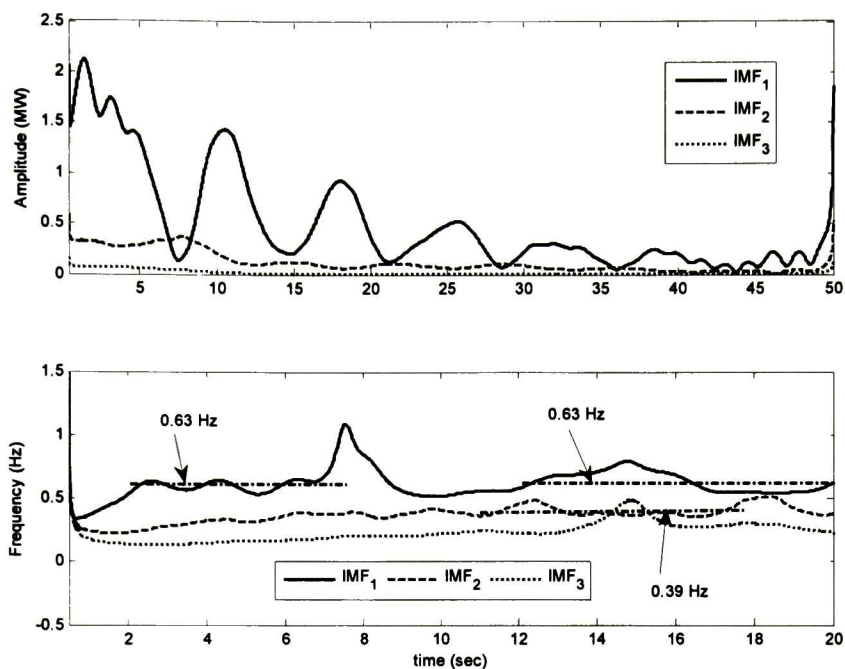
Figure 6.12. Instantaneous attributes of the 8-9 power signal. *Top:* Intrinsic mode functions, *Middle:* Instantaneous amplitude, *Bottom:* Instantaneous frequency.

Next, the standard HHT and the masking-based method are compared.

6.3 Masking technique to improve the existing HHT

Based on our previous results, the masking signal technique was used to improve the conventional HHT results.

For illustration purposes, the tie-line signal 50-51 was selected for study. In this analysis three different modeling approaches were developed and tested:

a) Conventional EMD with Fourier-based computation of the Hilbert transform. This is the same modeling approach used in section 6.2

b) EMD with masking technique Fourier-based computation of the Hilbert transform

c) EMD using masking technique and a convolution-based computation of the Hilbert transform

Figure 6.13 compares the IMFs obtained using the conventional approach and the masking signal technique. As may be observed from this plot, the conventional approach results in 3 IMFs and a trend while the masking approach results in four IMFs and a trend.

Further, Figure 6.14 compares the instantaneous amplitudes computed using the various approaches above. Simulation results show that the EMD with convolution-based Hilbert transform results in a smoother amplitude representation and reduces end-effects.
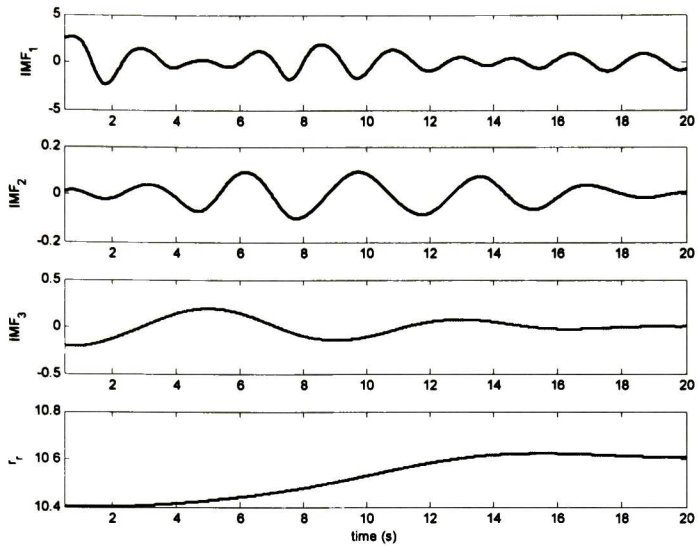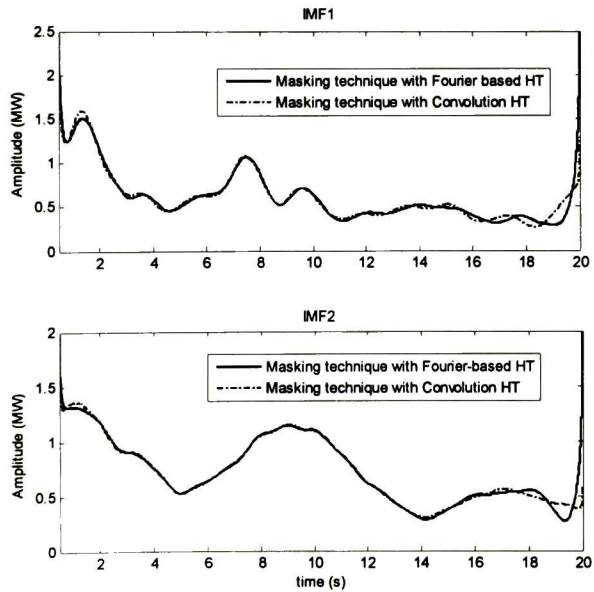
(a)
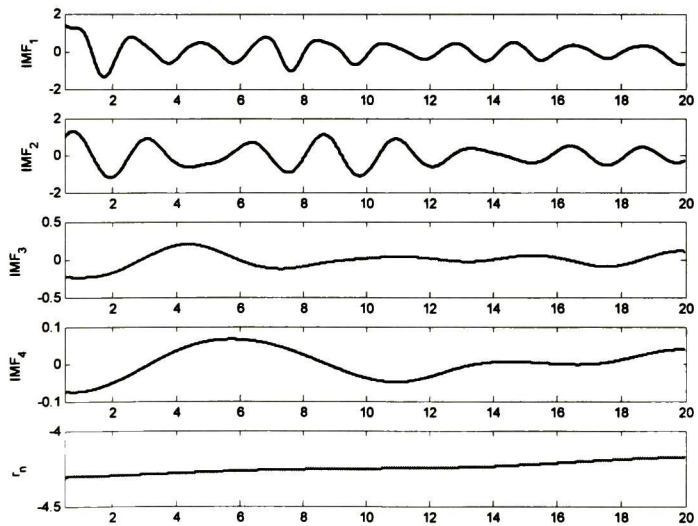
(b)

Figure 6.13. IMFs of tie-line 50-51 through: (a) conventional EMD method. (b) masking technique on EMD method.
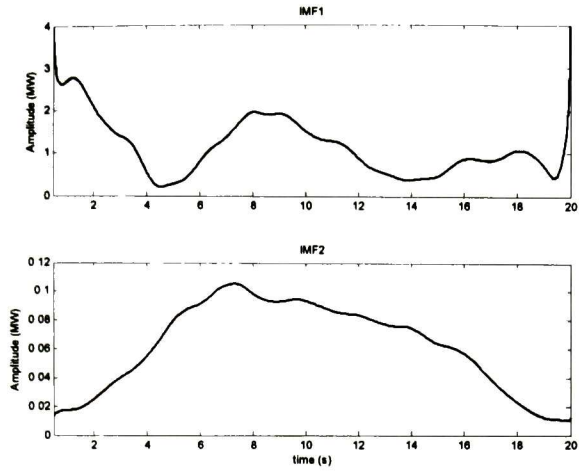
(a)

(b)

Figure 6.14. Instantaneous amplitude of IMFs in test power signal through: (a) EMD method with Fourier-based. (b) masking technique on EMD method comparison between Fourier-based HT and convolution HT.

In turn, the analysis of instantaneous frequency in Figure 6.15 confirms that the convolution method results in improved frequency characterization especially in the middle part of the plot. This contrast with the results with the conventional method in Figure 6.15a that show frequency modulation for IMF1 and increased end-effects. Again, the convolution-based method is found to perform better that the FFT-based method by Senroy.
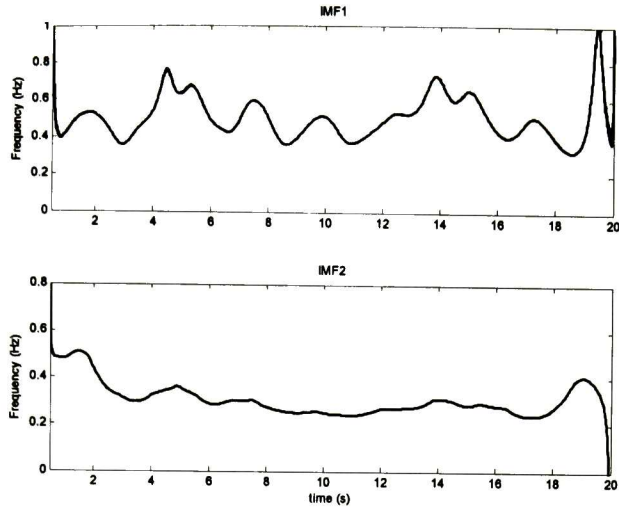
In Figure 6.15b the instantaneous frequency of IMF1 both convolution and conventional approaches are most meaningful that the Fourier-based approach, the fluctuations along of data recording have been demodulated. The IMF2 with convolution method presents demodulation in frequency regarding conventional method.

6.4 Damping identification

Much insight into the behavior of the temporal modes can be found by examining the instantaneous damping of critical modes. In this analysis two modeling approaches are investigated:

- A conventional approach based on the standard EMD and use of equation (2.95). We further assume that $\dot{\Lambda}_j(t)$ is a slowly varying function of time and can be negligible [3].

- The FREEVIB method in Chapter 4.

In all cases, the signal chosen for study is the tie-line power from bus 50 to bus 51.

(a)
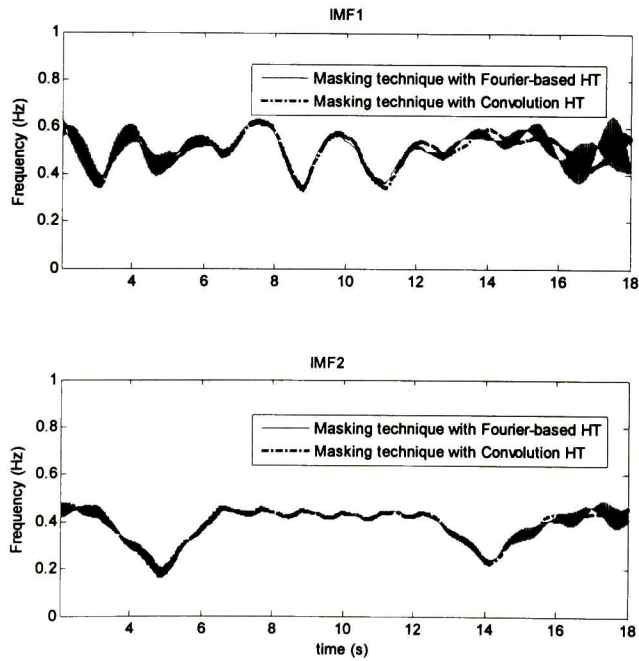
(b)

Figure 6.15. Instantaneous frequency of IMFs in test power signal through: (a) EMD method with Fourier-based. (b) masking technique on EMD method comparison between Fourier-based HT and convolution HT.

6.4.1 Conventional approach

Figure 6.16 shows the instantaneous damping of IMFs 1 and 2 obtained using conventional EMD. As observed in this plot, instantaneous damping exhibits strong variations about a mean value. The key point to emphasize is that instantaneous damping identifies two critical stages in system behavior: an unstable interval from 4 to 14 s and a stable interval from 14 to 19 s for both IMFs 1 and 2.
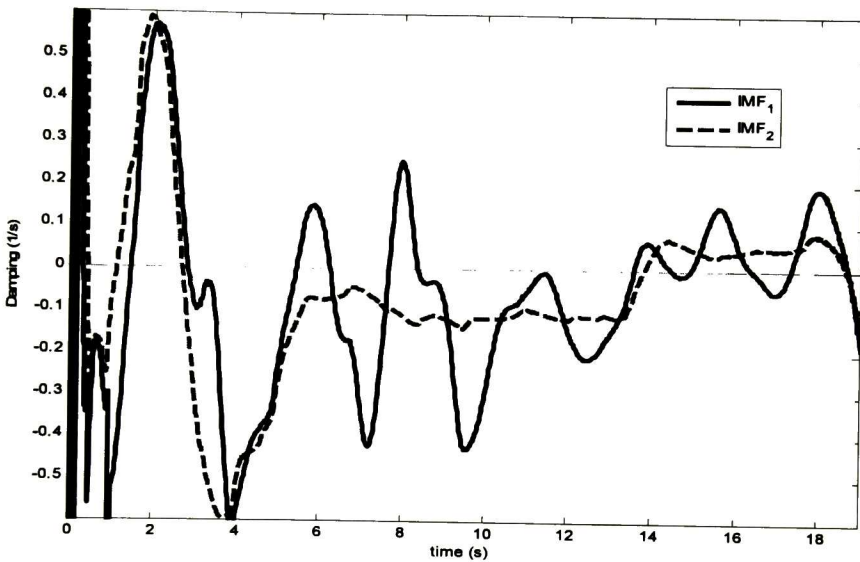

Figure 6.16. Instantaneous damping of the 50-51 power signal.

Further illustration of the ability of the method to capture temporal behavior is shown in Fig. 6.17 that compares damping obtained using the masking-based employing the conventional Hilbert transform with that obtained using FREEVIB. Compared with the FREEVIB method, the masking-based technique can provide a smoother characterization of the true damping pattern.
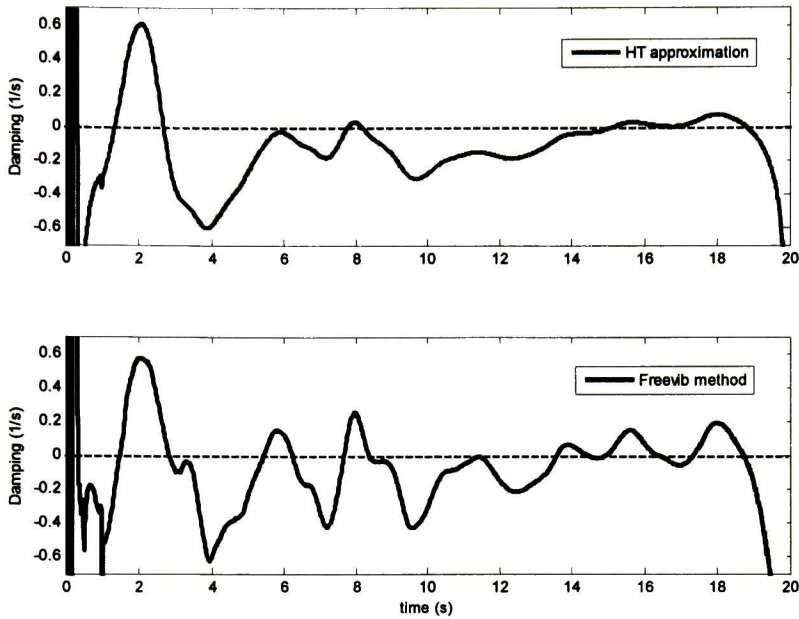
Figure 6.17. Comparison of the instantaneous damping of the 50-51 power signal.

Similar results are obtained for other signals and are not described here.

6.4.2 Instantaneous damping using masking technique

In this section we explore the use of the averaged damping technique to characterize instantaneous damping. Figure 6.18 compares the damping estimates using the masking-based algorithm with the instantaneous-average approach for the tie-line 50-51 signal.

The instantaneous estimates are found to provide a very characterization of damping. Comparison is found to be consistent with Prony analysis estimates in Table 6.2 that suggests that mode dominant modes are stable.
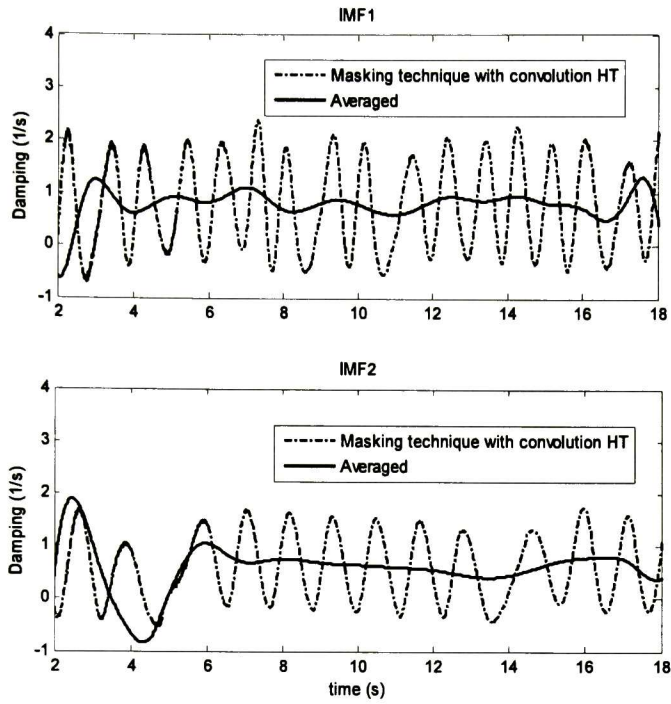
Figure 6.18. Averaged damping of dominants IMFs in test signal.

Table 6.2. Prony analysis for tie line 50-51 signal.

Mode	Frequency (Hz)	Damping /2π	Damping Ratio	Relative Energy
1	0.499431	0.010768	0.021555	1.000000
2	0.641810	0.008402	0.013090	0.998063
3	0.392111	0.009475	0.024158	0.330592
4	0.499338	-0.023080	-0.046171	0.005581

6.5 Coherency identification

A key feature of the proposed technique is its ability to extract instantaneous phase characteristics. Based on the algorithm proposed in Chapter 5, we next explore the use of phase analysis to identify dynamic coherency.

Figure 6.19 shows the time evolution of the instantaneous phases obtained from the proposed algorithm whilst Figure 6.20 shows the instantaneous phases referred to the center of inertia.

Comparison of this plot with the time evolution of the original signals in Figure 6.2a shows the correctness of the results.
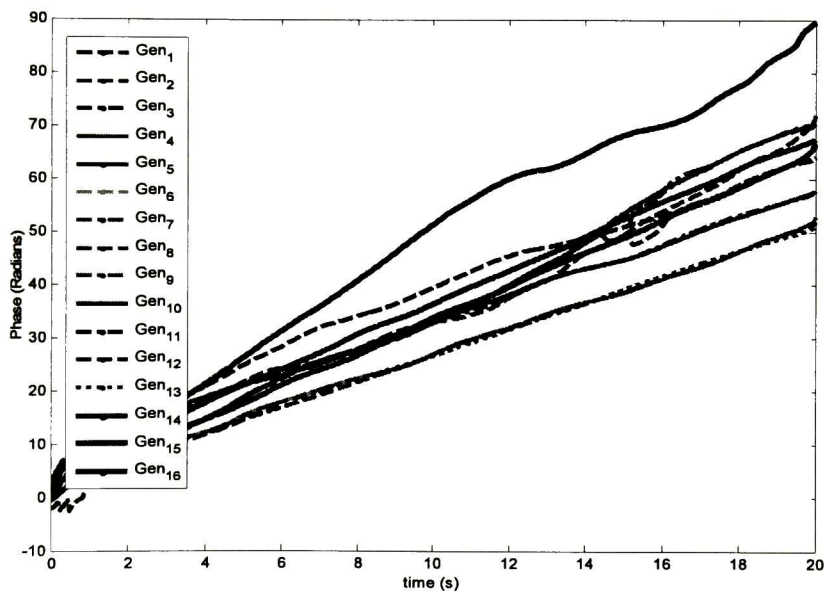

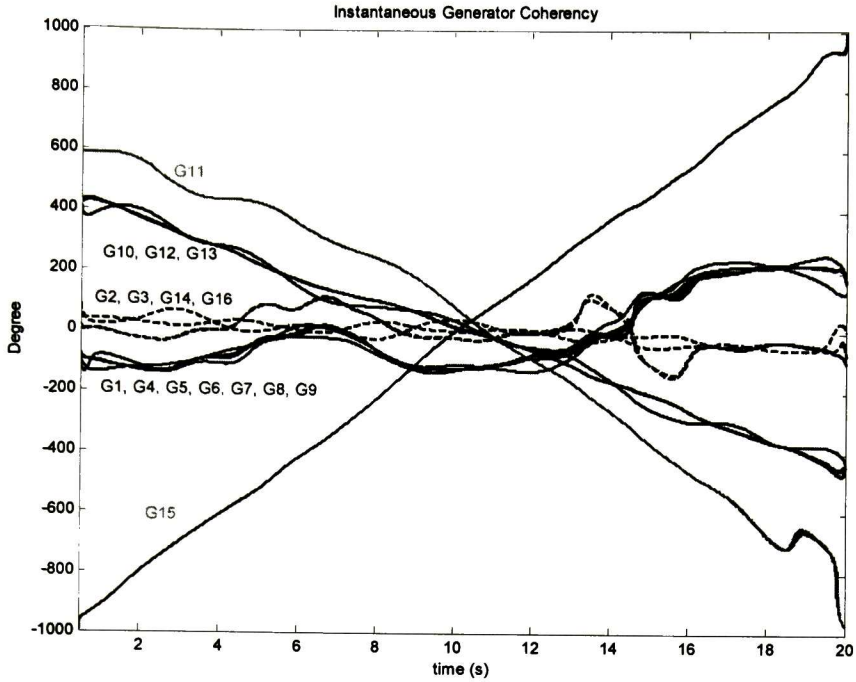Figure 6.19. Instantaneous phase of 16 generators of the test system.

Figure 6.20. Instantaneous phase of test system referring to inertia center.

6.6 Application to measured data

To further verify the ability of the method to analyze complex temporal oscillations, we consider measured data from phasor measurement units (PMUs).

Two real power signals are used to examine characteristics of quasi-stationary processes. These cases are:

Case 1. Active power signal ESA-MCD 230 kV line during the disturbance by fault on TC in phase B.

Case 2. Active power signal from a real event in northern Mexico.

Figures 6.21 and 6.22 show the instantaneous frequencies computed using the different approaches. From this analysis and other simulations several conclusions can be drawn:

- On comparison, the different approaches result in similar approximations to system frequency for periods of the signal that exhibit quasi-stationary behavior

- Second and fourth order central finite difference approximations provide better approximations to the instantaneous frequency, especially in regions in the signal with strong amplitude variations

- The standard and Barnes approximations produce larger spikes (positive and negative)

On comparison of the two curves it is seen that the several approaches give similar results.

While the conclusions may be difficult to generalize, these findings provide basic insight into the non-stationary behavior of nonlinear and non-stationary oscillations and the accuracy of the proposed techniques.
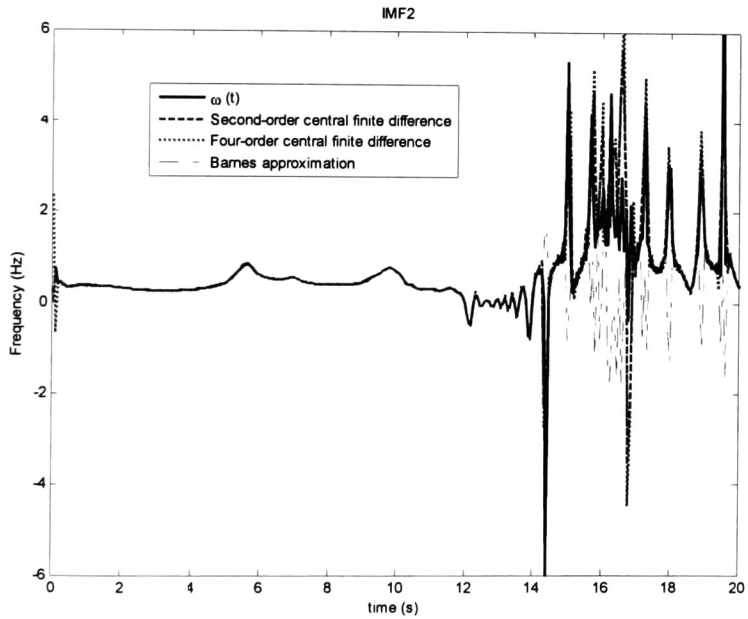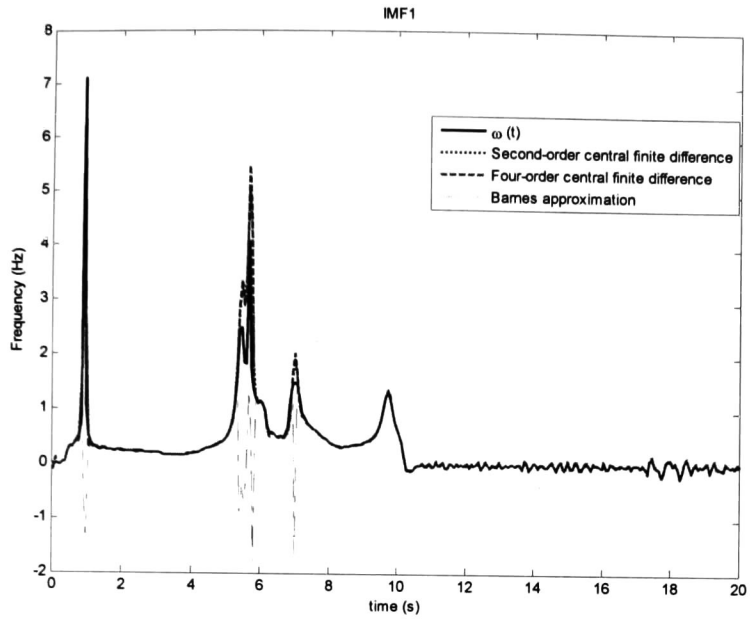
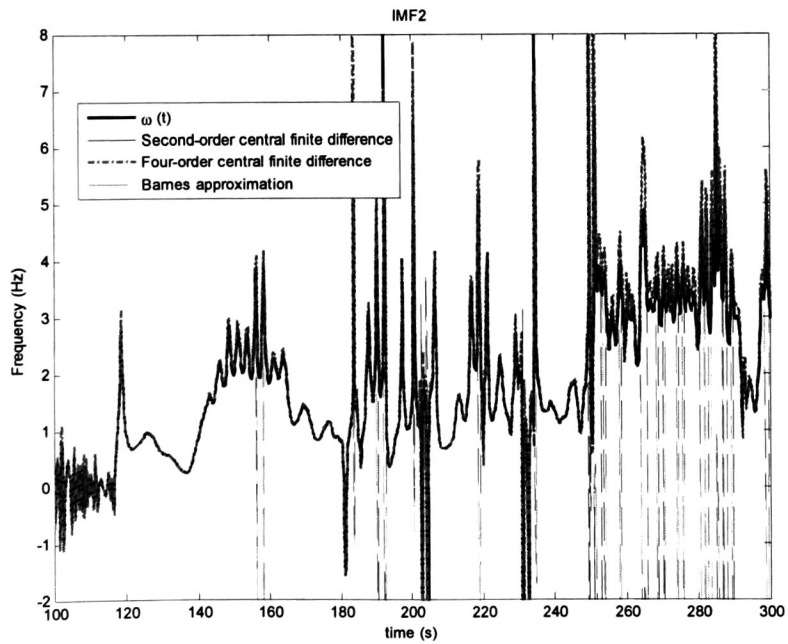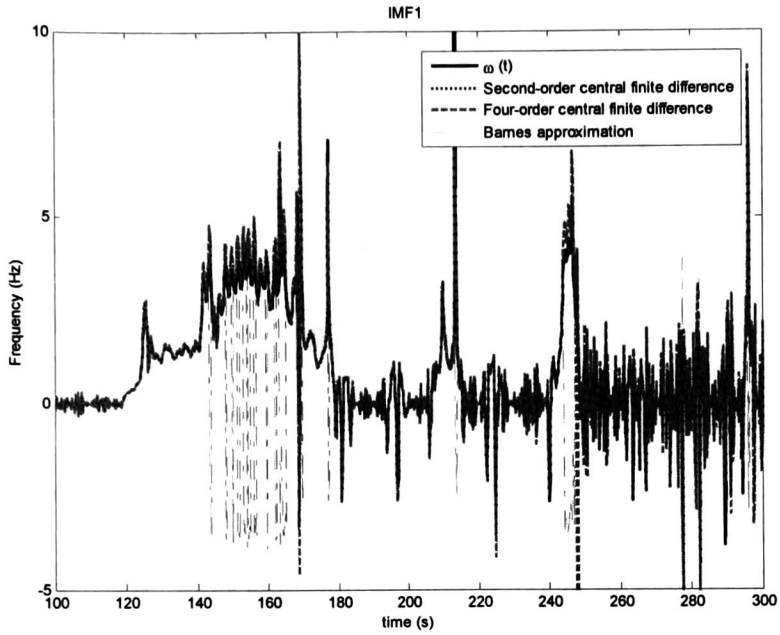Figure 6.21. Case 1. Comparison of instantaneous frequency in IMFs.

Figure 6.22. Case 2. Comparison of instantaneous frequency in IMFs.

6.7 Concluding remarks

In this chapter, the practical application of the proposed technique to the analysis of nonlinear and non-stationary oscillations has been demonstrated. The methods are effective for detection of both, oscillatory and abrupt changes in transient events of power systems. This permits direct comparison with conventional methods and its efficiency is demonstrated.

Significant improvement in the accuracy of the analytical procedure has been noted by adding masking and other processing techniques. Additional work is needed to further refine these methods.

Hilbert-based techniques for coherency identification have good potential for detection of dynamic patterns particularly in connection with protection actions. The extension of this approach to address modal coherency deserves further attention.

The use of time-controlled discrete switching control actions and wide-area mode control based on the detection of critical stability damping margins of observed oscillations and the introduction of Freevib method considering high harmonics for identification of nonlinear systems can be considered as future work.

6.8 References.

[1] G. Rogers, "Power System Oscillations," Ed. Kluwer Academic Publishers, ISBN , 1st ed., vol. 1, 2000.

[2] G. Rogers "Power System Structure and Oscillations," in *IEEE Computer Applications in Power*, Cap Tutorial, vol. 1, pp. 14–21, 1999.

[3] R. R. Zhang, L. VanDemark, J. Liang, and Y. Hu, "On estimating site damping with soil non-linerity from earthquake recordings," in *International Journal of Non-Linear Mechanics*, vol. 39, pp. 1501-1517, 2004.

Chapter 7
Conclusions

7.1 General conclusions

In this thesis, a new approach for the analysis and characterization of nonlinear, non-stationary power system oscillations, based on an innovate time-frequency-energy approach has been proposed.

The techniques developed in this thesis allow an in-depth analysis at the dynamical behavior of the system and permit to detect both, oscillatory and abrupt changes. Also, these approaches enable the systematic computation of IMFs to extract significant temporal modal information and its application is practical due to simplicity of the algorithms used in real events and simulated data. The proposed method has advantages over the conventional techniques that only offer partial results in the analysis of complex oscillations.

In addition, this adaptive time-frequency-energy method offers the possibility of application for the analysis on-line of inter-area oscillations.

Others main conclusions obtained from this work are:

- The application of masking signal techniques on conventional EMD can be used to solve the problem of mode mixing contained in the analyzed signal and improves the conventional HHT results.

- For the numerical calculation of the Hilbert transform several techniques are developed with the aim of eliminating numerical errors in the computing of instantaneous attributes in the initial and end data points.

- The use of the log decrement method make it is possible to estimate the averaged instantaneous damping of oscillatory phenomena.

- An alternative approach to computing the generator coherency is to use the phase of the generator oscillations, instead of the actual swing curves. Here is applied a new criteria to determine the dominant mode of each generator.

7.2 Future work

The futures areas of research identified in this thesis are:

The proposed method may be used into other areas of analysis. Further extensions and refinements are required for its on-line application.

The introduction of Freevib method considering high harmonics for characterization of instantaneous attributes in nonlinear time-varying power systems oscillations.

- The quantitative modal information obtained of the proposed method can be used to trigger control actions to stabilize the system, which are based on the detection of critical stability damping margins of oscillations present in the dynamic system behavior.

The application of generator coherency method in special protection system relying on wide-area measurements to improve system reliability and healing capability.

Appendix A
Interpolation by spline functions

Several procedures for fitting approximating polynomials to a set of tabular data are presented in [1]. Problems can arise when a single high-degree polynomial is fit to a large number of points. High-degree polynomials would obviously pass through all the data points themselves, but they can oscillate wildly between data points due to round-off errors and overshoot. In such cases, lower-degree polynomials can be fit to subsets of the data points. If the lower-degree polynomials are independent of each other, a piecewise approximation is obtained. An alternate approach is to fit a lower-degree polynomial to connect each pair of data points and to require the set of lower-degree polynomials to be consistent with each other in some sense. This type of polynomial is called a spline function, or simply a spline.

Splines can be of any degree. Linear splines are simply straight line segments connecting each pair of data points. Linear splines are independent of each other from interval to interval. Linear splines yields first-order approximating polynomials. The slopes (i.e., first derivatives) and curvatures (i.e., second derivatives) are discontinuous at every data point. Quadratic splines yield second-order approximating polynomials. The slopes of the quadratic splines can be forced to be continuous at each data point, but the curvatures (i.e., second derivatives) are still discontinuous.

Cubic spline

A cubic spline yields a third-degree polynomial connecting each pair of data points. The slopes and curvatures of the cubic spline can be forced to be continuous at each data point. In fact, these requirements are necessary to obtain the additional conditions required to fit a cubic polynomial to two data points. Higher-degree splines can be defined in a similar manner. However, cubic splines have proven to be a good compromise between accuracy and complexity.

The name spline comes from the thin flexible rod, called a spline, used by draftsmen to draw smooth curves through a series of discrete points. The spline is placed over the points and either weighted or pinned at each point. Due to the flexure properties of a flexible rod (typically of rectangular cross section), the slope and curvature of the rod are continuous at each point. A smooth curve is then traced along the rod, yielding a spline curve.

Figure A.1 illustrates the discrete x space and defines the indexing convection. There are $n+1$ total points, x_i $(i = 1,2,...,n+1)$, n intervals, and $n-1$ interior grid points, x_i $(i = 1,2,...,n)$. A cubic spline is to be fit to each interval. Thus,

$$f_i(x) = a_i + b_i x + c_i x^2 + d_i x^3 \qquad (i = 1,2,...,n) \qquad (A.1)$$

defines the cubic spline in interval $i, x_i \le x \le x_{i+1}$ $(i = 1,2,...,n)$. Since each cubic spline has four coefficients and there are n cubic splines, there are $4n$ coefficients to be determined. Thus, $4n$ boundary conditions, or constraints, must be available.

In the direct approach, the following constraints are applied.

1. The function values, $f(x_i) = f_i$ $(i = 1,2,...,n)$, must be the same in the two splines on either side of x_i at all of the $n-1$ interior points. This constraint yields $2(n-1)$ conditions.

114

2. The first derivative of the two splines on either side of point x_i must be equal at all of the $n-1$ interior points. This constraint yields $(n-1)$ conditions.

3. The second derivative of the two splines on either side of point x_i must be equal at all of the $n-1$ interior points. This constraint yields $(n-1)$ conditions.

4. The first and last spline must pass through the first (i.e., x_1) and last (i.e., x_{n+1}) points. That is, $f_1(x_1) = f_1$ and $f_n(x_{n+1}) = f_{n+1}$. This constraint yields 2 conditions.

5. The curvature [i.e., $f''(x)$] must be specified at the first (i.e., x_1) and last (i.e., x_{n+1}) points. That is, $f_1''(x_1) = f_1''$ and $f_n''(x_{n+1}) = f_{n+1}''$. This constraint yields 2 conditions.
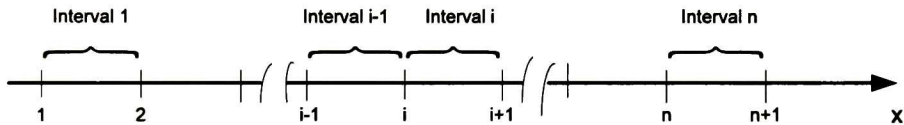
$n+1$ grid points, $x_i (i = 1,2,...,n+1)$

n intervals, $x_i \leq x \leq x_{i+1} (i = 1,2,...,n)$

n cubic splines, $f_i(x)(i = 1,2,...,n)$

$n-1$ interior grid points, $x_i (i = 2,3,...,n)$

Figure A.1. Cubic spline.

When all of the conditions given above are assembled, $4n$ linear algebraic equations are obtained for the $4n$ spline coefficients $a_i, b_i, c_i,$ and d_i $(i = 1,2,...,n)$. This set of equations can be solved by Gauss elimination. However, simpler approaches exist for determining cubic spline. The approach presented by Chapra and Canale is followed below [2].

115

From equation (A.1), it is obvious that the second derivative within each interval, $f_i''(x)$, is a linear function of x. The first-order Lagrange polynomial for the second derivative $f_i''(x)$ in the interval $i, x_i \leq x \leq x_{i+1}$ $(i = 1, 2, ..., n)$, is given by

$$f_i''(x) = \frac{x - x_{i+1}}{x_i - x_{i+1}} f_i'' + \frac{x - x_i}{x_{i+1} - x_i} f_{i+1}'' \qquad (A.2)$$

Integrating equation (A.2) twice yields expressions for $f_i'(x)$ and $f_i(x)$

$$f_i'(x) = \frac{x^2/2 - xx_{i+1}}{x_i - x_{i+1}} f_i'' + \frac{x^2/2 - xx_i}{x_{i+1} - x_i} f_{i+1}'' + C \qquad (A.3)$$

$$f_i(x) = \frac{x^3/6 - x^2 x_{i+1}/2}{x_i - x_{i+1}} f_i''(x) + \frac{x^3/6 - x^2 x_i/2}{x_{i+1} - x_i} f_{i+1}'' + Cx + D \qquad (A.4)$$

Evaluating equation (A.4) at x_i and x_{i+1} and combining the results to eliminate the constants of integration C and D gives

$$f_i(x) = \frac{f_i''}{6(x_{i+1} - x_i)} (x_{i+1} - x)^3 + \frac{f_{i+1}''}{6(x_{i+1} - x_i)} (x - x_i)^3$$

$$+ \left[\frac{f_i}{x_{i+1} - x_i} - \frac{f_i''(x_{i+1} - x_i)}{6} \right] (x_{i+1} - x)$$

$$+ \left[\frac{f_{i+1}}{x_{i+1} - x_i} - \frac{f_{i+1}''(x_{i+1} - x_i)}{6} \right] (x - x_i) \qquad (A.5)$$

Equation (A.5) is the desired cubic spline for increment i expressed in terms of the two unknown second derivatives f_i'' and f_{i+1}''.

An expression for the second derivatives at the interior grid points, f_i'' $(i = 2, 3, ..., n)$, can be obtained by setting $f_{i-1}'(x_i) = f_i'(x_i)$. An expression for $f_i'(x)$ can be obtained by differentiating equation (A.5). Applying that expression to intervals $i-1$ and i and evaluating those results at $x = x_i''$ gives expressions for $f_{i-1}'(x_i)$ and $f_i'(x_i)$. Equating those expressions yields

$$(x_i - x_{i-1})f''_{i-1} + 2(x_{i+1} - x_{i-1})f''_i + (x_{i+1} - x_i)f''_{i+1} = 6\frac{f_{i+1} - f_i}{x_{i+1} - x_i} - 6\frac{f_i - f_{i-1}}{x_i - x_{i-1}} \quad \text{(A.6)}$$

Applying equation (A.6) at the $n-1$ interior points gives $n-1$ coupled equations for the $n+1$ second derivatives, $f''_i \; (i = 1,2,...,n+1)$. Two more values of f''_i are required to close the system of equations.

The two additional conditions are obtained by specifying the values of f''_1 and f''_{n+1}. Several approaches are available for specifying these two values:

1. Specify f''_1 and f''_{n+1} if they are know. Letting $f''_1 = 0$ and/or $f''_{n+1} = 0$ speci-fies a natural spline.

2. Specify f'_1 and/or f'_{n+1} and use equation (A.2) to develop a relationship between f'_1 and/or f'_{n+1} and f'_1 f''_1 and f''_2, etc. This requires the evaluation of the constant of integration C.

3. Let $f''_1 = f''_2$ and $f''_{n+1} = f''_n$

4. Extrapolate f''_1 and f''_{n+1} from interior values of f''_i

The first approach, letting $f''_1 = f''_{n+1} = 0$, is the most commonly employed approach.

In actual analysis is used the command **spline** in MATLAB. This com-mand employs cubic spline interpolation where piecewise polynomials are the models of choice for fitting to arbitrary data.

References.

[1] J. H. Mathews, and K. D. Fink, "Numerical Methods Using Matlab", Ed. Prentice-Hall, ISBN 0-1327-0042-5, 3rd ed., vol. 1, 1999.

[2] J. D. Hoffman, "Numerical Methods for Engineers and Scientists," Ed. Marcel Dekker, ISBN 0-8247-0443-6, 2nd ed., vol.1, New York, 2001.

CENTRO DE INVESTIGACIÓN Y DE ESTUDIOS AVANZADOS DEL I.P.N.
UNIDAD GUADALAJARA

El Jurado designado por la   Unidad Guadalajara   del Centro de Investigación y de Estudios Avanzados del Instituto Politécnico Nacional aprobó la tesis

Interpretación y Visualización de Atributos Instantáneos en
Oscilaciones Inter-área

del (la) C.

Francisco Román LEZAMA ZÁRRAGA

el día 11 de Agosto de 2008.

Dr. Arturo Román Messina
Investigador CINVESTAV 3C
CINVESTAV Unidad Guadalajara

Dr. Deni Librado Torres Román
Investigador CINVESTAV 3A
CINVESTAV Unidad Guadalajara

Dr. Emilio Barocio Espejo
Profesor Investigador Titular C
Universidad de Guadalajara